POZNAN UNIVERSITY OF TECHNOLOGY

Faculty of Chemical Technology

Institute of Chemistry and Technical Electrochemistry

Field of study: Chemical Sciences

Emmanuel Pameté Yambou

Design of ionic liquid based electrical double layer capacitors operating very effectively at low temperature

Projektowanie kondensatorów podwójnej warstwy elektrycznej na bazie cieczy jonowych działających efektywnie w niskich temperaturach

DOCTORAL DISSERTATION

Promoter: **Prof. François Béguin**

Co-promoter: **Dr. inż. Barbara Gorska**

Poznań 2021

NATIONAL **S**CIENCE **C**ENTRE
POLAND

«Train people well enough so they can leave, treat them well enough, so they don't want to».

Richard Branson

Acknowledgments

This Ph.D. thesis has been accomplished in the Power Sources Group of the Poznań University of Technology. Its realization could not have been practical without many people's intellectual, moral, and physical effort to whom I wish to express my respectful gratitude.

First of all, I express my biggest gratefulness to my promoter, Professor François Béguin, for the opportunity he gave me to work on this ambitious research project. I am thankful for the research experience he instilled in me with his guidance and rich scientific discussions during these years. Merci Prof!

My sincere thanks go to my great co-promoter, Doctor Barbara Gorska, who has mentored me throughout this thesis. I thank her for her encouragement, understanding, availability, and indispensable help, which made this thesis work very enriching on the scientific and human levels. Dziękuję Pani Basia!

Thanks are due to the head of our Group, Professor Elzbieta Frackowiak, for her kind help and support for the smooth running of my thesis. Dziękuję!

These acknowledgments would be incomplete if I will not say a big thanks to Dr. Zhuanpei Wang for all her help, support, and contribution in the thermal and physicochemical characterization of ionogels. 太感谢了

I would like also to associate to the success of this thesis: Dr. hab. Mirosława Pawlyta, Dr. Agnieszka Chojnacka, Dr. Vladimir Pavlenko, Dr. Adam Ślesiński, Dr. Paula Ratajczak, MSc. Maciej Tobis and MSc. Xuexue Pan, for all their help and support.

May all the Power Sources Group members find in these few lines the expression of my deepest gratitude. I am thinking particularly of those on the so-called "8th floor" with whom I have shared all or part of these years.

Finally, I am grateful to M.Sc. Eng. Malgorzata Knas, for all her administrative help and support. Dziękuję Pani Malgosia!

Table of Contents

General introduction

Several countries worldwide are committed to reducing global carbon dioxide (CO_2) emissions to net-zero by 2050 (NZE2050). These targets are included in the Sustainable Development Scenario (SDS) of the International Energy Agency (IEA) - consistent with efforts to limit the long-term increase in average global temperatures to 1.5 °C. Yet, attention is increasingly turning to what it would mean for the energy sector globally to reach NZE2050, at a time when the world is trying to recover from the Covid-19 pandemic. Achieving net-zero CO_2 emissions by 2050 requires strengthened policies to speed the deployment of clean and efficient energy technologies. The most significant innovation needs concern advanced batteries, hydrogen electrolyzers, and direct air capture (a technology to capture CO_2 from the atmosphere) and storage. Together, these three technology areas are expected to make vital contributions to reducing CO_2 emissions between 2030 and 2050. Concerning the specific case of the battery technology, the goal set by the IEA to advance the energy transition between 2020 and 2030 is to double every two years their global manufacturing capacity.

In the past 20 years, the energy demand has led to increased scientific research on electrochemical energy storage; this mainly concerned developing new technologies or new materials in batteries and electrochemical capacitors (ECs). This crucial issue was recently immortalized by awarding the 2019 Nobel Prize in Chemistry to John Goodenough, M. Stanley Whittingham, and Akira Yoshino "for developing lithium-ion batteries". Their work created the appropriate conditions for a wireless and fossil-fuel-free society and benefits significantly to humankind. ECs represent an emerging class of energy storage systems that complement batteries in terms of power and conventional capacitors in terms of energy. They are used in numerous applications requiring high power (e.g., vehicles, tramways, and memory backup). When combined in a hybrid system with high energy density components such as batteries and fuel cells, ECs will increase their lifespan.

Among the various types of ECs, those based on activated carbon electrodes and organic electrolytes, so-called electrical double-layer capacitors (EDLCs), are the most advanced systems. EDLCs operate by a fast and reversible electrostatic accumulation of ions forming an electrical double-layer at the electrode/electrolyte interface. Since chemical reactions are not involved in the charging mechanism in EDLCs, the energy stored in these devices is lower than in lithium-ion batteries (LIBs). The advantages of the EDLCs operation include short charge/discharge time, high specific power, and long cycle life. The so-called Ragone plot (Figure 1) compares the specific energy and power of electrochemical energy storage devices.

As shown in this diagram, lithium-ion batteries can deliver high energy densities with relatively low power densities. In contrast, ECs provide very high power with lower energy density than batteries. Thanks to the physical type of their charge storage, ECs possess many other advantages, such as a time constant in the order of few seconds, and they can be charged/discharged up to million cycles without electrodes deterioration. Moreover, their power density and charge storage capacity can be enhanced significantly by using electrode materials characterized by a highly developed specific surface area and a high electrical conductivity.
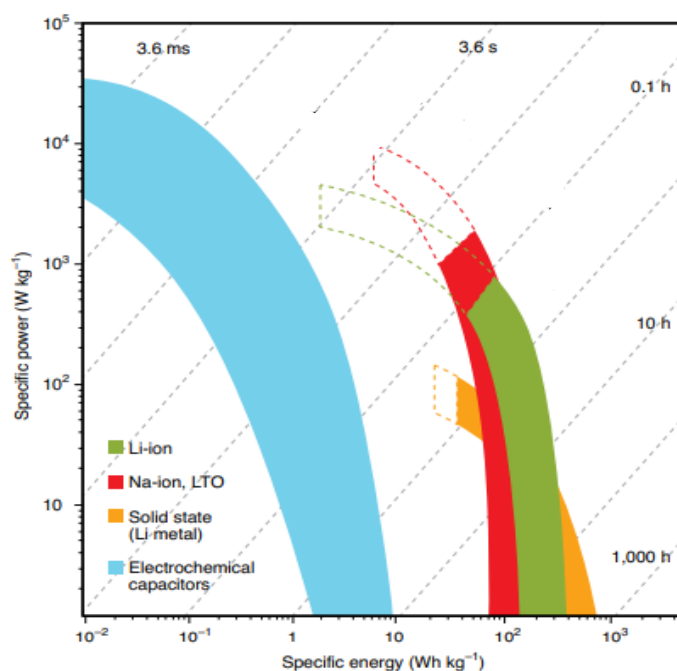
Figure 1. Ragone plot depicting the energy versus power density of few electrochemical energy storage systems [1]. Energy and power expressed per total mass of electrode materials.

According to the formula $E = \frac{1}{2}CU^2$ (C - capacitance), the specific energy (E) of EDLCs is strongly correlated with the operational cell voltage (U), which is mostly controlled by the electrolyte electrochemical stability window (ESW). For this reason, owing to their high ESW, ionic liquids (ILs) stand as a perspective solvent-free class of electrolytes for developing high-energy EDLCs; in addition, ILs are characterized by a high thermal stability, low toxicity, negligible vapor pressure, and non-flammability. Therefore, ILs are superior to conventional organic electrolytes, e.g., 1 mol L^{-1} TEABF$_4$ in acetonitrile, which poses safety and toxicity concerns. ILs commonly applied as electrolytes for EDLCs are imidazolium, [Im]$^+$,

pyrrolidinium, $[Pyr]^+$ or piperidinium, $[Pip]^+$ type cations coupled with bis(trifluoromethylsulfonyl)imide, $[TFSI]^-$, bis(trifluorosulfonyl)imide, $[FSI]^-$ or tetrafluoroborate, $[BF_4]^-$ anions. However, their relatively high melting point (T_m) restricts the scope of their applicability at low temperatures compared to traditional EDLCs implementing an organic electrolyte which perform from -40 °C up to +70 °C. The binary mixtures of ILs have been proposed as electrolytes to overcome these limitations and extend the operating range of IL-based EDLCs to sub-ambient temperatures.

The equimolar mixture of 1-butyl-4-methylpyridinium bis(fluorosulfonyl)imide [BMPyr][FSI] and 1-methyl-1-propylpiperidinium bis(fluorosulfonyl)imide [MPPip][FSI] has been demonstrated not to display neither first- nor second-order transition down to -80 °C and enabled EDLCs to operate at a low current power down to -30 °C when using various types of graphene-based electrodes, or -40 °C when the electrodes are made of nanotubes and carbon onions. It has been also reported that a graphite oxide-based cell incorporating an equimolar mixture of 1-butyl-4-methylpyridinium tetrafluoroborate $[BMPyr][BF_4]$ and 1-butyl-3-methylimidazolium tetrafluoroborate $[BMIm][BF_4]$ could demonstrate an EDLC performance at low power down to -40 °C. However, as graphite oxide or graphene-based electrodes have a relatively low density, the resulting low volumetric outputs of such EDLC are a concern in most applications.

To solve the disadvantages of the previously proposed solutions, the main objective of this thesis is to design IL-based EDLCs operating efficiently at low temperatures, while displaying realistic specific and volumetric energy and power outputs. More specifically: (i) to formulate ILs mixtures with an extended low-temperature liquidus range, as well as relatively low viscosity and high conductivity; (ii) to select/design micro/mesoporous carbon electrodes enabling efficient gravimetric and volumetric performances of ILs-based EDLCs at low temperatures (targeting -40 °C) and (iii) to increase the EDLCs safety by solving the leakage problem related with the use of liquid ILs electrolytes.

The first chapter of this thesis provides a literature review on EDLCs based on carbon electrodes. The general properties of EDLCs are discussed, followed by the explanation of the fundamental role played by the carbon porous texture and electrolytes on EDLCs' performance. Special attention is paid to the development of hierarchical carbon electrodes and eutectic mixtures of IL electrolytes. The weak points of the state of the art and the missing data on

IL-based EDLCs operating at low temperature are also highlighted. The last part of the review gives an overview on the synthesis and properties of solid-state electrolytes (so-called ionogels) without neglecting the temperature effects on the performance of ionogels based EDLCs.

Due to the relatively high melting point (T_m) of ILs, it is mandatory to design formulations with low T_m and good transport properties to enable an effective operation of EDLCs at sub-ambient temperatures. The publication entitled "*Binary mixtures of ionic liquids based on EMIm cation and fluorinated anions: physico-chemical characterization in view of their application*" and its summary presented in the chapter II show a strategy to reach these objectives. Three imidazolium-based ILs containing fluorinated anions (FSI^-, $TFSI^-$ and BF_4^-) were selected to formulate 27 binary mixtures - $[EMIm][TFSI]_x[FSI]_{(1-x)}$, $[EMIm][FSI]_x[BF_4]_{(1-x)}$ and $[EMIm][TFSI]_x[BF_4]_{(1-x)}$, with various molar ratios of the components. The thermal behaviour of these mixtures was investigated with differential scanning calorimetry (DSC) in a wide temperature range from -130 ℃ to 25 ℃. Among these formulations, 17 mixtures showed neither crystallization nor melting down to -130 ℃, but only a glass transition below -90 ℃, making them prospective low-temperature electrolytes. For such fluids, the density was measured at temperatures from 20 to 60 ℃, while the viscosity and conductivity were determined from -25 to 60 ℃ and -40 to 25 ℃, respectively. The ionicity of the mixtures was also estimated, and it is shown that according to the Angell classification, these binary mixtures are "good ILs". Finally, the electrochemical stability window of the mixture with the lowest viscosity and the highest conductivity is determined on a nanoporous carbon black electrode and compared with the data obtained on the parent neat ILs.

The third chapter includes the summary of the publication entitled "*Fitting the porous texture of carbon electrodes to a binary ionic liquid electrolyte for the realization of low temperature EDLCs*". It presents a strategy for the realization of IL-based EDLCs capable of efficient operation down to -40 ℃, while implementing the optimal ILs mixture described in the previous chapter, i.e. $[EMIm][FSI]_{0.5}[BF_4]_{0.5}$ which exhibits only a glass transition at -97 ℃, as well as a relatively low viscosity (33.0 mP s at 20 ℃) and good conductivity ($\sigma = 12.1$ mS cm^{-1} at 20 ℃ and 0.42 mS cm^{-1} at -40 ℃). To enhance the mass transport at low temperatures, electrodes made of two micro/mesoporous carbons were applied: i) a home-made hierarchical MgO-templated carbon named MP98B, having micropores interconnected with well-defined mesopores playing the role of transportation channels; and ii) the SC2A carbon black (from Cabot) with agglomerated dense microporous spherical particles creating

interparticle mesopores. The porous texture of the SC2A and MP98B electrodes analyzed by nitrogen adsorption/desorption at 77 K, and their pore size distribution determined by applying the 2D-NLDFT theory, are presented. The electrochemical properties of symmetric two-electrode pouch cells with both electrode types in the $[EMIm][FSI]_{0.5}[BF_4]_{0.5}$ binary electrolyte were evaluated from 20 °C to -50 °C with cyclic voltammetry (CV), galvanostatic charge/discharge (GC/GD) and electrochemical impedance spectroscopy (EIS) up to a cell potential of 3.0 V. Owing to the advantages of MP98B in terms of charge propagation and the high density of SC2A enabling to enhance the volumetric outputs, a mixed material (SCMP) made of an equal mass of these two carbons was implemented. The viability of this formulation is demonstrated with the Ragone plots realized at constant power by discharging the EDLCs with SC2A, MP98B, and SCMP electrodes from 3.0 V to 1.5 V. Finally, it is shown that the SCMP capacitor outperformed the cells with the single carbon component, delivering the highest retention of specific and volumetric energy at temperatures lower than -20 °C.

Given the results reported in chapter III, optimizing the electrode material and electrolyte properties is crucial to boost the volumetric outputs of IL-based EDLCs. The fourth chapter presents the properties of an optimized IL electrolyte and carbonaceous electrodes with adjusted density to realize devices demonstrating realistic energy and power outputs at low temperatures. Thus, the summary of the paper entitled "*Electrical double-layer capacitors based on a ternary ionic liquid electrolyte operating at low temperature with realistic gravimetric and volumetric energy outputs*" is presented. Since it is conceivable that the creation of an IL with desired characteristics is feasible by a judicious anion-cation combination, and based on the results reported in chapter II, the transport properties of the IL electrolyte have been optimized by mixing 1-ethyl-3-methylimidazolium tetracyanoborate - [EMIm][TCB] with [EMIm][FSI] and [EMIm][BF_4] in various molar ratios. The thermal and physicochemical properties of the $[EMIm][FSI]_x[BF_4]_y[TCB]_z$ ternary mixtures are discussed, and the best formulation ($[EMIm][FSI]_{0.6}[BF_4]_{0.1}[TCB]_{0.3}$) is selected as electrolyte for low-temperature EDLCs. Then, the textural/structural properties of a homemade hierarchical SiO_2-templated carbon (TC-2) analyzed by transmission electron microscopy (TEM) and nitrogen adsorption/desorption are reported. The potential limits of individual TC-2 electrodes in the $[EMIm][FSI]_{0.6}[BF_4]_{0.1}[TCB]_{0.3}$ electrolyte are determined and discussed in the light of a comparative analysis carried out using the neat [EMIm][FSI], [EMIm][BF_4] and [EMIm][TCB] ionic liquids. Next, the effect of low temperature on the electrochemical

performance of symmetric TC-2/TC-2 pouch cells in the $[EMIm][FSI]_{0.6}[BF_4]_{0.1}[TCB]_{0.3}$ electrolyte is investigated up to the cell potential of 3.2 V from 20 °C to -50 °C. Finally, the specific and volumetric energy outputs of the EDLC based on TC-2 electrodes and the $[EMIm][FSI]_{0.6}[BF_4]_{0.1}[TCB]_{0.3}$ electrolyte are compared with the performance of cells with alternative combinations of these components.

The fifth chapter presents the design of IL-based solid-state EDLCs operating from 20 °C to -40 °C. The applied ionogel films of different thicknesses (~100 and 200 µm) are based on the aforementioned optimized $[EMIm][FSI]_{0.5}[BF_4]_{0.5}$ binary mixture confined into a poly(vinylidene fluoride) (PVDF) network, and the solvent used for their preparation was N, N-Dimethylformamide (DMF). The morphology and microstructure of the PVDF and ionogel films are investigated by scanning electron microscopy (SEM), whereas DSC is used to compare the thermal properties of the films based on single ILs ($[EMIm][FSI]$ and $[EMIm][BF_4]$) and $[EMIm][FSI]_{0.5}[BF_4]_{0.5}$ from 25 to -140 °C. The MgO templated carbon, MP98B, with a hierarchical micro/mesoporous texture was used to enhance the mass transport of the ions, especially at low temperatures where the electrolyte present in the porosity exhibits a low conductivity. Globally, the electrochemical properties of the ionogel-based EDLCs at low temperature are discussed in light of a comparative study done with the liquid-state binary IL electrolyte.

The dissertation ends with a general conclusion highlighting and discussing the most critical results presented in the manuscript. Finally, perspectives for further research to optimize the low-temperature performance of EDLCs based on ILs electrolytes are suggested.

Chapter I

State of the art

1. Introduction

Improving the low energy density of electrical double-layer capacitors (EDLCs) remains a key challenge. This results in searching strategies to enhance either their cell voltage and/or their capacitance. The choice of an electrolyte with a high electrochemical stability window (ESW) and the design/selection of a suitable electrode material, which porous texture is compatible with the electrolyte ions, is the core issue to enhance the performance of EDLC devices, particularly their energy density. This review provides the state-of-the-art on EDLCs based on carbon electrodes and ionic liquid (ILs) electrolytes. For low-temperature applications of IL-based EDLCs, special attention is paid to the development of nanoarchitectured carbon electrodes and eutectic mixtures of IL electrolytes. The optimum properties of carbon porous texture and ILs mixtures for the low-temperatures operation of EDLCs with high volumetric outputs are detailed. However, since IL leakage may limit the operating range of EDLCs in practical applications, ionogels (ILs confined in solid scaffolds) as solid-like forms are proposed to overcome this critical issue.

2. Electrical double-layer capacitors

2.1. EDL models (on a flat surface)

The double-layer model proposed for the first time in 1853 by Helmholtz [2] describes the separation of charges at the interface of a solid electronic conductor and a liquid ionic conductor. When an electrode is polarized, the ions of opposite charge present in the electrolyte move towards its surface and form a rigid layer, the so-called inner Helmholtz double-layer or compact layer (Figure 2a). The potential in the electrode vicinity decreases linearly as the ions' distance to the electrode increases. The capacitance of the Helmholtz double-layer is expressed in the same way as that of a conventional electrical capacitor of capacitance C_H defined by equation (1).

$$C_H = \frac{\varepsilon_0 \varepsilon_r}{d} \cdot S \qquad\qquad (1)$$

In this equation, ε_0 is the vacuum permittivity ($\varepsilon_0 = 8.854 \cdot 10^{-12}$ F m^{-1}), ε_r is the dielectric constant of the electrolyte, S is the electrochemically accessible surface area, and d is the effective thickness of the double-layer.

Following Helmholtz, Gouy introduced in 1910 the notion of diffuse layer, crucial for dilute electrolytes: "the distribution of ions in the vicinity of the electrode, in the absence of specific adsorption (in the compact layer), is governed by thermal agitation and Coulomb forces" [3]. Chapman established the diffuse layer theory in 1913 (Figure 2b) using the Boltzmann and Poisson equations [4]. The assumptions of the Gouy-Chapman theory are that:

- ➢ the ions are considered as point charges,
- ➢ only the Coulomb interactions are taken into account,
- ➢ the solvent is a continuous dielectric medium of uniform electrical permittivity.

The Gouy-Chapman theory was improved in 1924 by Stern [5] by introducing the dimension of ions and solvent molecules in the modeling. The space charge is then divided into two distinct zones: a so-called compact layer made up of ions adsorbed on the surface of the electrodes and the diffuse layer as defined by Gouy and Chapman. The model used nowadays is the Stern one (Figure 2c), which combines the compact and diffuse layers. The two layers are equivalent to two capacitors in series: the capacitance of the compact Helmholtz layer (C_H) and the capacitance of the diffuse Gouy-Chapman layer (C_{diff}) as expressed in equation (2):

$$C_{dl} = \left(\frac{1}{C_H} + \frac{1}{C_{diff}} \right)^{-1} \qquad (2)$$
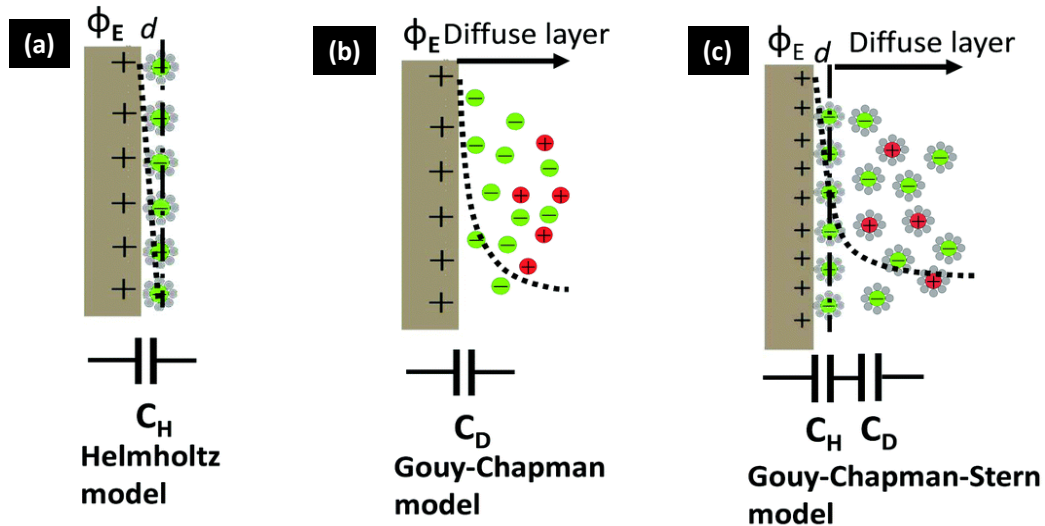
Figure 2. (a) Helmholtz, (b) Gouy-Chapman, and (c) Gouy-Chapman-Stern models of the electrical double-layer formed at a positively charged electrode in an electrolyte with solvent. The dashed lines indicate the potential drop (Φ_E) in each model. The bottom insets present the simplified equivalent circuits (adapted from [6]).

In the three above described models, the adsorption of ions on the electrode surface is considered to be non-specific. However, desolvated anions, in particular, can be irreversibly adsorbed on the electrode surface. In 1947, Grahame developed a three-region model which divides the Stern layer in the inner Helmholtz plane (IHP) and the outer Helmholtz plane (OHP) [7]. IHP is the plane formed by the centres of the specifically adsorbed ions, whereas OHP represents the locus of the electrical centers of the positive charges [8].

Another EDL model described in 1963 by Bockris, Devanathan and Müller (BDM model) [9] introduces a final component to the Grahame one. The BDM model included the action of the solvent molecules (adsorbed on the electrode surface) in the interface. The dipoles of the solvent are oriented according to the nature of the charges on the surface of the electrode, where they form a layer together with the specifically adsorbed ions of the electrolyte. In the case of a negatively polarized electrode (Figure 3), the IHP passes through the centers of the specifically adsorbed cations and solvent molecules, which are oriented parallelly to the electric field. These solvent molecules can be associated with the first solvation sphere of the electrode. The OHP of the adsorbed solvated cations, which pass through the solvated ions centers (outside the IHP), can be identified as the second sphere of electrode solvation. Behind the OHP, there is a diffuse layer region, yet the total EDL thickness depends on the concentration of the electrolyte and the size of the ions.
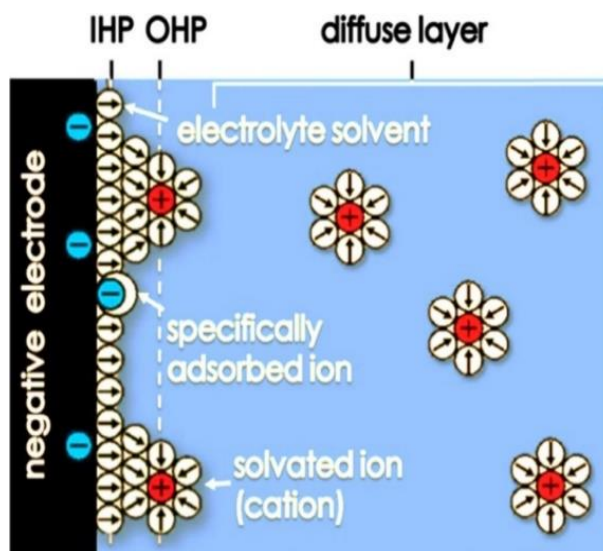
Figure 3. Schematic representation of the Bockris, Devanathan and Müller (BMD) double-layer model on a negatively polarized electrode [10].

2.2. Working principle and properties of EDLCs

The operation principle of EDLCs is based on a fast and reversible electrostatic accumulation of ions, forming an electrical double-layer at the electrode/electrolyte interface [11]. EDLCs are made of two metallic current collectors on which the active materials impregnated with an electrolyte are deposited. The two electrodes are separated by an insulating and porous membrane (separator) to ensure ionic conduction (Figure 4). The simplified circuit of an EDLC is a series assembly comprising two capacitors corresponding to the two electrode/electrolyte interfaces and a resistor (Figure 4). Accordingly, when an electric potential difference is applied between the electrodes, anions are attracted to the positive electrode and cations to the negative one, forming the EDL interfacial regions.
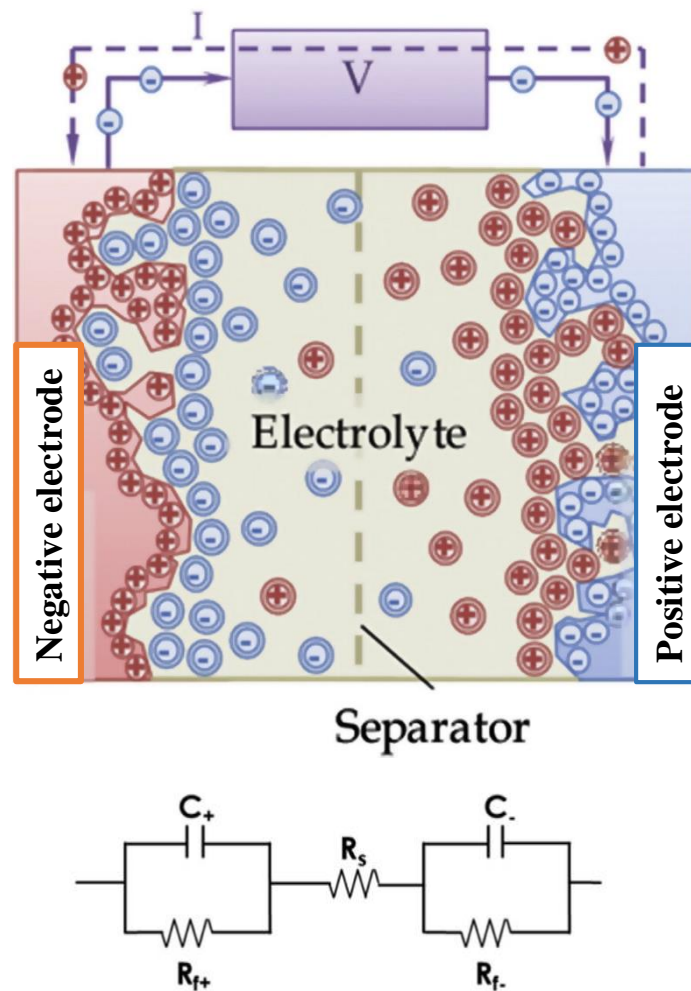
Figure 4: Schematic representation of an EDLC and its simplified equivalent circuit (adapted from [12]).

Hence, the overall capacitance which characterizes an EDLC is given by equation (3):

$$C = \left(\frac{1}{C_+} + \frac{1}{C_-} \right)^{-1} \tag{3}$$

According to equation (3), the electrode with the lowest capacitance value determines the capacitance of the system.

To evaluate the practical applicability of EDLC, their energy (E) and power (P) are the most important parameters to be determined and compared, usually on the Ragone plot basis (Figure 1). They can be expressed per mass of the device, then one speaks about gravimetric or specific energy (E_s in Wh kg^{-1}) and power (P_s in W kg^{-1}) or per volume and referred to as volumetric (energy E_v in Wh L^{-1} and power P_v in W L^{-1}) [6]. The energy outputs depend on the device's capacitance (C in F g^{-1}), cell voltage (U in V), and mass (*m* in kg), as expressed by equation (4):

$$E = \frac{C}{2m} \cdot U^2 \tag{4}$$

and the power (equation (5)) on the discharge time (t in h) and the equivalent series resistance (ESR in Ω).

$$P = \frac{E}{t} \quad or \quad P = \frac{1}{4R_s \, m} \cdot U^2 \tag{5}$$

Still, caution should be used because the values of energy and power given by the researchers do not represent the performance of a real device e.g., they are normalized to the mass of the active material [13].

Another critical parameter of an EDLC is its time constant (τ), corresponding to the time required to release half of the energy stored in the device [14]. It is expressed in seconds and given by the equation (6):

$$\tau = R_s C \tag{6}$$

On the Ragone plot shown in Figure 1, the time constant is represented by the diagonal dashed lines, obtained by dividing the energy density by power; they inform how fast the energy can be distributed at a certain power.

Coming back to the equation (1) above, one can expect that the greater the specific surface area (SSA) of the active material, the greater the number of ions adsorbed on the surface, and the higher the capacitance and energy of EDLCs. However, it has been shown that the capacitance does not change proportionally with the increase of SSA but rather depends on the pores size of the carbon materials [15-17]. The authors of ref. [17] showed that the specific capacitance is proportional to the BET and DFT surface area only up to around 1500 m^2 g^{-1} and 1200 m^2 g^{-1}, respectively; at higher SSA, the pore walls become so thin that they cannot accommodate more charges. Hence, it is essential to control the pore size distribution to achieve enhanced capacitive performance [18-21]. This condition is also vital to realize high volumetric energy and volumetric power in EDLCs, because the density of the electrode materials strongly influences the volumetric characteristics [22, 23]. Yet, there are drawbacks to introducing too much porosity; a very high porosity leads to a low electrode density, resulting in low volumetric outputs of the EDLCs.

The choice of an appropriate electrolyte is also decisive for enhancing the specific energy and power of EDLCs. Indeed, as the energy and power of EDLCs is related to the cell voltage (according to equations 4 and 5), it closely depends on the electrochemical stability window (ESW) of the electrolyte. Therefore, an electrolyte for EDLC should display a high ESW, a high ionic conductivity, a low viscosity, a high boiling point, a low melting point, a high flash point, a high dielectric constant, and high chemical stability. Additionally, the porous texture of the electrode material should be compatible with the electrolyte ion dimensions.

To date, the most widely used electrolytes for EDLCs in academic research are the aqueous ones. They are characterized by a high conductivity, thus enabling good power performance of EDLCs. However, since the thermodynamic stability window of water is 1.23 V, the voltage range of EDLCs based on these electrolytes is reduced. Therefore, the cell voltage of capacitors is usually less than 1 V with aqueous KOH and H_2SO_4 electrolytes. However, neutral aqueous alkali sulfates (e.g., Li_2SO_4 and Na_2SO_4) enable increased cell voltage of carbon/carbon EDLCs up to ca. 1.5 V [24-26], owing to the negative shift of the Nernst hydrogen evolution potential provoked by the water reduction and hydroxyl (OH^-) ion generation inside the porosity of the negative electrode [27, 28]. Recently, a new class of aqueous electrolytes has been reported,

so-called "water-in-salt", i.e., highly concentrated solutions of salt in water, more precisely having salt to water mass (m_{salt}/m_{water}) or volume (V_{salt}/V_{water}) ratios greater than 1 [29], enabling carbon/carbon cell voltage value of 1.8 V in 8 mol kg^{-1} NaTFSI [30] and 20 mol kg^{-1} LiTFSI [31] or 2.3 V in 17 mol kg^{-1} NaClO$_4$ [32].

Although extensive studies have focused on the aqueous-based EDLCs, organic electrolytes dominate the commercial market due to their high operation potential window, typically in the range of 2.5 to 2.8 V [33]. The conventional organic electrolytes mainly consist of the tetraethylammonium tetrafluoroborate (TEABF$_4$) conductive salt dissolved in acetonitrile (ACN) or propylene carbonate (PC) [33]. However, compared to the aqueous electrolytes, the organic ones usually have a higher cost, a lower conductivity (leading to a smaller specific capacitance of EDLCs), and safety concerns related to the flammability, volatility, and toxicity of the solvent [11, 34]. Furthermore, an organic electrolyte has to be carefully purified, and the EDLCs must be assembled in a strictly controlled environment to remove any residual impurities (e.g., water) that can lead to considerable performance degradation and serious self-discharge issues.

PC is usually considered as a safe electrolyte solvent since it is less toxic and has a higher flash point than ACN, which is volatile and flammable. However, PC-based electrolytes exhibit inferior transport properties compared to their ACN-counterparts – resulting in worse EDLCs performance [35]. It has been shown that the aging of a single electrode dominates the aging rate of symmetric EDLCs in either ACN or PC and that the maximum safe potential of each electrode (in a two-electrode cell with reference experiments) depends directly on the solvent [36, 37]. In ACN-based electrolyte, the positive electrode ages much more rapidly than the negative one due to the electrolyte degradation, while in electrolyte using PC as solvent, the negative electrode exhibits faster aging than the positive one – due to the formation of carbonates and the evolution of gaseous species (H$_2$ and CO$_2$) [36]. Noticeably, along with the temperature decrease, ACN-based EDLCs retain almost unchanged dependence of specific energy vs. power from 45 °C to -30 °C (Figure 5a) [38] or discharge capacity from 20 °C to -40 °C (Figure 5b) [39]. The authors of ref. [39] believed that the low-temperature operation of EDLCs with organic electrolytes could be extended beyond -40 °C by adding methyl acetate (MA) as a co-solvent to ACN. However, the performance of the resulting capacitor deteriorated, and its discharge capacity decreased at a temperature below -40 °C (Figure 5c) [39]. Still, the safety concern and environmental unfriendliness of ACN or MA remained

unsolved. Therefore, ionic liquids (ILs) have been proposed as solvent-free electrolytes for EDLCs [40].
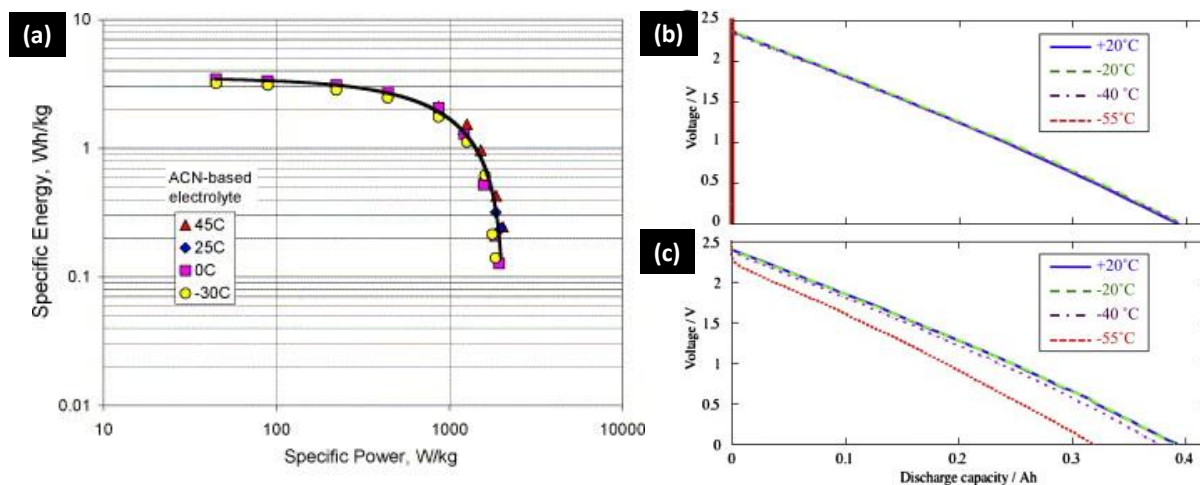
Figure 5. (a) Ragone plots for an ACN-based capacitor at various low temperatures [38]. Galvanostatic discharge curves of cells (b) in ACN and (c) ACN + MA (67:33 in volume) electrolytes at 20, -20, -40 and -55 °C [39]. The salt used in both cases is TEABF$_4$.

3. Ionic liquids as electrolytes for EDLCs

Ionic liquids (ILs) are a solvent-free perspective class of electrolytes for high voltage EDLCs. They are characterized by a high electrochemical stability, a high heat conductivity, a low vapor pressure, a wide range of thermal and chemical stability. ILs are neither volatile nor flammable, and their decomposition temperature is typically higher than 300 °C [41]. Therefore, ILs are superior to conventional organic electrolytes, which pose safety and toxicity concerns. In addition, the possibility of adjusting their physicochemical characteristics by varying the type of anion and/or cation or by modifying the substituents carried by the cation is a significant advantage. For EDLCs applications, the most commonly implemented ILs combine one of the following cations (Figure 6): N-methyl-N-propylpiperidinium [MPPip]$^+$, 1-ethyl-3-methylimidazolium [EMIm]$^+$, 1-butyl-3-methyl-imidazolium [BMIm]$^+$, N-butyl-N-methyl-pyrrolidinium [BMPyrr]$^+$ with one of the following anions: bis(trifluoromethylsulfonyl)imide [TFSI]$^-$, bis(trifluosulfonyl)imide [FSI]$^-$ and tetrafluoroborate [BF$_4$]$^-$.
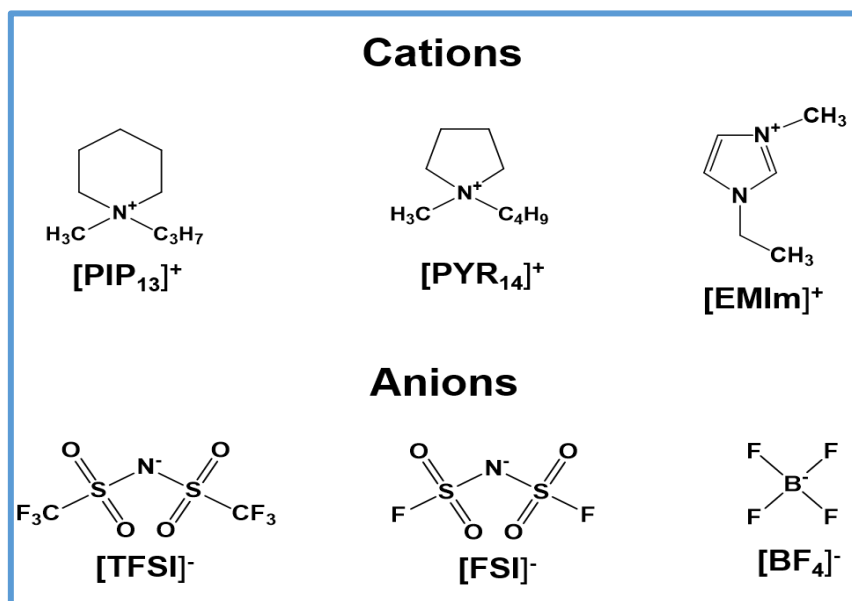
Figure 6. The most commonly used cations and anions of IL electrolytes for EDLCs.

3.1.   Thermal properties of ILs

ILs are characterized by a relatively low melting point and a high decomposition temperature (350 - 400 °C), hence have a vast liquid state temperature range (~ 200 - 300 °C), and a substantial thermal stability range [42]. The melting point of an IL depends on the nature of the cation and the anion [43]; the larger the anion, the lower the melting point of the IL. Likewise, bulky cations with asymmetric substituents enable ILs with a lower melting point [44]. It has been shown by differential scanning calorimetry (DSC) that ILs can remain supercooled, adopt quasi-amorphous phases or even assemble in the form of liquid crystals and thus present a melting point (T_m) and/or a glass transition (T_g) [45, 46]. Generally, ILs with short alkyl chain cations are crystalline solids in which the interactions are strong in the solid state. Those which carry alkyl chains of moderate length have large liquid domains and tend to solidify in the glassy state [47, 48]. Finally, the ILs with long alkyl chains behave like amphiphilic compounds, leading to mesophases and crystallization in sheets [47].

However, the relatively high melting point (Table 1) of ILs restricts the scope of their applicability as low-temperature electrolytes, which is a requirement for commercial EDLCs. To overcome this limitation, their binary mixtures have been proposed as electrolytes. Figure 7 shows the DSC thermograms of the individual ILs and an equimolar eutectic mixture of N-methyl-N-propylpiperidinium bis(fluorosulfonyl)imide [PIP$_{13}$][FSI] and

N-butyl-N-methylpyrrolidinium bis(fluorosulfonyl)imide [PYR$_{14}$][FSI]. The neat [PIP$_{13}$][FSI] and [PYR$_{14}$][FSI] show a melting point of 6 °C and -18 °C, respectively, whereas the DSC curve of the binary mixture displayed neither first nor second-order transitions between -80 and 100 °C [49]. Therefore, this mixture is considered for physico-chemical characterizations (density, viscosity, conductivity) as a prospective low-temperature electrolyte for EDLCs.

Table 1: Melting point of ILs commonly implemented as electrolyte for EDLCs.

ILs	[PIP$_{13}$] [FSI]	[PIP$_{13}$] [TFSI]	[PYR$_{14}$] [FSI]	[PYR$_{14}$] [TFSI]	[PYR$_{13}$] [FSI]	[PYR$_{13}$] [TFSI]	[EMIm] [TFSI]	[EMIm] [FSI]	[EMIm] [BF$_4$]
T$_m$ (°C)	6	12	-18	-6	-9	12	-16	-13	15
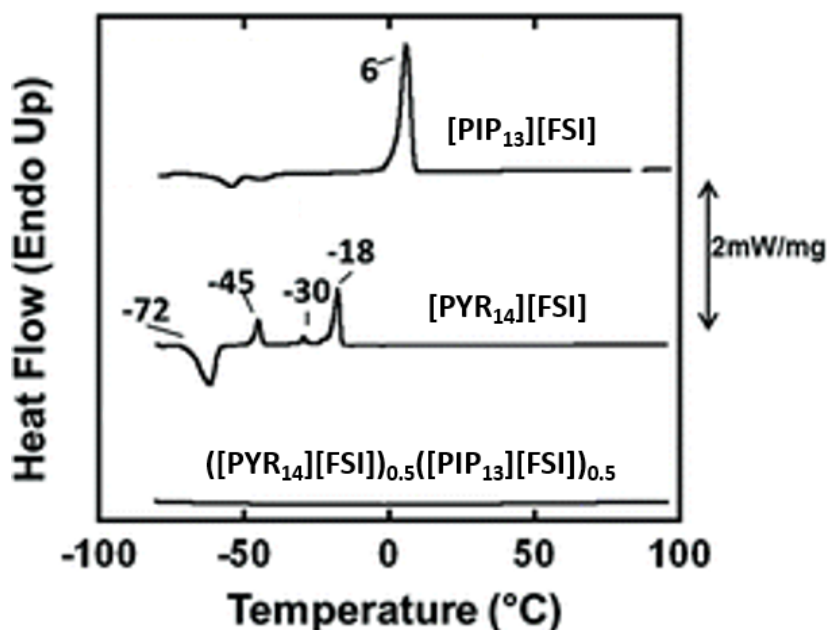
Figure 7. DSC profiles of [PIP$_{13}$][FSI], [PYR$_{14}$][FSI] and ([PYR$_{14}$][FSI])$_{0.5}$([PIP$_{13}$][FSI])$_{0.5}$ [49].

3.2. *Physico-chemical properties of ILs*

For EDLCs applications, the most often reported properties of ILs are their density (ρ), viscosity (η), ionic conductivity (σ), ionicity (α), and electrochemical stability window (ESW). The vast majority of ILs have a density between 1 and 1.6 g cm^{-3}, which is greater than the density of water [44, 50]. For an imidazolium-type cation, it has been shown that the density

decreases with increasing the length of the alkyl chain [45]. Usually, the density of ILs composed of the same anion and various cations decreases in the following order: pyridinium > imidazolium > ammonium > piperidinium [50]. Considering ILs based on the same cation and different anions, the increase of density is as follows: methanesulfonate $[CH_3SO_3]^- \approx [BF_4]^-$ < trifluoroacetate $[CF_3CO_2]^-$ < trifluoromethanesulfonate $[CF_3SO_3]^-$ < heptafluorobutyrate $[C_3F_7CO_2]^-$ < $[TFSI]^-$. Overall, the variations in density of ILs based on the same cation follow the ILs' anion molar mass: the higher the anion molar mass, the lower the IL density [51]. Along with a temperature increase, the density of ILs linearly decreases and can be correlated by the equation (7):

$$\rho \ (g \ cm^{-3}) = = \ a \ + \ bT \tag{7}$$

where a (g cm^{-3}), b (g cm^{-3} K^{-1}) are fitting parameters, and T (K) is the temperature.

One of the important parameters reported when applying ILs as electrolytes for EDLCs is their viscosity. The viscosity of ILs is much higher than that of water, and it decreases with increasing temperature. Usually, higher viscosity values are reported for ILs with a small size of anion, which display stronger electrostatic interactions and hydrogen bonds [42]. It has been observed that the viscosity decreases as follows: chloride $[Cl]^- >$ hexafluorophosphate $[PF_6]^- > [CH_3SO_3]^- \approx [CH_3CO_2]^- > [CF_3SO_3]^- > [CF_3CO_2]^- > [TFSI]^-$ for anions (with the same common cation) and piperidinium > pyrrodinium > imidazolium for cations (with the same common anion) [48, 52]. Generally, the Arrhenius type equation (8) is applied to describe the temperature dependence of viscosity of ILs containing asymmetric cations without functional groups on the alkyl chains [53, 54].

$$\eta = \eta_0 \ exp\left[-\frac{E_a}{RT}\right] \tag{8}$$

where η_0 (mPa s) is the viscosity at infinite temperature, E_a (kJ mol^{-1}) the activation energy for a viscous flow and R (8.314 J mol^{-1} K^{-1}) the universal gas constant.

In the presence of ILs with small and symmetrical cations of low molar mass, the Vogel-Tamman-Fulcher (VTF) equation (9) is recommended [55, 56]:

$$\eta = \eta_0 \, exp\left[\frac{B_\eta}{T - T_{0,\eta}}\right] \tag{9}$$

where, $T_{0,\eta}$ is the temperature at which the viscosity goes to zero or glass transition temperature, and B_η is a constant corresponding to the slope of the VTF plots.

The relatively low conductivity of ILs cannot be simply explained as the consequence of a high viscosity. For example, at 20 °C [EMIm][BF$_4$] (σ = 12.16 mS cm^{-1}, η = 41.2 mPa s) displays a higher conductivity than [EMIm][TFSI] (σ = 7.14 mS cm^{-1}, η = 39.2 mPa s) despite its slightly higher viscosity [57]. Thus, other factors such as the ion size [58-60], charge delocalization [58, 60], density, and species aggregation [61-64] contribute to the conductivity of ILs. For ILs based on the same anion, the conductivity increases in the following order: pyridinium < ammonium < sulphonium < imidazolium [50]. It has also been observed that for IL with the same cation, the ionic conductivity decreases as follows: [FSI]$^-$ > [BF$_4$]$^-$ > [TFSI]$^-$ [65]. The temperature dependence of ILs conductivity is generally expressed by the classical linear Arrhenius behavior (equation (10)):

$$\sigma = \sigma_0 \, exp\left[-\frac{E_a}{RT}\right] \tag{10}$$

where σ_0 (mS cm^{-1}) is the conductivity at infinite temperature, E_a (kJ mol^{-1}) the activation energy for a viscous flow and R (8.314 J mol^{-1} K^{-1}) the universal gas constant. When the Arrhenius law is not respected, the VTF model is applied (equation (11)):

$$\sigma = \sigma_0 \, exp\left[-\frac{B_\sigma}{T - T_{0,\sigma}}\right] \tag{11}$$

where $T_{0,\sigma}$ is the ideal glass transition temperature where the conductivity goes to zero and B_σ is a constant corresponding to the slope of the plots.

The conductivity and the viscosity of an IL are correlated by the fractional Walden rule (equation (12)) [48, 66, 67]:

$$\Lambda \eta^\alpha = Constant \tag{12}$$

where α is a constant between zero and unity ($0 < \alpha \leq 1$) corresponding to the slope of the Walden plot (Figure 8), which correlates the logarithm of molar (or equivalent) conductivity log (Λ) (S cm^2 mol^{-1}) vs. the logarithm of fluidity log ($1/\eta$) (Poise^{-1}). Such plotted data are compared to a reference, the so-called ideal KCl line (0.01 mol L^{-1}), representing an aqueous solution of completely dissociated salt where all the ions have the same mobility [68]. Depending on whether the ion mobility is strongly correlated to the viscosity or not, the ILs electrolytes have an ideal behavior ($\alpha = 1$) or not ($\alpha \neq 1$) [48, 66, 69-75]. According to the Walden diagram (Figure 8), ILs can be classified as superionic glasses, superionic liquids, good ionic liquids, poor ionic liquids, or non-ionic liquids [76].
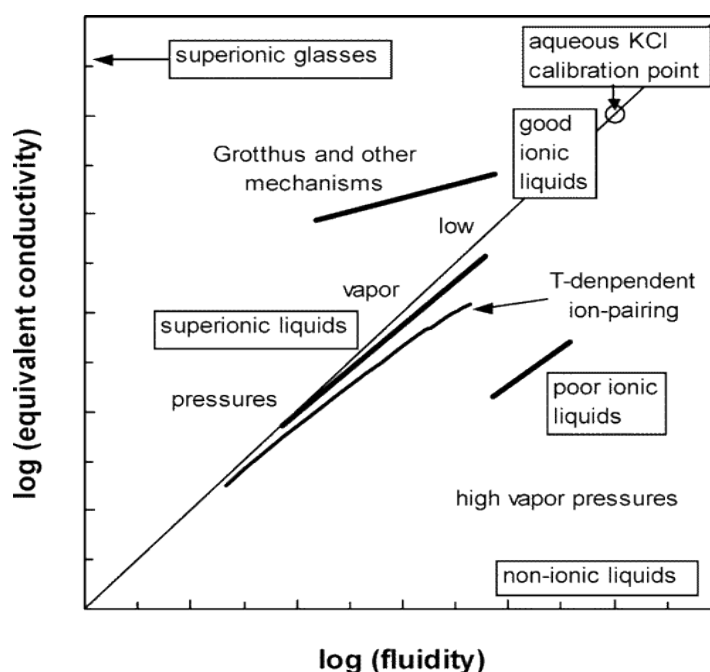
Figure 8. Diagram classifying the ionic liquids on the basis of the Walden rule [76].

3.3. *Electrochemical stability of ILs*

The electrochemical stability window (ESW) on a given electrode is the potential range within which the electrolyte is neither reduced nor oxidized. Therefore, it is an important property which plays a significant role in using ILs as electrolytes for EDLCs. The ESW of ILs is usually measured by linear sweep voltammetry or cyclic voltammetry on an inert electrode, e.g., glassy carbon (GC) or platinum in a three-electrode cell configuration. Figure 9 shows the limiting reduction and oxidation potentials (E_{red} and E_{ox}, respectively) of [EMIm][BF$_4$] measured by

cyclic voltammetry at room temperature on a platinum working electrode [77]. E_{red} and E_{ox} are defined as the potentials at which the limiting current density reached 1 mA cm^{-2}. Here, the ESW between the onset of E_{red} and E_{ox} is 4.5 V for [EMIm][BF$_4$] on platinum [77]. However, it should be highlighted that depending on the applied electrochemical method and the type of working electrode, the ESW of an electrolyte can be different, especially when implementing an activated carbon electrode.
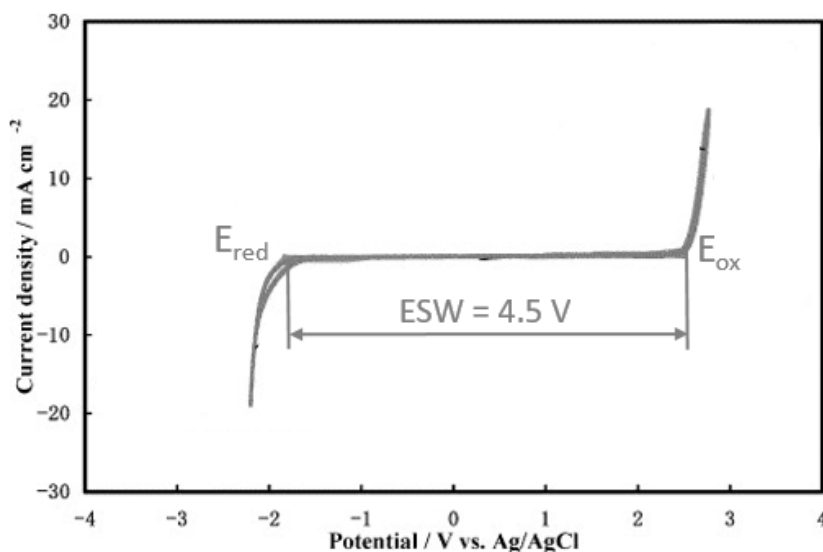
Figure 9. Linear sweep voltammogram of the [EMIm][BF$_4$] ionic liquid at 25 °C. Scan rate: 1 mVs^{-1}; working and counter electrode: platinum; reference electrode: Ag/AgCl [77].

To determine the ESW of electrolytes accurately on activated carbon (AC) electrodes, and on the basis of preliminary works developed by Xu et al. [78], Kötz et al.[79] proposed a window opening method, the so-called S-method. Briefly, the S-method consists of recording cyclic voltammograms (CVs) on separate electrodes under negative and positive polarizations by steps of 0.1 V until observing in each case a noticeable redox signature (Figure 10). In Figure 10, the purely box-like shape of the CV loops characterizing the EDL charging represents the electrochemical stability region. In contrast, the CVs with the appearance of parasitic redox peaks reveal the decomposition of the electrolyte.
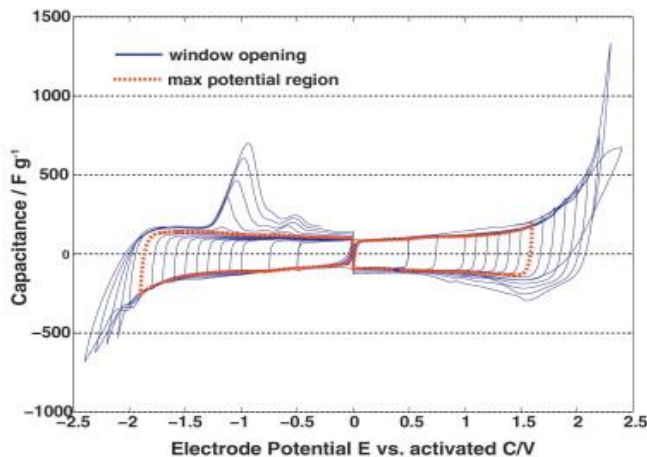
Figure 10. Window opening experiments on BP2000 working electrodes with [EMIm][BF$_4$] electrolyte by cyclic voltammetry at a scan rate of 1 mV s^{-1}. Reference and counter electrodes: YP17. The red dashed lines indicate the anodic and cathodic limits [79].

Subsequently, the S-values are calculated for the positive and negative polarizations, using the equations (13) and (14), respectively:

$$S_{pos} = \frac{Q_+}{Q_-} - 1 \qquad (13)$$

$$S_{neg} = \frac{Q_-}{Q_+} - 1 \qquad (14)$$

where Q_+ and Q_- are the integrated charges during the anodic and cathodic scans, respectively. Then, the S-values are plotted vs. the corresponding vertex potentials as presented in Figure 11.
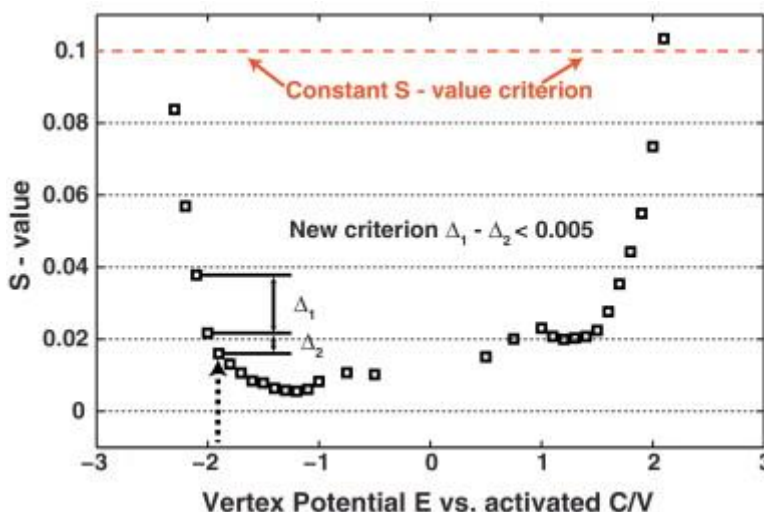
Figure 11. Plot of S-value vs. vertex potential based on the new criterion for [EMIm][BF$_4$] with the carbon BP2000 at room temperature [79].

The ESW (Table 2) is found based on the statement (so-called 'new criterion' proposed in ref. [80]) that the difference between the S-values of two successive points should not exceed 0.005. Practically, this means that the system is considered unstable as soon as the voltammetric charge (in mAh g^{-1}) increases by 5% in a 0.1 V voltage step. The positive and negative potential limits of a few ILs obtained on high specific surface area carbon black (BP2000) electrodes using the new criterion are reported in Table 2. By subtracting the values of their cathodic potential limit from the anodic one, [BMIm][BF$_4$] demonstrates the higher ESW of 3.6 V and [Pyr$_{14}$][TFSI] the lowest (3.1 V). Interestingly, one may observe that the ESW of [EMIm][BF$_4$] obtained based on the new criterion with BP2000 electrode is 1 V lower than the value (4.5 V [77]) reported above on platinum by linear sweep voltammetry, what confirms that the ESW of an electrolyte depends on the type of working electrode and the applied electrochemical method.

Table 2: Potential limits of positively (E$_+$) and negatively (E$_-$) polarized BP2000 electrodes in various IL electrolytes and their corresponding ESW based on the new criterion (from [79]).

	[EMIm] [BF$_4$]	[BMIm] [BF$_4$]	[EMIm] [TCB]	[EMIm] [TFSI]	[Pyr$_{14}$] [TFSI]
E $_+$ (V vs AC)	1.6	1.6	1.6	1.5	1.4
E $_-$ (V vs AC)	-1.9	-2.0	-1.8	-1.9	-1.7
ESW (V)	3.5	3.6	3.4	3.4	3.1

3.4. *IL ions size*

Since ILs consist entirely of ions, they were found to be appropriate electrolytes for the assessment of the relationship between the effective ion size, given by its dimension adopted for pore entering, and size of the pores itself, both factors having an influence on the capacitance of EDLCs. The early study showed that when using one type of porous carbon electrodes for EDLCs, the specific capacitance decreases with increasing the length of alkyl substituent on the phosphonium cation of IL (from 0.8 to 2 nm), demonstrating the requirement of pore-to-ion size compatibility [81]. The following research showed that, when using various microporous carbons with (relatively) controlled pore size and the [EMIm][TFSI] IL electrolyte (Figure 12), a maximum specific capacitance of 160 F g^{-1} was obtained for the pores matching the IL ions [82]. It was also demonstrated that the capacitance decreases when the

pores are i) smaller than ions, hence sterically hindered from their entering as well as ii) bigger than ions because they still could accommodate only one ion, while the double-layer thickness increases [82]. It should be highlighted that both research [81, 82] support the assumption that elongated ions enter pores with the orientation enabling them to align their largest dimension to the pore walls. It means that more of them can be packed in the pore confinement [83].
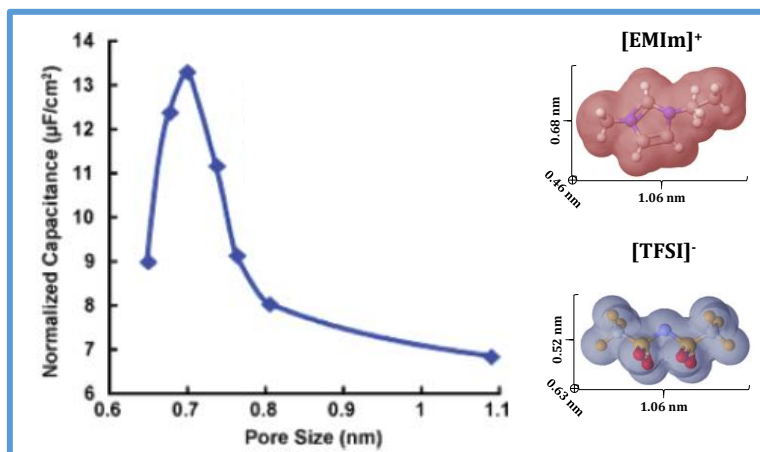
Figure 12. Normalized capacitance (i.e., specific capacitance divided by the SSA) versus the pore size of a series of carbide derived carbons (adapted from [82]), and structure and molecular size of the cation and anion in [EMIm][TFSI] IL. (*Thanks are due to M. Tobis for the models of [EMIm]$^+$ and [TFSI]$^-$ ions*).

4. Active materials for IL-based EDLCs

Thanks to their moderate cost, high availability and high electrical conductivity, carbons are the most widely used electrode materials in EDLCs. The different forms of carbon tested as electrode material for EDLCs include, but are not limited to, activated carbons, graphene, carbon nanotubes, carbide-derived carbon, carbon blacks and templated carbons.

4.1. Porous texture of carbons

According to the International Union of Pure and Applied Chemistry (IUPAC) classification, the pores of carbons include: micropores (pores smaller than 2 nm), mesopores (pores in the range between 2 and 50 nm), and macropores (pores larger than 50 nm) [84]. Accordingly, their isotherms can be grouped into six types (Figure 13).

In the type I or Langmuir isotherm found for microporous substrates having pores below 2 nm, the maximum amount of gas adsorbed is reached without any inflection and the shape indicates the formation of only a monolayer. For materials with narrow micropores of width < 1 nm, the isotherms are of type I(a); those having a pore size distribution over a broader range, including wider micropores and possibly narrow mesopores (< 2.5 nm), display a type I(b) isotherm. The type II isotherms are for nonporous or macroporous materials with a monolayer-multilayer formation in the adsorption process. At point B, the monolayer is formed, and the multilayer adsorption at high relative pressure occurs. Isotherms of type III are assigned to both microporous and nonporous materials characterized by weak attractive forces between the adsorbate and the adsorbent. The type IV(a) isotherms are a variation the of type II presenting the adsorption of a monolayer at low relative pressure and a hysteresis loop at high relative pressure due to a multilayer formation in mesopores. Some micro/mesoporous carbons combine both types I and type IV(a) isotherms. Type IV(b) isotherms are given for conical and cylindrical mesopores that are closed at the tapered end [85]. Type V isotherms present at low relative pressure the characteristics of type III isotherms with a hysteresis loop characteristic of capillary condensation occurring in mesopores. Finally, the isotherm of type VI is particular for materials having a uniform nonporous surface, where each step on the isotherm indicates the formation of a monolayer.
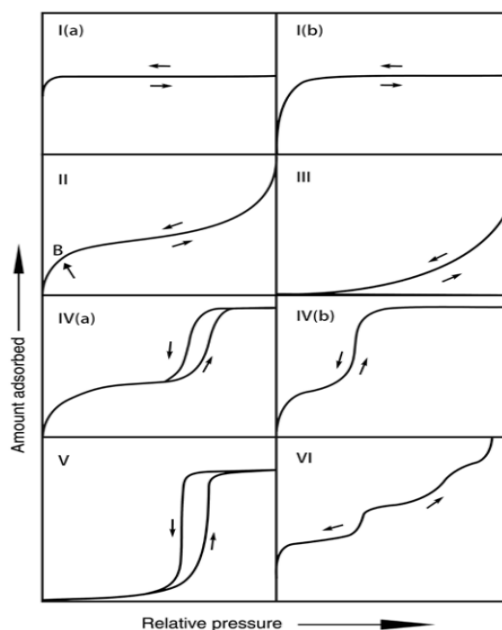
Figure 13. Types of adsorption/desorption isotherms according to the IUPAC [85].

As mentioned above, the type IV(a) and V isotherms present at high relative pressure hysteresis loops, and are classified into five types by IUPAC (Figure 14). The type H1 is assigned for adsorbent with mesopores of narrow and regular distribution [86]. Materials that give rise to a H2 hysteresis loop have a more complex porous texture with significant network effects, e.g., pore-blocking/percolation. The type H2(a) hysteresis loops characterized by very steep desorption branches are attributed either to pore-blocking/percolation in a narrow range of pore necks or cavitation-induced evaporation [85]. The hysteresis loops of type H2(b) are also associated with pore blocking, but in this case, the size distribution of neck widths is much larger. Isotherms with a type H3 hysteresis loop do not exhibit any limiting adsorption at high relative pressure; this is caused by the existence of non-rigid aggregates of plate-like particles or assemblages of slit-shaped pores. The types H4 hysteresis loops are generally observed with complex materials containing both micropores and mesopores. The H3 and H4 hysteresis loops have a characteristic step-down in the desorption branch associated with the hysteresis loop closure [87]. The type H5 hysteresis loops are unusual, and they have a distinctive form related to specific pore structures containing both open and partially blocked mesopores.
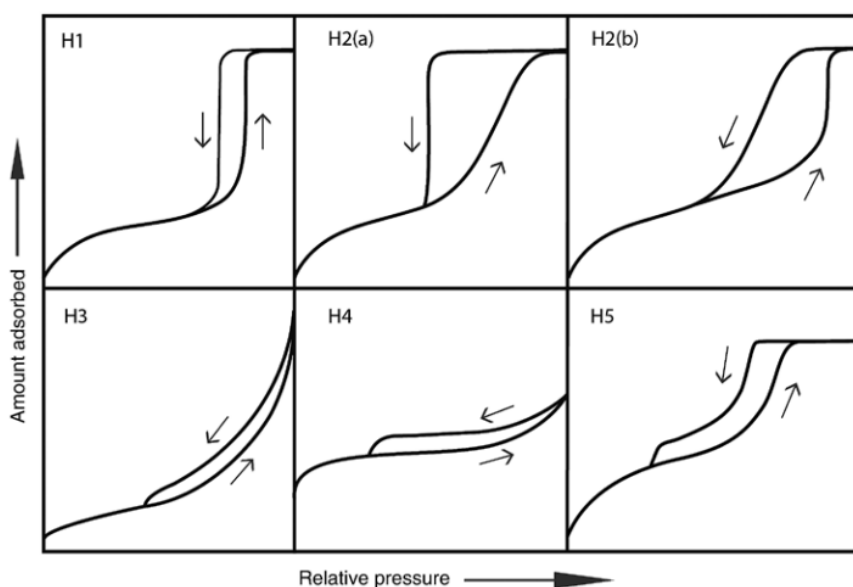
Figure 14. Types of hysteresis loops according to IUPAC [85].

The technique mainly used to evaluate the porous texture of materials is the low temperature gas adsorption, most often nitrogen adsorption at 77 K. Calculating the accessible surface area, the average pore size, and the pore size distribution is essential to characterize porous materials

properly. The specific surface area (SSA) is usually obtained using the Brunauer-Emmett-Teller (BET) method [84]. The BET equation directly relates the amount of gas adsorbed in the material to the amount of gas adsorbed on the surface for a given P/P_0 pressure. Thus, with several values of P/P_0, it is possible to determine the quantity of gas adsorbed on the material's surface. Therefore, if the surface occupied by a gas molecule is known, it is easy to calculate the corresponding specific surface area. However, the BET method is not suitable for estimating the pore size distribution of microporous materials (it overestimates the SSA in case of pores larger than 0.9 nm or underestimates it in case of pores smaller than 0.9 nm) [86], yet because of its ease of use, it is still widely used today.

A better estimation of the SSA can be carried out using the Non-Local Density Functional Theory (NLDFT) method applicable for materials of various porous texture characteristics. The NLDF theory does not consider both chemical and geometrical heterogeneities of the pore walls but takes into account a chemically and geometrically smooth surface model. Consequently, a mismatch between the theoretical assumption of smooth and homogeneous surfaces and the inherent molecular-scale heterogeneity of actual adsorbents is that theoretically calculated NLDFT isotherms display multiple steps related to the formation of a monolayer, a second adsorbed layer, and a multilayer, which cause a gap in the pore size distributions (PSD) of microporous samples between 1 and 2 nm [88-93]. Therefore, the Quenched Solid Density Functional Theory (QSDFT) was proposed to improve the NLDFT model for carbon samples that assumed flat, structureless, and graphitic pore walls [94]. The two-dimensional - Non-Local Density Functional Theory (2D-NLDFT) was also proposed for estimating the cumulative surface area as well as the pore size distribution (PSD) of carbon materials [95, 96].

When using the 2D-NLDFT theory to calculate the PSD of hierarchical micro/mesoporous carbons characterized by a type IV isotherm including an H1 hysteresis loop, while assuming slit pores with a heterogeneous rough surface (2D-HS-SLIT model), an unexpected artifact was observed ca. 3.5 nm [97]. Therefore, a dual shape pore model (which applies the 2D-HS-SLIT model to the adsorption isotherm up to $P/P_0 = 0.2$ and a cylindrical pore model to the desorption isotherm down to $P/P_0 = 0.2$) has been recently proposed to analyze the gas adsorption data of hierarchical micro-mesoporous carbons [97]. Interestingly, applying this dual shape pore model to hierarchical micro/mesoporous carbons of various mesopore sizes and oxygenated surface functionalities showed an excellent fit with the experimental isotherms.

Moreover, the mesopore peak in the PSDs was narrower, and the artifact observed at ca. 3.5 nm was eliminated [97].

4.2. *Surface functionality of carbons*

Significantly, the life span of EDLCs based on any of these carbons can be strongly deteriorated due to the presence of surface functional groups. Yet, before their usage as electrode material for EDLCs, carbon surface functional groups should be eliminated, e.g., by high-temperature treatment in a neutral atmosphere. The types of functional groups present on the surface of carbon materials contain oxygen, nitrogen, and/or sulfur heteroatoms (Figure 15). Those groups include carboxyl, phenol, hydroxyl, lactone, amine, amide, pyridine, lactam, pyrrole, carbonyl, ether, pyrone, and sulfonic acid. In addition, the wettability of the carbon electrode can be affected by the surface groups, which can also affect the electrochemical performance of the cell through faradic contributions (considerable capacitance enhancement) [98].
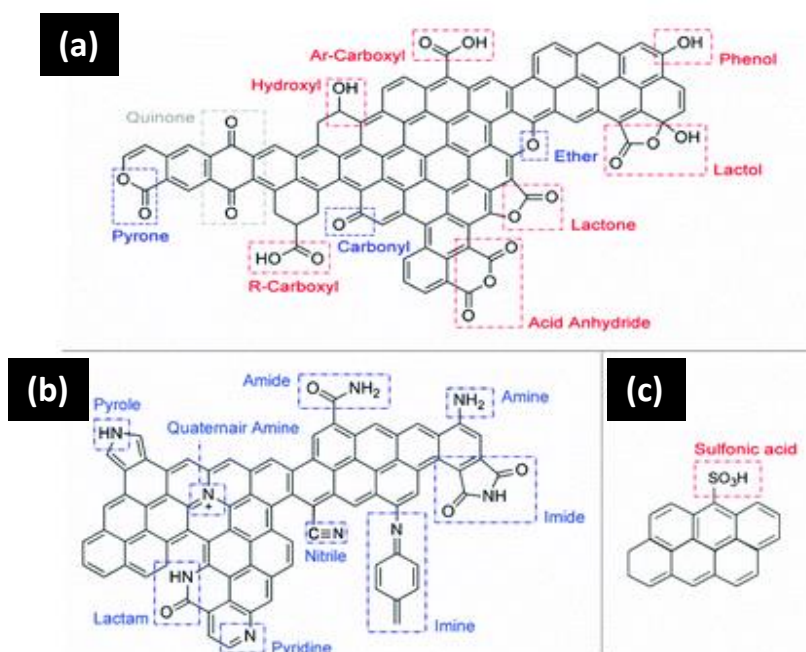
Figure 15. Variety of functional groups on a carbon surface including: (a) oxygen, (b) nitrogen, and (c) sulfur heteroatoms. The basic functionalities are indicated in blue, and the acid ones are in red [99].

A number of experimental techniques are used to determine the surface functionality of carbons. The Boehm titration method is used to estimate the amount of both basic and acidic (carboxylic acid, lactonic acid and phenolic) oxygenated surface functional groups on carbon samples [100], whereas the potentiometric methods provide an insight into the population of acidic sites [101]. Both chemical and potentiometric techniques are classified as "wet methods". Other techniques, namely "dry methods", include infrared spectroscopy (IR), X-ray photoelectron spectroscopy (XPS), and (the most used) temperature-programmed desorption (TPD) [102]. TPD uses the coupling of thermogravimetric analysis (TGA), aiming at desorbing the groups from the solid surface by increasing the temperature, with mass spectrometry (MS) needed for the detection of the evolving gases (the most often are CO, CO_2, and H_2O). Then, the nature and amount of functionalities present on the carbon surface are obtained by deconvoluting the TPD profiles using Gaussian [103] or Lorentzian [104] functions.

4.3. Activated carbons and carbide-derived carbons for low-temperature IL-based EDLCs

Activated carbons (ACs) are the most widely used as electrode materials in EDLCs, thanks to their high specific surface area, abondance and moderate cost. ACs are generally obtained by physical or chemical activation of a carbon precursor (coke, coconut shells, wood, pitch, etc.). The physical activation of carbon precursors is carried out at high temperatures (between 700 °C and 1000 °C), in an oxidizing atmosphere, such as steam, carbon dioxide, air or a mixture of these gases [105]. On the contrary, the chemical activation takes place at a lower temperature (400 °C - 700 °C), with activating agents such as phosphoric acid (H_3PO_4), potassium hydroxide (KOH), sodium hydroxide (NaOH), or zinc chloride ($ZnCl_2$).

Carbide-derive carbons (CDCs) are 3D materials prepared by extracting metals or metalloid atoms from carbide precursors (TiC, SiC, Ti_2AlC, VC, Mo_2C…) by reaction with a gaseous halogen (F_2, Cl_2, Br_2, I_2 or mixtures thereof) at high temperatures, transforming the carbide structure into pure carbon [106]. This synthesis method allows obtaining amorphous carbons with a highly controlled pore size distribution dependent on the carbide precursor.

The nitrogen adsorption/desorption isotherms of exemplar AC (YP80F) and TiC-CDC at 77 K and their corresponding pore size distribution are shown in Figure 16 a,b. The isotherms of AC and TiC-CDC are of type I(b) and I(a), respectively, characteristic of microporous materials. The specific surface area of ACs and CDCs generally varies between 1000 and 3000 m^2 g^{-1}. The pore size of CDCs can be adjusted with angstrom precision by varying synthesis

parameters, such as temperature and time [107-110]. Nevertheless, compared to some other carbon types, ACs and CDCs are characterized by a relatively low conductivity, which imposes the use of a conductive additive (carbon black) during EDLCs electrode manufacturing [111, 112].
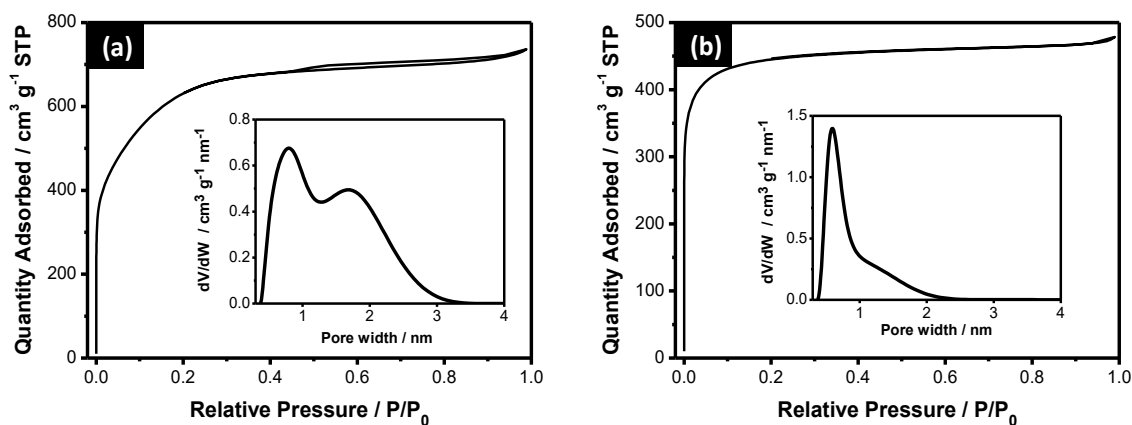
Figure 16. Nitrogen adsorption/desorption isotherms of YP80F (a) and TiC-CDC (b) at 77K. Their pore size distribution obtained using the 2D-NLDFT theory is represented in the insets.

Many authors have reported the room temperature performance of AC-based EDLCs with various types of IL electrolytes [113-117]. AC/AC cells with a pyrrolidinium-based IL electrolyte were claimed to operate at a high cell potential of 3.7 V (though this value did not account for the high ohmic drop) [118]; the cell performance is limited by the relatively high viscosity and low ionic conductivity of the IL (78 mPa s and 3.0 mS cm^{-1} at 25 °C [119]). EDLCs with imidazolium-based ILs typically operate with a smaller cell potential of $\leq$ 3.5 V but perform better even at higher rates due to their more favorable physical properties (e.g. [EMIm][BF$_4$] with η = 37 mPa s [120] and σ = 14 mS cm^{-1} at 25 °C [121]). However, due to the AC texture, which is essentially microporous, their usage as electrode materials for low-temperature EDLCs with ILs electrolytes is limited [122]. As it can be seen in Figure 14, an AC/AC (YP17) cell using the [BMIm][BF$_4$] electrolyte demonstrates a capacitive behavior from 20 to 0 °C, yet the specific capacitance of the device is reduced by ca. 72 % between 20 and -20 °C. Since YP17 is dominantly microporous, the ions' movement within the pores is hindered, and the diffusion resistance increased by lowering temperature [122]. Although the authors of this work did not report the volumetric outputs of the device, it is obvious that the low density (0.3 g cm^{-3} [123]) of the electrodes made of YP17 would lead to low volumetric capacitance, energy and power of the cell.
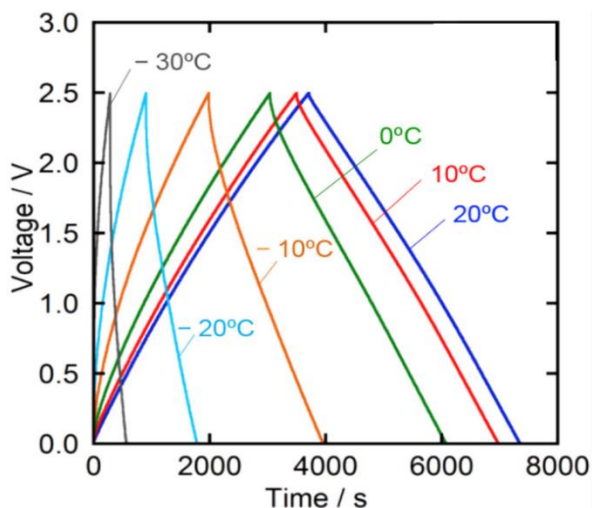
Figure 17. Galvanostatic (0.2 mA cm^{-2}) charge/discharge characteristics of a YP17 AC-based cell in [BMIm][BF$_4$] from 20 to -30 °C [122].

The beneficial effect of micropores on the EDL capacitance is well established, since ions are essentially accumulated herein [124, 125]. Nonetheless, mesopores play an essential role in ion transportation [126, 127], and their presence leads to an enhanced capacitance retention under harsh currents [128]. Therefore, carbons having well-fitted micropores are highly desirable for enhancing the gravimetric and volumetric capacitance, and the presence of mesopores is mandatory for the transportation of IL ions, especially when low-temperature applications are targeted [122]. Therefore, carbon nanotubes, graphene, carbon black, and templated carbons were considered in the literature for ELDCs operating at sub-ambient temperatures.

4.4. *Carbon nanotubes and carbon onions for low-temperature IL-based EDLCs*

To address the ion transport limitations in nanometer pores of AC or CDC, exohedral carbons, namely carbon nanotubes (CNTs) and onion-like carbons (OLCs), have been used as electrode material for EDLCs. CNTs are cylindrical carbon allotropes with a one dimensional (1D) structure [129], whereas OLCs are spherical or polyhedral carbon nanoparticles, consisting of concentric defective sp^2-hybridized graphene shells [130]. The TEM image of Figure 18a shows multiwalled carbon nanotubes with diameters between 5 and 10 nm and 4 to 7 carbon layers [49]. The image of OLCs (Figure 18b) reveals nanoscopic carbon particles with a nearly spherical shape made of multiple enclosed fullerene-like carbon shells [131], with a small diameter around a few tens of nanometers [130]. The nitrogen adsorption/desorption isotherms of CNTs and OLCs are shown in Figures 18c [130] and 18d [131], respectively. Both isotherms

are of type IV(a) with H3 (for CNTs) and H4 (for OLCs) hysteresis loops closing at a relative pressure (P/P$_0$) ca. 0.4, indicating the existence of mesopores. The S$_{BET}$ of CNTs in Figure 18c is 113 m^2 g^{-1} [132], whereas OLCs in Figure 18d exhibit an S$_{BET}$ of 842 m^2 g^{-1} [133]. The two materials are essentially mesoporous with a pore size distribution (inset Figure 18c) centered at 3.4 nm for CNTs [132] and 3.7 nm for OLCs [133]. Hence, the external surface of CNTs and OLCs is entirely accessible for anions and cations of IL electrolytes, and their exohedral carbon nanoparticles can overcome the ion transfer limitations of EDLCs.
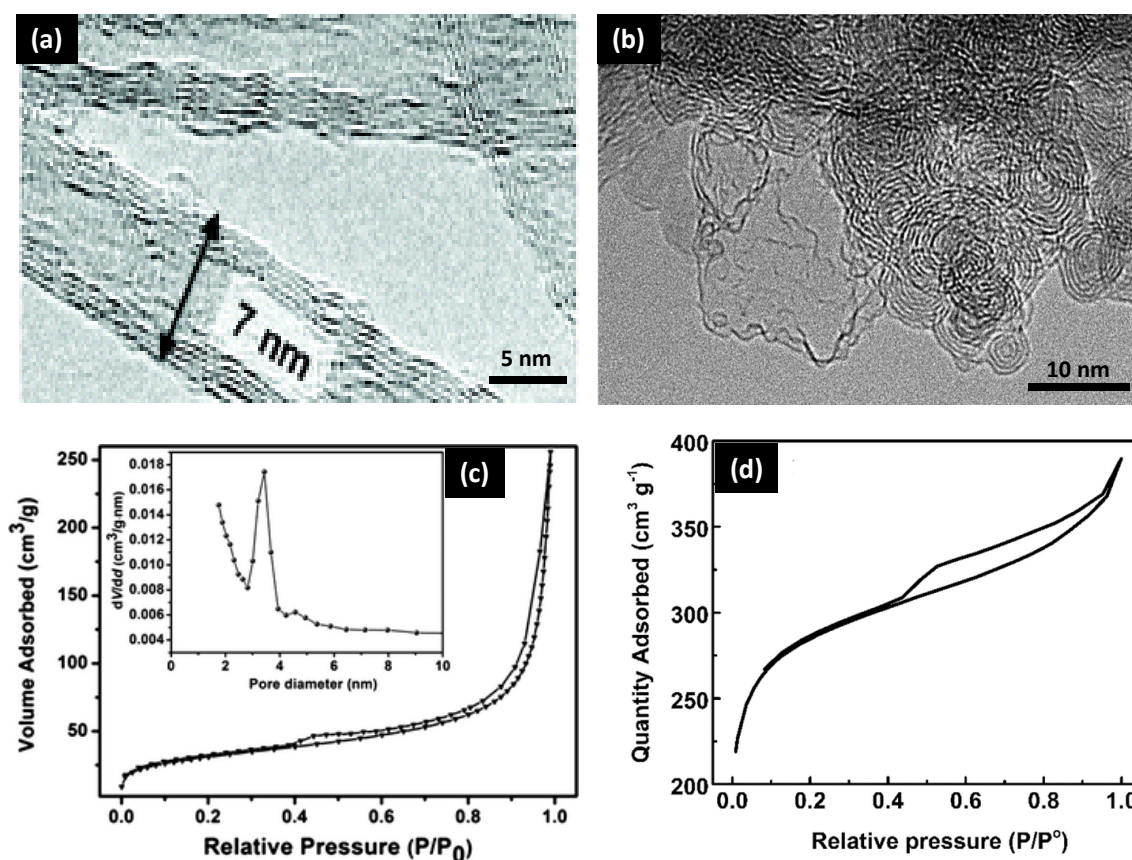
Figure 18. Transmission electron microscopy images of (a) CNTs [49] and (b) OLCs [130]. Nitrogen adsorption/desorption isotherms at 77 K of (c) CNTs [132] and (d) OLCs [133]. The inset in (c) shows the corresponding pore size distribution of CNTs.

The first and only work to date on low-temperature performance of CNT and OLCs-based EDLCs with IL electrolyte was reported by Simon et al., as shown in Figure 19 [134]. The authors formulated an equimolar binary mixture of [PIP$_{13}$][FSI] and [PYR$_{14}$][FSI] and used it as an electrolyte for EDLCs and determined the electrochemical properties from -50 °C to 100 °C. When the electrodes were made of OLCs (Figure 19a), the capacitor exhibited

a fish-like shape of CVs (at 100 mV s^{-1}) at -20 °C up to 2.8 V, and a capacitance < 100 F g^{-1} (per electrode). In contrast, the device made of CNTs electrodes (Figure 19b) operated efficiently at 5 mV s^{-1} down to -50 °C up to a cell voltage of 3.5 V, yet the capacitance was < 50 F g^{-1} (per electrode) [134]. Despite an interesting charge propagation, owing to the opened external surface of the two materials, their low specific energy is a concern. Moreover, one of the significant weak points of this work is the lack of indication about the volumetric outputs of the devices, which is probably very low. Additionally, CNTs are hard to process due to their poor dispersibility; in particular, they exist as ropes and bundles heavily entangled to form agglomerates [135].
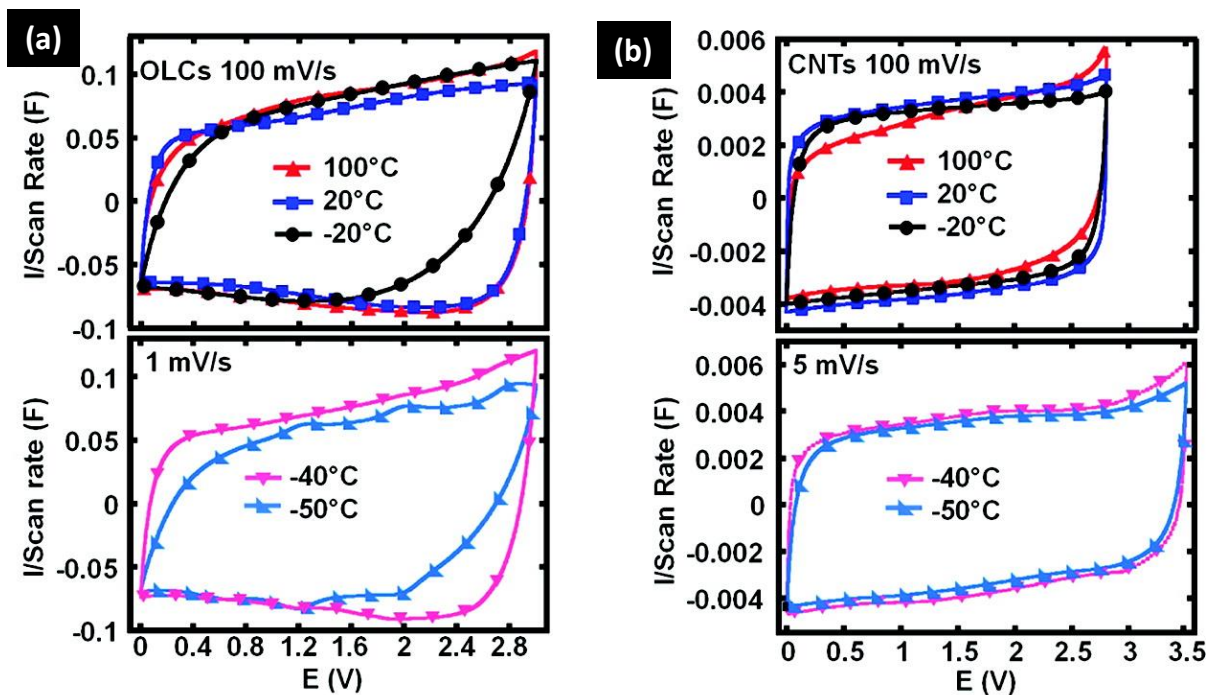
Figure 19. Effect of temperature on the CVs of (a) OLCs and (b) CNTs based EDLCs in equimolar binary mixture of IL electrolyte [134].

4.5.   Graphene for low-temperature IL-based EDLCs

Graphene is a carbon material consisting of a single layer of carbon atoms with a theoretical thickness of around 0.335 nm [136]. It is claimed to have a strong potentiality in energy storage due to its electrical, mechanical, and thermal characteristics [137, 138]. Different graphene types with various structures such as 1D (fiber and yarn types), 2D (graphene-based films), and

3D (graphene foams, aerogels, and sponges) have been reported [136, 139-142]. Figure 20 shows the transmission electron microscopy image and adsorption/desorption isotherms of 2D graphene. The isotherm is of type IV(a) with a type H1 hysteresis loop, and the pore size distribution (inset in Figure 20b) derived from the adsorption branch of the isotherms exhibits a sharp peak centered at 8.9 nm [137]. The BET specific surface area and total pore volume were calculated to be about 661 $m^2 g^{-1}$ and 1.59 $cm^3 g^{-1}$, respectively. Thanks to such porous properties, high electrical conductivity, and fast charge transfer, graphene has been considered as electrode material for low-temperature IL-based EDLCs.
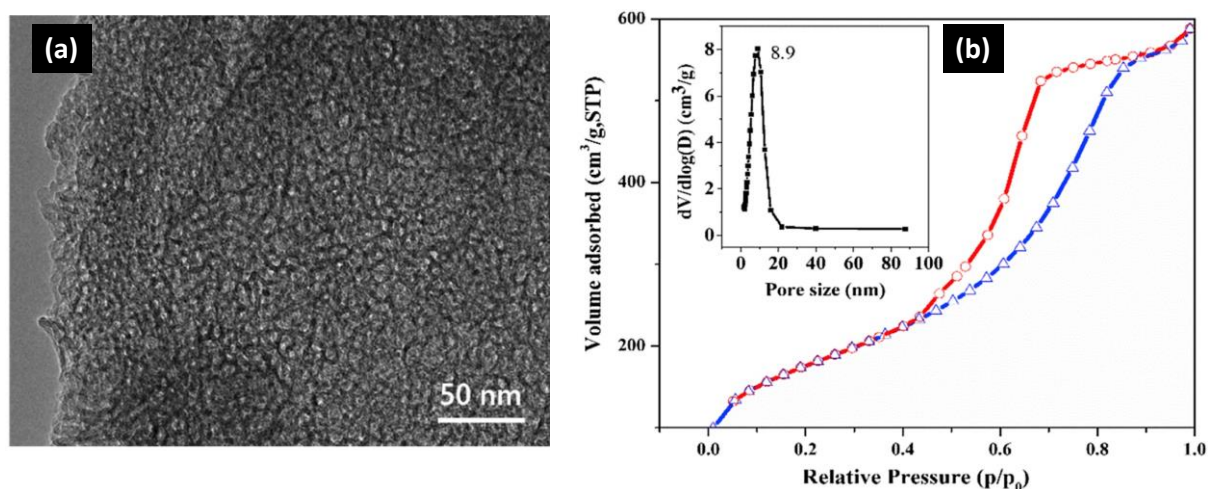
Figure 20. (a) Transmission electron microscopy image and (b) nitrogen adsorption/desorption isotherms of graphene at 77 K. The inset in (b) is the corresponding pore size distribution [137].

A graphite oxide-based EDLC with an equimolar binary mixture of 1-butyl-4-methylpyridinium tetrafluoroborate [BMPyr][BF$_4$] and 1-butyl-3-methylimidazolium tetrafluoroborate [BMIm][BF$_4$] showed rectangular CVs (5 mV s^{-1}) down to -40 °C with 16 % of capacitance drop from room temperature (C = 109 F g^{-1}) to -40 °C (C = 92 F g^{-1}) [143]. Symmetric cells based on graphene display almost rectangular CVs at -20°C (at a very slow scan rate of 1 mV s^{-1}) (Figure 21a) [144] or even -40 °C when the electrodes were made of activated graphene [145] in ([PYR$_{14}$][FSI])$_{0.5}$([PIP$_{13}$][FSI])$_{0.5}$ IL binary mixture electrolyte. However, due to the low electrolyte conductivity (4.9 mS cm^{-1} at 20 °C and ~0.1 mS cm^{-1} at -40 °C), the cell demonstrated a resistive character at low temperatures, as illustrated by the high equivalent series resistance (ESR) on the Nyquist plots (Figure 21b). The non-capacitive nature of the device at sub-ambient temperature is also well-evidenced by the low-frequency region of the curves which are not parallel to the

imaginary (Z") axis (Figure 21b). Moreover, although graphene has broad pores facilitating the mass transport at low temperatures, its low electrode density may deteriorate the volumetric energy and power required in most applications [146].
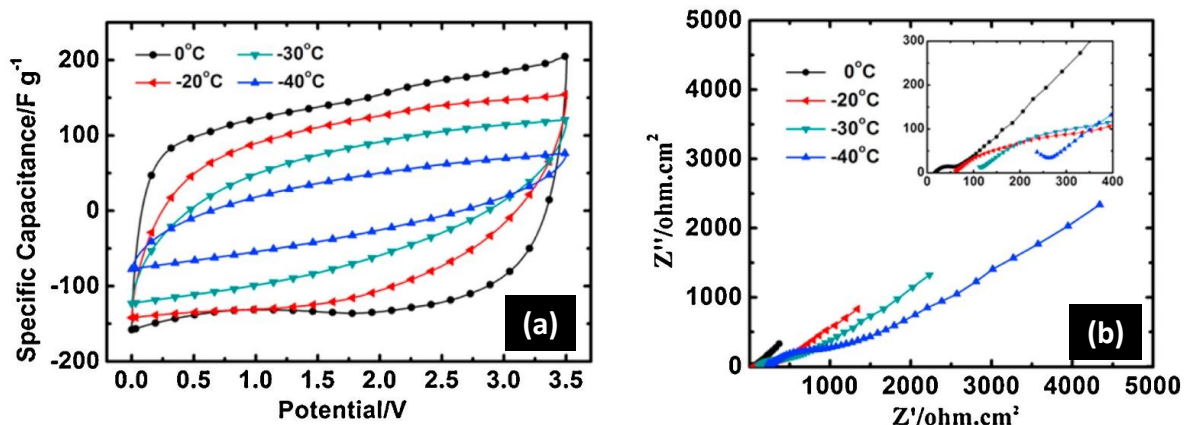
Figure 21. Low-temperature electrochemical characterizations of graphene-based EDLC in a binary mixture of IL electrolytes. (a) CVs at 1 mVs^{-1} and (b) Nyquist plots at 0 V [144].

4.6.   Carbon black for low-temperature IL-based EDLCs

Carbon black (CB), which is essentially a pure form of soot, is manufactured industrially on a large scale, primarily for use as a filler in rubber products [147]. The CB's most important preparation method is the "furnace black" process, which involves the partial combustion of petrochemical or coal tar oils [148]. CB consists of quasi-spherical particles with sizes ranging from about 10 nm to 500 nm, often joined together in clusters or "necklace" chains [149]. The essential advantages of carbon black include high conductivity, micro and mesoporosity, and high density [150]. Many studies have proposed models of carbon blacks with a tendency toward the concentric alignment of graphene layers roughly parallel to the external surface of the carbon particles (Figure 22a). According to the high-resolution transmission electron microscopy (HRTEM) observations, the individual graphene layer in primary carbon black particles is the basic building unit [151-153], instead of graphite crystallites as concluded by XRD [154] and Raman [155] measurements.

Conventional CB, such as acetylene black (C65 by Imerys), is primarily used in low quantities (~10 wt %) as an electronically conductive additive in composite electrode materials. Due to

its low specific surface area (< 100 m^2 g^{-1}), C65 does not provide any significant capacitance, and its electrochemical performance remains well below that of activated carbons. However, high surface area CB such as Black Pearls (BP2000, S_{BET} = 1500 m^2 g^{-1} [156]) or SC2A (S_{BET} = 1440 m^2 g^{-1} [150]) can overcome this issue. The texture of the SC2A carbon black is formed by aggregates of primary particles with a diameter of about 15-20 nm [157]. A high resolution TEM image (Figure 22b) shows that SC2A particles consist of a compact arrangement of concentric carbon layers with a relatively low 002 interlayer distance, what suggests a high density for this material. The nitrogen adsorption/desorption isotherm of the BP2000 carbon black (Figure 22c) is of type I(a) at low relative pressure, and the hysteresis loop of type H3 at high relative pressure is attributed to the presence of mesopores formed by the agglomeration of particles. The PSD of BP2000 related to mesopores is relatively broad, with a maximum at ca. 27 nm (Figure 22d).
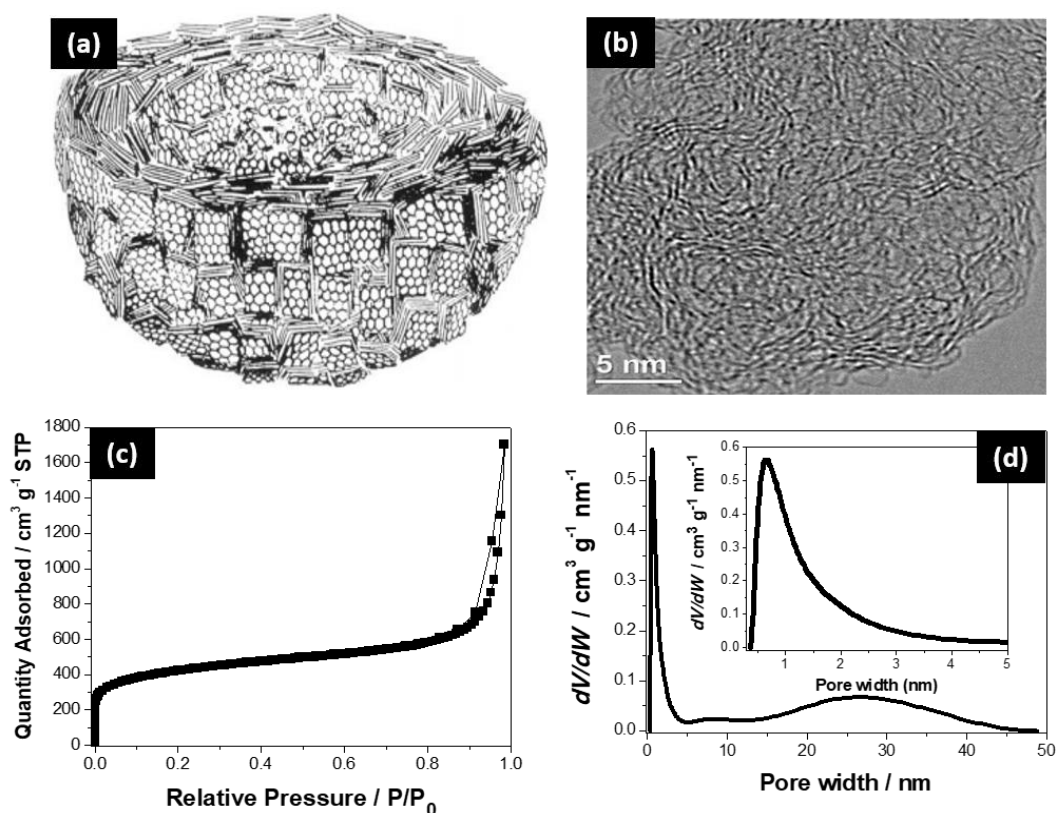
Figure 22. (a) Modeled structure of carbon black [149] and (b) HRTEM image of the SC2A carbon black [157]. (c) Nitrogen adsorption/desorption isotherms at 77 K and (d) pore size distribution of the BP2000 carbon black. The inset in (d) is the magnification of the micropores region. The PSD is obtained using the 2D-NLDFT theory.

4.7. *Templated carbons for low-temperature IL-based EDLCs*

The word "templated" denotes various preparation processes to control the porous texture of carbon materials, aiming to differentiate the templated carbon materials from conventional ACs and underline their preparation without activation. Compared to ACs, the texture of templated carbons has the advantage to be hierarchical, what is beneficial for IL ions electrosorption. The most commonly used methods for producing porous carbons with a hierarchical texture usually involve either salt templating [123, 158-161] or hard templating [162-164]. Another approach for making very high surface area (2500 m^2 g^{-1}) multi-modal porous carbons has been recently reported by combining the salt templating and the hard templating methods [165, 166].

The salt templating method involves carbonizing a carbon precursor around a molten salt (NaCl, $ZnCl_2$, LiCl, KCl, LiBr) at an elevated temperature [167]. However, this technique mainly results in the production of microporous carbons (with small mesopores) due to the small size of the cations (Li^+, Na^+, K^+, Zn^{2+}) and anions (Cl^-, Br^-) of the inorganic salts used as templates [162, 168]. Therefore, hierarchical porous carbons (HPCs) are commonly prepared by various hard-templating methods in which the carbon nanostructure is replicated from a rigid mold of a well-defined size [169]. Different type of templates such as ordered mesoporous silica [170-172], colloidal silica [165], silica gels [162], aluminosilicate [170, 173], or MgO [164, 174] are often mixed with a carbon precursor (e.g., glucose) to obtain a mixture which is further subjected to a high-temperature carbonization treatment under neutral atmosphere, followed by the removal of the inorganic matrix with an etching agent [164, 165].

Owing to its chemical and thermal stability (no structural and compositional changes, no reaction with carbon up to the carbonization temperature of the precursors, and its easy dissolution into a diluted acidic solution), MgO is a template ceramic of choice for preparing template carbons. Different MgO precursors of reagent grade, MgO itself, magnesium acetate $Mg(CH_3COO)_2$, magnesium citrate $Mg_3(C_6H_5O_7)_2$, magnesium gluconate $Mg(C_{11}H_{22}O_{14})$, and magnesium hydroxy-carbonate $3MgCO_3 \cdot Mg(OH)_2 \cdot 3H_2O$ are used [164]. Figure 20a shows the process of preparing MgO-templated carbons by carbonizing magnesium citrate hydrate ($C_{12}H_{10}Mg_3O_{14} \cdot 3H_2O$) under a neutral atmosphere, leading to obtaining MgO particles coated with carbon shells [175]. Then MgO is dissolved in an acidic solution, leaving a carbon material which is the negative replica of the MgO particles (Figure 23a). The typical texture/structure of a hierarchical MgO-template carbon is presented on the HRTEM image (Figure 23b), which

shows curved and strongly defected carbon layers arranged in parallel at about 0.35 nm. In addition, the main space of this material is occupied by hollows (intraparticle mesopores), which result from the leaching of MgO leaving behind carbon shells [157, 164]. The nitrogen adsorption/desorption isotherm of this material at 77 K (Figure 23c) is of type I(b) at low relative pressure (presence of micropores) and type IV(a) (with type H2(a) hysteresis loop) at high relative pressure, typical for adsorbents having a considerable proportion of mesopores. The mesopore size distribution of this MgO-template carbon (Figure 23d) is quite narrow, with a maximum at 3.5 nm [175]; its porous texture data are S_{BET} = 1875 m^2 g^{-1}, V_{micro} = 0.35 cm^3 g^{-1}, V_{meso} = 1.30 cm^3 g^{-1} [157].
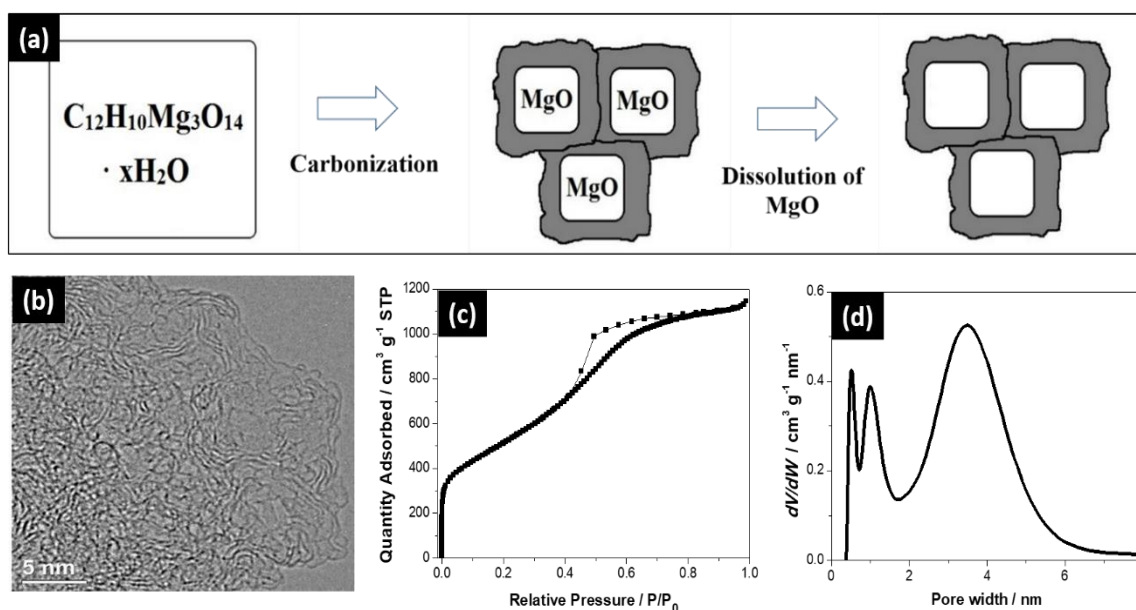
Figure 23. (a) Scheme of the process to form micro/mesoporous MgO-templated carbons (adapted from [164]); (b) HRTEM image; (c) nitrogen adsorption/desorption isotherm at 77 K and (d) pore size distribution of the MgO-templated carbon obtained using the 2D-NLDFT theory [157].

The low-temperature electrochemical performance of EDLCs incorporating the 1-butyl-3-methylimidazolium tetrafluoroborate [BMIm][BF$_4$] IL electrolyte (T_m = -39 °C [176]) and electrodes made of a MgO-templated carbon (MPC) is presented in Figure 24a [122]. The cell exhibits a gradual decrease of the discharge time from 20 to -20 °C. Below -20 °C, the diffusion resistance of the ions in the pores is significant even though the latter are micro/meso-sized [122]; this is due to poor electrolyte properties (σ = 3.5 mS cm^{-1} and η = 180 mPa s at 20 °C [121]). Nevertheless, the capacitor using the MPC carbon demonstrated

a much better capacitance retention (Figure 24b) than another device made of conventional microporous activated carbon (AC = YP17) electrodes [122]. The better operation of the MPC/MPC cell is attributed to the hierarchical porous texture of the MgO-templated carbon, advantageous on the point of view of charge propagation for all the considered sub-ambient temperatures. Therefore, formulating mixtures of IL electrolytes with enhanced thermal and transport properties (low viscosity and high ionic conductivity) might be an excellent compromise to designing EDLCs using electrodes made of MgO-templated carbons operating efficiently at low temperatures.
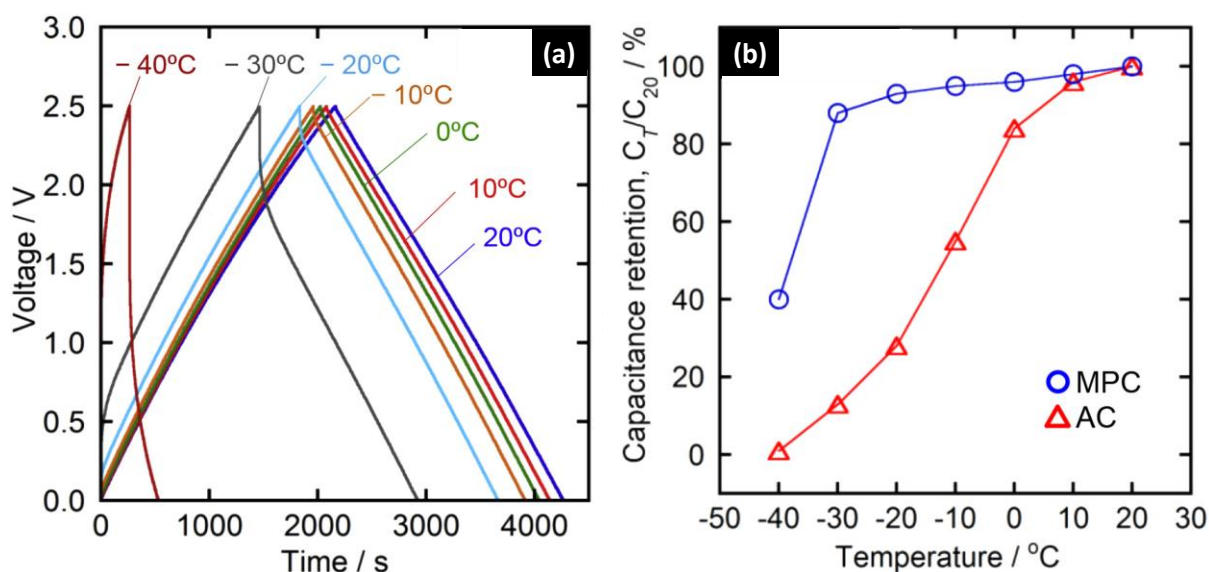
Figure 24. (a) Galvanostatic charge/discharge charatcteristics at 0.2 mA cm^{-2} for EDLCs based on a MgO-templated carbon (MPC) in [BMIm][BF$_4$] electrolyte and (b) capacitance retention from 20 to -40 °C compared to a microporous activated carbon - AC [122].

The structural/textural parameters of HPCs can be tuned by the size/shape of the applied template - which imposes the pore size of the resulting carbon material, and the template/carbon precursor mass ratio determining the number of pores [177]. Figure 25a schematizes the process to form hierarchical SiO$_2$-templated carbons by the pyrolysis of a mixture of colloidal silica and glucose in optimized proportions, followed by etching the mold [157]. The most distinct advantage of this approach is the obtained material contains relatively wide and ordered mesopores. The TEM images of HPCs based on the SiO$_2$-templated method consist of irregularly shaped particles [162], which are fluffier and less compact than in the case of the MgO-templated carbon [178]. The surface of SiO$_2$-templated HPCs is very uneven and strongly developed, whereas the mesopores are more prominent and better visible than in the MgO

HPCs. Similarly, the nanostructure is better ordered, and the carbon layers are closer and more parallel at a constant distance of approximatively 0.35 nm (Figure 25b), leaving few empty spaces (micropores) between them [157]. Figure 25c shows that the N_2 adsorption/desorption isotherm at 77 K of a SiO_2-template HPC (TC-2 from ref [157]) is of type I(b) at low P/P_0 (presence of micropores) and type IV(a) at high relative pressure, with a hysteresis loop of type H1 at $P/P_0 \geq 0.6$. In Figure 25d, it is worth noticing that this carbon is characterized by a narrow mesopore size distribution with a maximum at 9.5 nm, owing to the almost monomodal size (12 nm) of the colloidal silica template used for the preparation.
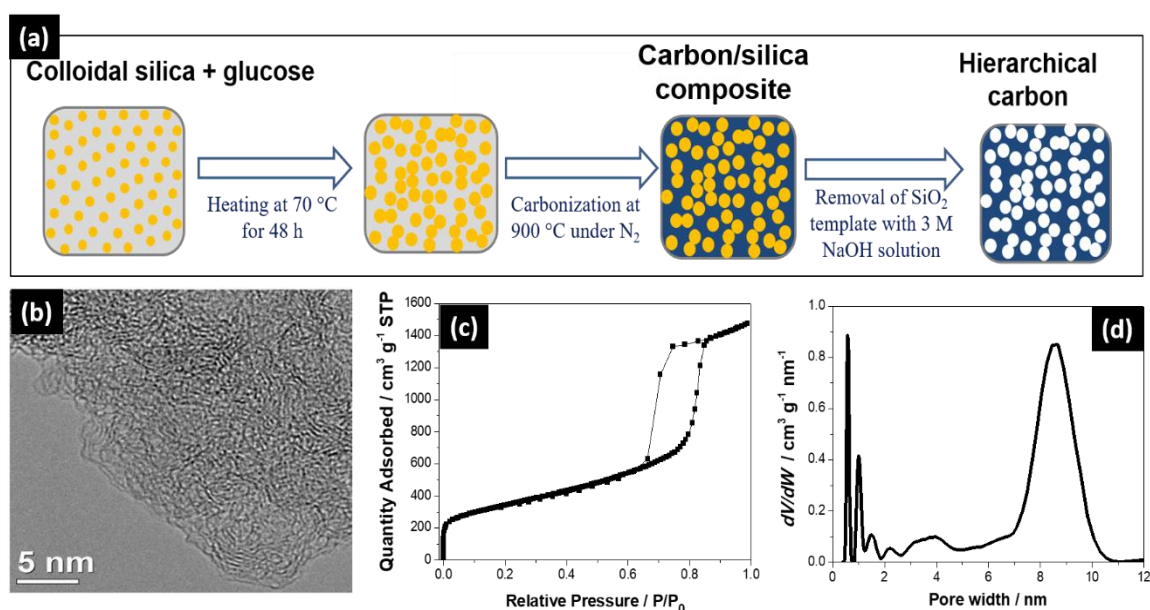
Figure 25. (a) Scheme of the process to form hierarchical SiO_2-templated carbons (adapted from [165]). (b) HRTEM image; (c) nitrogen adsorption/desorption isotherm at 77 K and (d) pore size distribution of a SiO_2-templated carbon (TC-2) from ref. [157].

5.   EDLCs based on ionogels

The risk of leakage of ILs remains an issue for their use in EDLCs. Solid-state electrolytes obtained by entrapping an ionic liquid in a host network (e.g., silica, PVdF), also known as ionogels, have been proposed to replace liquid electrolytes in energy storage devices, including batteries and ELDCs [179-182]. The ionic motion in such a system is liquid-like, whereas the polymeric network provides a mechanical integrity to the material [183]. Ionogels possess

many distinct advantages over their liquid electrolyte counterparts, such as less reactivity and no leakage, improved safety, limiting packaging constraints, better EDLCs manufacturing integrity, good thermal properties, and good interfacial stability [180, 183-186].

Silica-based ionogels obtained by encapsulating [EMIm][TFSI] in a tetramethoxysilane (TMOS) or dimethy-l-dimethoxysilane (DMDMS) network have been reported to display a relatively good ionic conductivity of 4.0 mS cm^{-1} at 20 °C [180] or 3.0 mS cm^{-1} at 25 °C [179], respectively. However, the preparation process of ionogels based on a silica matrix is very long (3 to 7 days), and the obtained ionogels are fragile, which leads to difficult cell manufacturing [179-181, 186-191]. Therefore, polymer hosts such as poly(vinylidene fluoride) (PVdF) or biopolymers (cellulose [192, 193], guar gum [194], agarose [195], and gelatin [196]) have been proposed owing to their low cost, easy assembly, and flexible packaging. Nevertheless, the operating voltage of EDLCs with biopolymer-based ionogels is less than 2.0 V, and the operation is limited at high temperatures [197]. By contrast, PVdF-based ionogels display good properties such as a high thermal stability, a strong mechanical strength, a realistic electrochemical stability window (up to 3.0 V), and a good resistance to aging [183-185, 198].

The ionic conductivity and DSC thermograms of neat [EMIm][TFSI] and its corresponding PVdF-based ionogel are shown in Figures 26a and 26b, respectively. At 20 °C, the ionic conductivity is 9 mS cm^{-1} and 3 mS cm^{-1} for the neat IL and ionogel, respectively; the conductivity of the ionogel decreases continuously and considerably along with the temperature lowering from 100 °C to -40 °C; the neat [EMIm][TFSI] demonstrates a comparable tendency, yet its conductivity suddenly drops at -10 °C, due to the phase transition from the liquid to the solid-state. Such a drop is not observed with the ionogel, which conductivity fades steadily down to a lower temperature of -40 °C; the higher ionic conductivity of the ionogel from -10 °C to -40 °C is due to its confinement, which quenches part, but not all, the liquid-to-solid transition. These results are supported by the DSC thermograms in Figure 26b, showing a slight shift in melting and cold crystallization temperatures. The glass transition temperature values of the neat IL (184 K) and ionogel (182 K) are within the limit of experimental error.
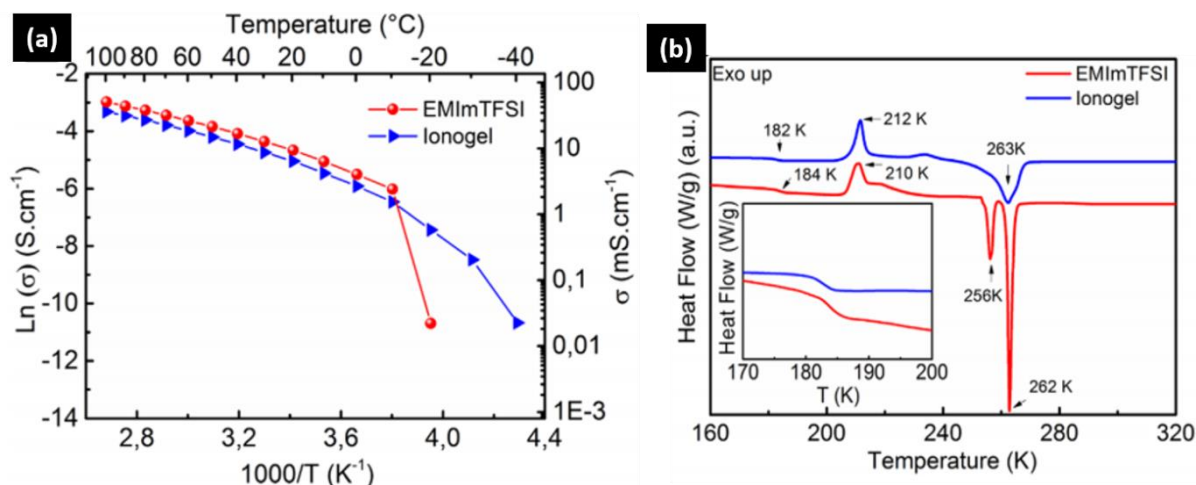
Figure 26. Thermal properties of neat [EMIm][TFSI] and [EMIm][TFSI]/PVdF ionogel: (a) ionic conductivity vs. temperature and (b) DSC profiles [190].

Despite the lower ionic conductivity of ionogels than that of their neat ionic liquid counterpart, many authors reported comparable performance of EDLCs based on the two types of electrolytes from room to high temperatures [188, 199, 200]. However, information about their low-temperature operation is limited due to the relatively low ionic conductivity of ionogels and the above-mentioned high melting point of ILs. Some efforts have been made to overcome these limitations and extend the operating range of ionogel-based EDLCs to sub-ambient temperature [201, 202].

To enhance the ionic conductivity of the ionogel based on [BMIm][BF$_4$], crystalline succinonitrile (SN) of high dielectric constant has been used as a nonionic additive in a PVdF gel matrix [201, 203]. As a result, the ionic conductivity of the ionogel film with SN at room temperature was 3.5 times higher (6.4 mS cm^{-1}) than that without SN (1.8 mS cm^{-1}), and it was even higher than the neat [BMIm][BF$_4$] IL (4.0 mS cm^{-1}) [201]. The EDLCs based on the PVdF/[BMIm][BF$_4$]/SN ionogel and AC electrodes (YP50F) operated at a cell voltage of 2.5 V with capacitive characteristics from 80 °C (C = 112 F g^{-1}) down to -30 °C (C = 91 F g^{-1}) [201]. However, the ESR values were as high as 9.35 Ω at RT and 22 Ω at -30 °C (Figure 27a), what was attributed to the microporous texture of AC which limits the migration of ions as the temperature decreases [201]. Still, the cell could not operate down to the required low-temperature limit of -40 °C due to the relatively high melting point (-39 °C [176]) of [BMIm][BF$_4$]. Additionally, the capacitor demonstrated a fast self-discharge at room temperature, with a 40% voltage drop after 25h (Figure 27 b).
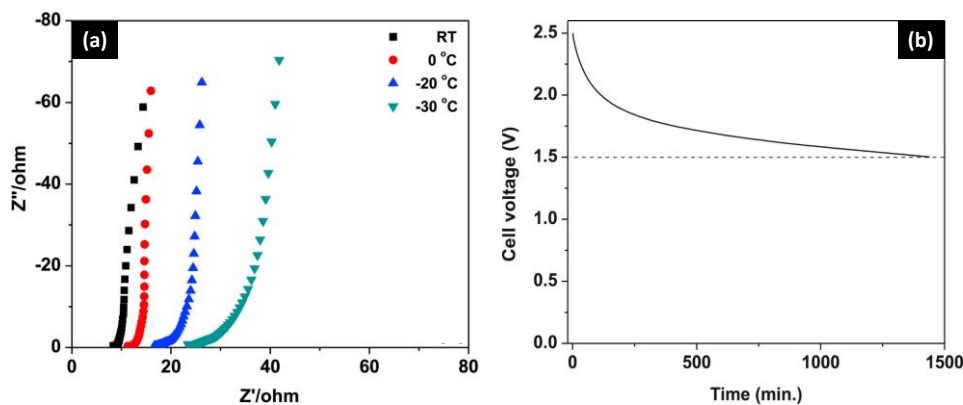
Figure 27. Properties of AC/AC cells based on the PVDF/[BMIm][BF$_4$]/SN ionogel: (a) Temperature dependence of Nyquist plots in the frequency range from 100 kHz to 10 mHz; (b). Self-discharge at RT, after a charge at 0.35 A g^{-1} up to 2.5 V followed by a 1 hour voltage hold at 2.5 V [201].

To overcome the limitation related to the high melting point of neat ILs and extend the operation of ionogel-based capacitors to low temperatures, it has been proposed to trap the ([PYR$_{14}$][FSI])$_{0.5}$([PIP$_{13}$][FSI])$_{0.5}$ binary mixture into an inorganic silica network [202]. However, the cell demonstrated a very poor performance and a high resistance (due to the low conductivity of this electrolyte) at temperatures lower than 0°C (Figure 28) [202]. Another reason of the poor low-temperature performance of this cell could be related to the active material used for electrode preparation, which was a micro- slightly mesoporous activated carbon (PICACTIF) of high SSA 2300 m^2 g^{-1} [204]. At this point, it should be reminded that the usage of carbons with a pore size well-adapted to the dimensions of IL ions is mandatory to enhance the performance of EDLCs, especially at low-temperature [122].
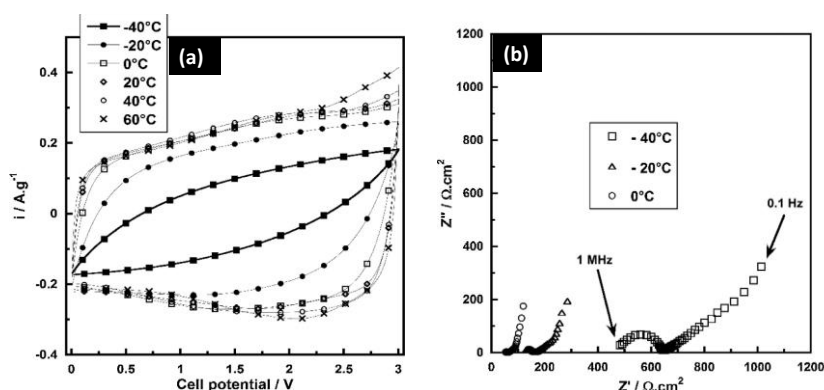
Figure 28. Temperature dependence of the electrochemical performance of an EDLC using an ionogel based on a binary IL mixture trapped in a silica matrix: (a) CVs at 5 mV s^{-1} and (b) Nyquist plots at 0 V [202].

6. Conclusion

Ionic liquids (ILs) show great promise to endow electric double-layer capacitors (EDLCs) with a high energy density. Indeed, ILs as electrolytes in EDLCs instead of organic electrolytes offer several advantages, such as extending the electrochemical potential window (consequently increasing the specific energy) and improving the safety. Among the most often implemented ILs in EDLCs, pyrrolidinium and piperidinium-based ILs display greater electrochemical stability window than their imidazolium counterpart, yet the latter exhibit a higher conductivity and lower viscosity. However, the application of ILs as electrolytes for EDLCs is not possible at sub-ambient temperatures due to their high melting point (T_m). Hence, decreasing the melting temperature, T_m, of most ILs is required to enable EDLCs to operate at low temperatures; the most convenient strategy to reach this objective is the preparation of binary mixtures. A proper design of the carbon electrode in conjunction with an IL mixture or ionogel electrolyte formulation also offers an opportunity to expand the operating range of EDLCs under extreme climatic conditions.

The compatibility of ions size of an IL electrolyte with the pores of carbon is an essential parameter for EDLCs application. The usage of microporous carbons as electrode materials for low-temperature EDLCs with IL electrolytes limits the cell operation at 0 °C. This low-temperature limit can be extended to − 30 °C when using electrodes made of carbon nanotubes, onion-like carbons, or graphene. However, the low density of these electrodes results in a low volumetric output of the EDLCs, which is a concern in most applications (e.g., cars) requiring a reduced size of the devices.

High surface area carbon blacks (BP2000 and SC2A) are constituted of microporous particles (with a relatively low 002 interlayer distance between the graphene planes) which are aggregated, providing an open mesoporosity to these materials. When used as electrodes for EDLCs, the mesopores serve as pathways for the transportation of ions, whereas micropores provide sites for their electrosorption. However, hierarchical porous carbons (HPCs) with well-interconnected meso/micropores provide adequate structural/textural properties for their usage as electrode material for low-temperature IL-based EDLCs. Various HPCs can be prepared by hard templating methods and further applied to manufacture EDLC electrodes.

Though the EDLCs with binary IL electrolytes demonstrated relatively good low-temperature performance down to ca. -30 °C, the leakage problem of IL may limit their usage in practical

applications. Hence, ionogels (ILs confined in solid scaffolds) can help to overcome this critical issue while adding other advantages such as remarkable mechanical and thermal properties, thus limiting the packaging constraints and offering better manufacturing integrity. Various kinds of ionogels have been developed for multiple energy storage devices operating from room to high temperature. However, only sporadic reports on the low-temperature properties of ionogel-based EDLCs can be found.

In this context, to design IL-based EDLCs displaying realistic specific and volumetric outputs at low temperatures, the following points should be addressed successively:

- the formulation of ILs mixtures with an extended low-temperature liquidus range, as well as relatively low viscosity and high conductivity;
- the selection/design of micro/mesoporous carbon electrodes enabling the efficient performance of IL-based EDLCs at low temperatures down to at least -40 °C;
- the enhancement of the volumetric performance at low temperature by simultaneously optimizing the IL-electrolyte formulation and HPC porous texture;
- the increase of EDLCs safety (leakage problem with liquid IL electrolyte) by designing an optimized ionogel formulation.

Chapter II

Binary mixtures of ionic liquids based on EMIm cation and fluorinated anions: physico-chemical characterization in view of their application as low-temperature electrolytes

1. **Summary of the publication** [J. Mol. Liq., 298 (2020) 111959]

This paper reports the physico- and electrochemical characterization of binary mixtures of ionic liquids (ILs) performed in a wide temperature range, with a particular interest to their properties at sub-ambient conditions. The parent ILs were made of the common 1-ethyl-3-methylimidazolium [EMIm]$^+$ cation and one of the fluorinated anions: bis(fluorosulfonyl)imide [FSI]$^-$, bis(trifluoromethanesulfonyl)imide [TFSI]$^-$ or tetrafluoroborate [BF$_4$]$^-$, since they are acknowledged to display good transport properties. The objective of the study was to determine binary mixtures of ILs that remain liquid at low temperature (at least down to -40 °C) and exhibit a relatively low viscosity and high conductivity (also at such harsh conditions), because the targeted application was harnessing them as non-freezing electrolytes in energy storage devices (ESDs).

Raison d'être: *Generally, ILs, which have been widely examined as electrolytes for EDLCs, suffer from relatively high melting points, excluding their application at low temperatures. The recognized approach to tune physicochemical properties of ILs, in particular, to decrease their melting point, is a formulation of their mixtures, especially binary ones. So far, the research related to the development of IL electrolytes has been focused on the mixtures prepared form ILs constituted of piperidinium or pyrrolidinium cations coupled with fluorinated anions. These ILs are known to display great electrochemical stability, yet relatively poor viscosity and conductivity. For this reason, it was believed that for low-temperature applications, the binary mixture of the imidazolium-based counterparts would offer improved transport properties with a minor decrease in electrochemical stability.*

The following mixtures, [EMIm][TFSI]$_x$[FSI]$_{(1-x)}$, [EMIm][FSI]$_x$[BF$_4$]$_{(1-x)}$ and [EMIm][TFSI]$_x$[BF$_4$]$_{(1-x)}$, were formulated, where the x (molar ratio) values varied from 0.1 to 0.9 every 0.1. First, their thermal behavior was investigated with differential scanning calorimetry (DSC), revealing changes in the phase transitions as compared to the parent ILs. In general, the neat ILs exhibited first order transitions, crystallization and melting, whereas their mixtures showed lower temperatures of theses thermal events. For the particular mixtures, where x ranges from 0.5 to 0.8 for [EMIm][TFSI]$_x$[FSI]$_{(1-x)}$ or from 0.1 to 0.6 for [EMIm][FSI]$_x$[BF$_4$]$_{(1-x)}$ or 0.2 to 0.8 for [EMIm][TFSI]$_x$[BF4]$_{(1-x)}$ only glass transition around -90 °C was detected.

Accordingly, only non-freezing representatives were selected for further investigation, and their density, viscosity, and conductivity were determined in a wide temperature range. In all the cases, the density of the ILs' mixtures was linearly dependent on the temperature, demonstrating similar sensitivity to its change. The density values of the mixtures were intermediate between those of their parent ILs reflecting their ratio and density. The dynamic viscosity of the tested liquids decreases, while the ionic conductivity increases as the temperature rises. In both cases, an Arrhenius type dependence on temperature was not detected; hence the Vogel-Tamman-Fulcher (VTF) model, which is commonly utilized for glass forming liquids, was applied. At 20 °C, the determined viscositt values of the $[EMIm][FSI]_x[BF_4]_{(1-x)}$ mixtures were consistent with the average values calculated on the basis of an ideal mixing (which considers the ratio of components and the viscosity of neat ILs), unlike in the case of $[EMIm][TFSI]_x[FSI]_{(1-x)}$ and $[EMIm][TFSI]_x[BF_4]_{(1-x)}$. In the latter cases, significant dissimilarities were attributed to the steric effects contributing to a substantial change in the ion organization. In the case of conductivity, no clear trend was observed for the mixtures, highlighting the complexity of the factors governing this property of the ILs. Still, according to the obtained Walden plots, the examined mixtures were classified as "good ILs", even below 0 °C.

Finally, the electrochemical stability of the representative mixture, the one with the lowest viscosity and the highest conductivity, $[EMIm][FSI]_{0.6}[BF_4]_{0.4}$, was determined on nanoporous electrodes. The obtained window of 3.1 V was intermediate between the values detected for its parent ILs, showing an impact of the less stable component, $[EMIm][FSI]$.

The presented research proves the mixing of ILs to be an effective strategy for adjusting their physicochemical properties. Moreover, the obtained mixtures display lower viscosity and higher conductivity, superior to the ones so far reported in the literature, giving an opportunity for designing ESDs operating more efficiently at low temperature.

Chapter III

Fitting the porous texture of carbon electrodes to a binary ionic liquid electrolyte for the realization of low temperature EDLCs

1. **Summary of the publication** [Electrochim. Acta, 350 (2020) 136416]

This paper presents the progress in the development of electrical double-layer capacitors (EDLCs) based on an ionic liquid (IL) electrolyte and carbonaceous electrodes, with a particular attention to the improvement of their performance at low temperatures (even -40 °C). The examined EDLCs incorporated an equimolar binary mixture of 1-ethyl-3-methylimidazolium bis(fluorosulfonyl)imide and [EMIm][FSI], and 1-ethyl-3-methylimidazolium tetrafluoroborate [EMIm][BF$_4$], as a non-freezing electrolyte, whereas electrodes were made of bimodal (micro-mesoporous) active materials: carbon black (SC2A) with an external porosity or hierarchical MgO-templated carbon with uniform and relatively narrow mesopores. The investigations aimed at realizing EDLCs with enhanced specific and volumetric outputs compared to a few examples known from the literature.

Raison d'être: *Generally, ILs-based EDLCs reported to operate at low temperature, even -50 °C, utilized a binary mixture of 1-butyl-4-methylpyridinium bis(fluorosulfonyl)imide [BMPyr][FSI] and 1-methyl-1-propylpiperidinium bis(fluorosulfonyl)imide [MPPip][FSI] in the 1:1 molar ratio, and carbonaceous electrodes with an external porosity like carbon nanotubes (CNTs) or carbon onions. Taking into account that this mixture of ILs suffers from relatively poor transport properties, e.g., a conductivity of 4.9 mS cm^{-1} at 20 °C and ~0.1 mS cm^{-1} at 40 °C, an interest in harnessing mixtures made from imidazolium-based ILs was developed to improve the electrolyte characteristics. Furthermore, considering that the above-listed electrode materials exhibit a low density, imposing low volumetric outputs of the EDLCs, the utilization of alternative ones is required to solve this issue.*

The electrolyte of choice was the equimolar mixture of [EMIm][FSI] and [EMIm][BF$_4$] displaying a relatively low viscosity (33.0 mP s at 20 °C) and good conductivity (12.1 mS cm^{-1} at 20 °C and 0.42 mS cm^{-1} at 40 °C), which were superior to these exhibited by the above-mentioned mixture of [BMPyr][FSI] and [MPPip][FSI] in the 1:1 molar ratio.

The selected electrode materials were both mesoporous, yet characterized in that they represent different kinds of textures. In the case of carbon black, the spaces created between its particle's agglomerates give rise to a so-called external porosity. Accordingly, at middle-to-high relative pressure, its gas adsorption isotherm resembles those commonly found for CNTs, where mesopores are formed within their entangled pieces, wherein carbon black is a relatively dense

material, unlike CNTs. In turn, the hierarchical carbon offers uniform mesopores of approximately 3.5 nm, which are considered to play the role of both well-accessible ion reservoirs and smooth transportation channels to the micropores. The hierarchical character of the carbon texture is reflected in the H2(a)-type hysteresis loop on its gas adsorption isotherm. It is worth noticing that these two carbons exhibit similar values of DFT cumulative specific surface area, around 1500 m^2 g^{-1}, facilitating a comparative analysis.

The EDLCs with both types of electrodes were able to show some operation even at -50 °C, yet at 'soft' investigation conditions provided by cyclic voltammetry at 1 mV s^{-1}. The electrodes made from the hierarchical carbon enabled the cell to retain a pure box-like shape of cyclic voltammograms down to -40 °C with a little capacitance loss compared to the values obtained at room temperature. In the case of the cell with carbon black electrodes, an apparent performance deterioration was detected already at -30 °C. Moreover, the EDLC with hierarchical carbon exhibited excellent specific outputs (capacitance and energy, and greater retention of these when the temperature was lowered), which were higher than those obtained by a capacitor with carbon black electrodes. Contrarily, the EDLCs based on carbon black were superior in terms of volumetric parameters.

To realize EDLCs exhibiting the desired performance in all respects, i.e. providing good specific and volumetric metrics from room-to-low temperature, the electrodes were prepared from the mixture of both carbons. Importantly, the EDLC with such mixed electrode components exhibited specific outputs similar to the ones of the capacitor with electrodes based on the hierarchical carbon, whereas its volumetric energy was alike in the case of carbon black from 20 °C down to 0 °C, and even better at sub-zero temperatures.

Overall, the proposed constructions of EDLCs enabled their improved performance in terms of energy and power at low temperatures, bringing more realistic solutions for implementing IL-based electrolytes.

Chapter IV

Electrical double-layer capacitors based on a ternary ionic liquid electrolyte operating at low temperature with realistic gravimetric and volumetric energy outputs

1. **Summary of the publication** [ChemSusChem, 14 (2021) 1196 - 1208]

This paper reports further advancement in the development of electrical double-layer capacitors (EDLCs) based on an ionic liquid (IL) electrolyte and carbonaceous electrodes, where the primary goal was to make their low-temperature performance presenting (more) realistic energy and power outputs. The research shows the next stage in the IL electrolyte improvement realized through the formulation of ILs' ternary mixture with better transport properties compared to the previously proposed binary one. Furthermore, a hierarchical carbon with better-adjusted mesopore size and greater density was implemented as electrode material. Both fine-tuned components enabled a considerable enhancement of the resulting EDLC operation, especially at low temperatures.

Raison d'être*: Despite the beneficial hierarchical texture of the MgO-templated carbon from the point of view of charge propagation on the previously reported EDLC (chapter 3) at sub-ambient temperatures, the low volumetric outputs of the device require particular attention. That is why another carbonaceous material offering both well-accommodated mesopores and reasonable density was still needed. To boost the low-temperature performance of the EDLC yet more, the transport properties of the electrolyte required to be improved as well.*

In this context, 1-ethyl-3-methylimidazolium tetracyanoborate, [EMIm][TCB] exhibiting noticeably low viscosity against other imidazolium-based ILs emerged as an attractive IL-electrolyte for low-temperature EDLCs. However, the too high melting point of the neat [EMIm][TCB] and also of its binary mixtures with, e.g., 1-ethyl-3-methylimidazolium, bis(fluorosulfonyl)imide [EMIm][FSI], precludes their utilization in such application. To solve the issue, ILs' ternary mixtures consisting of [EMIm][TCB], [EMIm][FSI] and 1-ethyl-3-methylimidazolium, tetrafluoroborate [EMIm][BF$_4$] with various component molar ratios were prepared. The viscosity of the obtained ternary electrolytes was decreased by the presence of [EMIm][TCB], e.g., compared to the binary [EMIm][FSI]$_{0.5}$[BF$_4$]$_{0.5}$ mixture, whereas [EMIm][FSI]$_{0.6}$[BF$_4$]$_{0.1}$[TCB]$_{0.3}$ emerged as superior formulation owing to its lower viscosity and higher conductivity.

To benefit from the properties of the electrode material, the carbon texture was imposed through the templating technique and resulted from the size of a silica 'mold', while its density

by the appropriate carbon-to-template ratio. Such material exhibited a narrow range of uniform mesopores evidenced by the H1-type hysteresis loop on its gas adsorption analysis. Replicating from the spherical SiO_2 particles introduced alike shape of the carbon mesopores, as revealed by the images of transmission electron microscopy.

At 20 °C, the ternary $[EMIm][FSI]_{0.6}[BF_4]_{0.1}[TCB]_{0.3}$ mixture displayed a high electrochemical stability of 3.2 V on the proposed carbon electrodes. At a low temperature, -30 °C, it was enlarged to 3.9 V, mainly owing to the extended cathodic potential limit. It resulted from the inhibition of the parasitic redox reactions related to the acidic and labile hydrogen on the ring of imidazolium cation. Conveniently, the electrodes of a symmetric carbon/carbon EDLC operated within the determined stability limits of the electrolyte without balancing their masses. It was confirmed in the accelerated aging test.

Interestingly, the carbon/carbon EDLC with the ternary $[EMIm][FSI]_{0.6}[BF_4]_{0.1}[TCB]_{0.3}$ mixture was able to operate at 'mild' current regime (5 mV s^{-1} and 0.2 A g^{-1}) down to -50 °C, which reveals a significant progress compared to the previously proposed cell construction (chapter 3). The improvement was mainly elucidated in terms of specific and volumetric energy outputs; their greater retention below -20 °C was apparent.

The results of this study support the idea of constructing IL-based EDLCs competitive to the ones with typical organic electrolytes.

Chapter V:

An all-solid-state electrical double-layer capacitor operating at low temperature with the help of an ionogel electrolyte and a hierarchical micro-mesoporous carbon

1. Introduction

Electrical double-layer capacitors (EDLCs) display the advantage of high power density, long cycle life, fast charge/discharge ability at high current density [33, 83]; however, compared to Li-ion batteries, they deliver a moderate energy density of 5-10 Wh kg^{-1} [205]. Therefore, further improvements in the energy density of EDLCs are required to meet society's growing demands for energy storage devices. The specific energy of an EDLC depends essentially on the cell potential. Hence, selecting an electrolyte with a high electrochemical stability window is crucial for improving the specific energy.

Ionic liquids (ILs) exhibit a wide electrochemical stability window and other noteworthy properties such as non-flammability, high thermal stability, and low vapor pressure. However, their relatively high melting point restricts their low-temperature applications [206]. The melting point of ILs can be effectively decreased by realizing binary mixtures; for example, it has been demonstrated that an equimolar mixture of N-methyl-N-propylpiperidinium bis(fluorosulfonyl) imide ([PIP$_{13}$][FSI]) and N-butyl-N-methylpyrrolidinium bis(fluorosulfonyl) imide ([PYR$_{14}$][FSI]) remains liquid down to -80 °C and displays a conductivity of 4.9 mS cm^{-1} at 20 °C and ~0.1 mS cm^{-1} at -40 °C [207]. The capacitor realized with this electrolyte and electrodes based on onion-like carbon or carbon nanotubes exhibited a box-like shape of CVs (at 5 mV s^{-1}) down to -40 °C and -50 °C, respectively [207]. When the electrodes were made of porous KOH-activated microwave exfoliated graphite oxide (a-MEGO) and compact graphene films, the capacitors using the binary mixture of ([PIP$_{13}$][FSI])$_{0.5}$([PYR$_{14}$][FSI])$_{0.5}$ operated in a large temperature range from -50 to 80 °C and from -30 to 80 °C, respectively [144, 208]. The equivalent series resistance (ESR) of the cell-based on a-MEGO electrodes using this binary electrolyte decreased from 300 to 3.4 Ω cm^{-2} upon increasing the temperature from -50 to 20 °C. A graphite oxide-based EDLC with another binary mixture of 1-butyl-4-methylpyridinium tetrafluoroborate [BMPyr][BF$_4$] and 1-butyl-3-methylimidazolium tetrafluoroborate [BMIm][BF$_4$] (1:1 by molar ratio) showed rectangular CVs (5 mV s^{-1}) from -40 to 80 °C, and the ESR of the cell using this IL mixture (1.9 Ω cm^{-2} at 20 °C) was remarkably reduced compared to the value obtained with another device made of neat [BMIm][BF$_4$] (7.2 Ω cm^{-2} at 20 °C) [143].

In chapter II, we have shown that the equimolar mixture of 1-ethyl-3-methylimidazolium bis(fluorosulfonyl)imide ([EMIm][FSI]) and 1-ethyl-3-methylimidazolium tetrafluoroborate

([EMIm][BF$_4$]) exhibits only a glass transition at - 97 °C, a relatively low viscosity of 33.0 mP s and relatively good conductivity of 12.1 mS cm^{-1} at 20 °C and 0.42 mS cm^{-1} at -40 °C [57]. This conductivity is 4 times higher than reported for ([PIP$_{13}$][FSI])$_{0.5}$([PYR$_{14}$][FSI])$_{0.5}$ at -40 °C. In chapter III, we showed that from 20 to -40 °C, a capacitor made of [EMIm][BF$_4$]$_{0.5}$[FSI]$_{0.5}$ IL with MP98B electrodes displayed a high specific capacitance and energy down to -40 °C [209]. However, one shortcoming of ILs or their mixtures is the leakage problem, which leads to internal short circuits, increases the ESR, and affects the life of EDLCs. Therefore, solid-state electrolytes also known as ionogels (ILs confined in solid matrices) are proposed to get rid of this issue.

Recently, ionogels received increasing attention due to their remarkable properties – non-leakage, improved safety, and good interfacial stability [181, 182]. For example, silica-based ionogels were prepared by the sol-gel method with: i) tetramethoxy-silane (TMOS) and dimethyl-dimethoxysilane (DMDMS) as a co-silica precursor, ii) 1-ethyl-3-methylimidazolium bis(trifluoromethylsulfonyl)imide ([EMIm][TFSI]) as IL and iii) formic acid (FA) as a catalyst [179, 180]. The resulting ionogel exhibited an ionic conductivity of 3.0 mS cm^{-1} at 25 °C with [TMOS/DMDMS]/IL:FA molar ratio of [70/30]/33:1 [179] and 4.0 mS cm^{-1} at 20 °C with increasing IL molar ratio to [70/30]/50:1 [180]; these values are lower compared to the conductivity of the bulk [EMIm][TFSI], i.e. 9 mS cm^{-1} at 25 °C [57]. In addition, the sol-gel process takes very long time for gelation and aging, generally 3 to 7 days for brittle SiO$_2$-based ionogel (at a molar ratio 1: 7.8: 1 of TMOS: FA: IL) and even longer (~15 days) for compliant ionogels by decreasing FA and increasing IL proportions to a molar ratio 1: 6: 6 of TMOS: FA: IL [210]. Other kinds of ionogel with controllable thickness were prepared by encapsulating an IL in polymer matrices, which have been extensively developed due to their low cost, easy assembly, and flexible packaging. Among the various polymer hosts reported to date, biopolymers (cellulose [192, 193], guar gum [194], agarose [195], and gelatin [196]) have shown many advantages, e.g., a widespread source, low cost, and biodegradability. However, EDLCs based on biopolymer-based ionogels do not operate efficiently at high temperatures owing to their physical cross-linking by hydrogen-bonding or hydrophobic interactions. Poly(vinyl alcohol) was also used as a polymer network for solid-state electrolytes [211-213]; in this latter case, the proton-conducting polymer relies on the presence of water to achieve a high conductivity [211-213]. Consequently,

the operating voltage of a capacitor based on such quasi-solid electrolytes is less than 2.0 V [213].

Therefore, the attention has recently been shifted to poly(vinylidene fluoride) (PVdF) or poly(vinylidene fluoride-co-hexafluoropropylene) (PVdF-HFP) for synthesizing IL-based ionogels [181, 185, 198]. Their advantages include a high thermal stability, a relatively high ionic conductivity, a strong mechanical strength and a good resistance to aging [183-185]. Moreover, there is no covalent association between the polymer network and the ILs in PVdF or PVdF-HFP-based ionogels, leading to the liquid-like properties of ILs in these ionogels. A PVdF-HFP-based ionogel containing 71% of 1-ethyl-3-methyl imidazolium dicynamide ([EMIM][DCA]) exhibited a conductivity of 3.4 mS cm^{-1} at room temperature, which is lower than that of the neat IL (~25 mS cm^{-1}) [214]. When 80 wt.% of 1-butyl-3-methylimidazolium iodide ([BMIM][I]) was used, the conductivity was 3.9 mS cm^{-1} at room temperature [215].

Most solid-state EDLCs based on ionogel electrolytes have been reported to operate at room and high temperatures [188, 199, 200, 216]. However, it is still a major challenge to improve the performance of such systems at low temperatures due to the high melting point and low conductivity of IL in these conditions. To overcome these limitations, and develop ionogel performing at low-temperature, crystalline succinonitrile (SN) was used as a nonionic additive in the solid-state electrolyte, owing to its high dielectric constant (~55 at 25 °C), which leads to enhance the ionic mobility [201, 203]. A PVdF-HFP/SN based ionogel prepared using 1-butyl-3-methylimidazolium tetrafluoroborate ([BMIm][BF$_4$]) exhibited a conductivity of 6.4 mS cm^{-1} at room temperature, which is higher compared to the values obtained for the neat [BMIm][BF$_4$] (σ = 4.0 mS cm^{-1}) and PVdF-HFP/[BMIm][BF$_4$] (σ = 1.8 mS cm^{-1}), i.e. ionogel without SN. The solid-state capacitor based on PVdF-HFP/[BMIm][BF$_4$]/SN ionogel operated in the temperature range from -30 to 80 °C. However, the plastic phase of SN is stable only from -35 to 62 °C, which hinders applications in a wider temperature range [201, 217].

As already mentioned above, the high melting point of neat ILs can be lowered by formulating mixtures. For example, it has been proposed to realize a solid-state electrolyte based on the equimolar mixture of [PIP$_{13}$][FSI] and [PYR$_{14}$][FSI] trapped inside an inorganic silica network [38]. Surprisingly, it was claimed that the synthesized ionogel exhibits a comparable ionic conductivity with the liquid binary mixture from 20 to 60 °C (σ = 10 mS cm^{-1} at 60 °C), and even a higher value was obtained for the ionogel at -40 °C (0.2 mS cm^{-1} vs. 0.1 mS cm^{-1}) [202]. However, the operation of a capacitor-based on this ionogel with activated carbon electrodes

was limited to a temperature of -20 °C. Moreover, the ionogels based on a silica matrix are generally very thick (1.5 - 2.0 mm), fragile and require a long time of preparation (up to 5 days) [186, 187, 189-191, 202], which is unfavorable from an application perspective. Therefore, confining a binary mixture of ILs in a PVdF-HFP polymer network would be a good compromise for developing solid-state EDLCs in a wide temperature range.

In this work, an ionogel film based on the PVdF-HFP polymer was prepared in a totally oxygen/moisture free atmosphere by using the equimolar mixture of [EMIm][FSI] and [EMIm][BF$_4$], which was revealed to be superior in terms of low-temperature properties in liquid electrolyte. The synthesized so-called ionogel-binary (Scheme 1) demonstrated a relatively high conductivity of 5.8 mS cm^{-1} at 20 °C. At -40 °C, its conductivity (0.75 mS cm^{-1}) was even higher than the one of the liquid IL mixture (0.42 mS cm^{-1}). To uphold the mass transport of the carbon-based EDLCs at low temperatures, we applied electrodes made of a hierarchical micro/mesoporous MgO-templated carbon, MP98B. Below -20 °C, the solid-state MP98B/MP98B capacitor with the designed ionogel film exhibited a better energy retention and life span than the cell using the liquid-state binary mixture electrolyte.
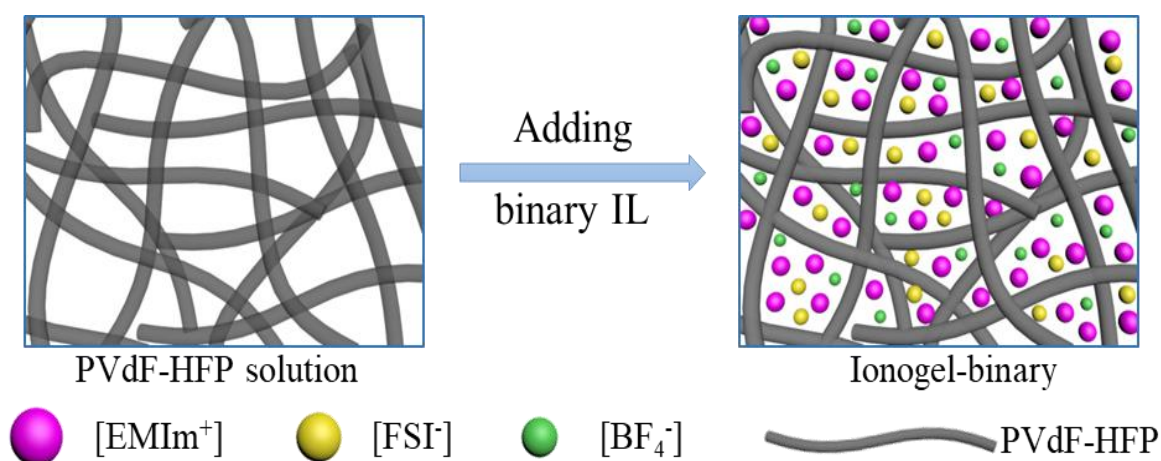
Scheme 1. Illustration of synthesizing the ionogel based on the binary [EMIm][FSI]$_{0.5}$[BF$_4$]$_{0.5}$ mixture.

2. Experimental

2.1. Preparation of the ionogel and PVdF-HFP film

In an argon filled glove box (MBraun, H_2O < 1 ppm and O_2 < 1 ppm), to prepare ca. 100 or 200 μm thick ionogel membranes, 0.3 g or 0.6 g of PVdF-HFP (Kynar Flex® 2801, Arkema) was dissolved in 3 mL or 6 mL of DMF under stirring for 30 minutes (in a hermetically closed vessel); then 0.7 g or 1.4 g of either 1-ethyl-3-methylimidazolium bis(fluorosulfonyl)imide ([EMIm][FSI]; H_2O < 20 ppm, 99.9%, Solvionic), or 1-ethyl-3-methylimidazolium tetrafluoroborate ([EMIm][BF$_4$], H_2O < 200 ppm, 99.0%, Sigma Aldrich), or the equimolar binary mixture of [EMIm][FSI] and [EMIm][BF$_4$] was added to the previously prepared solution and mixed during 1 hour under magnetic stirring. The mixture was poured into a Petri dish (S = 63.58 cm²), which was immediately introduced in a desiccator. Then, to evaporate DMF, the desiccator was slowly evacuated with a rotary-vane pump (Rotary-vane pumping unit PC 3/RZ 6, Vacuubrand) protected with a liquid nitrogen trap, and kept under vacuum during 4 - 6 hours at 24 °C. After this time, the vacuum pump was isolated, and the desiccator was filled with argon from the glove-box atmosphere to collect the film; the mass of the membrane was ~1 g or ~2 g, which is equal to the total mass of PVdF-HFP and IL, proving that DMF was totally removed during this treatment. As targeted, the thickness of the obtained ionogel film was ~100 or ~200 μm. A 100 μm thick PVdF-HFP film used as reference was also prepared in the same conditions, without adding an IL to the solution of PVdF-HFP.

2.2. Characterization of the ionogel and PVdF-HFP films

The morphology of the ionogel-binary and PVdF-HFP films was imaged by scanning electron microscopy (SEM) and energy dispersive X-Ray (EDX, JEOL JSM-7001F) was used for controlling the elemental composition of the ionogel and for the mapping of elements. The Raman spectra of DMF, PVdF-HFP film, binary IL, and ionogel-binary were recorded with a DXR-2 computer-controlled Raman spectroscope (ThermoFisher Scientific®, USA) using a laser excitation wavelength of 532 nm and a power of 2 mW with an exposure time of 1 min to avoid damaging the samples. The thermal properties of the PVdF-HFP film, ionogel-binary, ionogel-[EMIm][FSI], and ionogel-[EMIm][BF$_4$] were investigated with a differential scanning calorimeter (DSC, NETZSCH DSC 204 F1 Phoenix) coupled with a CC 200 liquid nitrogen supply and control system (NETZSCH). The samples were cooled from 25 °C to -140 °C, kept at -140 °C for 10 min, and then heated to 25 °C twice at a scan rate of

10 °C min^{-1} to ensure that the thermograms were reproducible; all the data provided in this work are from the second cycle. The conductivity of the ionogels was determined by sandwiching a film of 12 mm diameter between two aluminum current collectors in a Swagelok-type vessel; the resistance R (Ω) was measured by electrochemical impedance spectroscopy (EIS) with a sinusoidal signal of 5 mV s^{-1} in the frequency range from 100 kHz to 10 mHz. The conductivity (σ) was calculated from the ionogel resistance, according to equation (15) [218].

$$\sigma = \frac{1}{R} \cdot \frac{e}{A} \tag{15}$$

where A and e are the cross-sectional area and the ionogel thickness, respectively.

2.3. Cells manufacturing and electrochemical measurements

The carbon (MP98B, home-made carbon, S_{BET} = 1875 m^2 g^{-1}, V_{micro} = 0.35 cm^3 g^{-1}, V_{meso} = 1.30 cm^3 g^{-1} [157]) sheet electrodes employed for the electrochemical measurements were prepared following the description reported in ref. [209]. The electrodes were attached to an etched aluminum foil (Blue Solutions, 35 µm thickness) coated with conductive, chemically-resistant Dag®EB-012 (Acheson™). The assembly was further calendared to ensure proper contact of the components and dried under vacuum at 120 °C for 12 h (Vacucell® drier). Pouch cells were assembled in an argon-filled glove-box (MBraun, < 1 ppm of O$_2$ and H$_2$O): the electrodes were positioned to sandwich an ionogel film (3 cm × 3 cm, 100 or 200 µm thickness) or a glassy microfiber separator (3 cm × 3 cm; Whatman GF/A, 260 µm thickness) soaked with the liquid IL electrolyte, and then introduced into a pouch case made of aluminum laminated film. Each cell was degassed for 15 seconds under vacuum before closing with a vacuum sealer (Jumbo Plus, Henkelman).

The electrochemical measurements with cyclic voltammetry (CV, 5 mV s^{-1}), galvanostatic charge/discharge (GC/GD, 500 mA g^{-1} – per average active mass of one electrode) and electrochemical impedance spectroscopy (EIS, with a sinusoidal signal of 5 mV s^{-1} in the frequency range from 100 kHz to 1 mHz) were performed using a VSP 3 multichannel potentiostat/galvanostat (Biologic, France). The tests were carried out in an ultra-low temperature climatic chamber (MC-712, ESPEC), from 20 °C to -50 °C; the temperature was stabilized for 3 hours before each measurement. The constant power Ragone plots were obtained following the description reported in ref. [219]. The accelerated aging tests were realized by potentiostatic floating consisting of a hundred 2-hour periods (at 3.0 V) interspaced

by five galvanostatic (500 mA g^{-1}) charge/discharge cycles [25] to determine the cell capacitance and equivalent series resistance (ESR). The specific capacitance (C$_S$, F g^{-1} expressed per average active mass in one electrode) was calculated by integrating the area under the discharge curves as described in ref.[220], and the equation (16) was applied:

$$C_S = \frac{2E_{Int/D}}{U^2} \qquad (16)$$

where E$_{int/D}$ (W s) is the discharge energy and U (V) is the maximum cell potential from which the ohmic drop was subtracted.

3. Results and discussion

3.1. Thermal and physicochemical properties of the ionogels

Solid-state ionogel films based on ILs trapped into a PVdF-HFP network were implemented to avoid the leakage risk of liquid IL electrolyte in the EDLC application. As low temperatures are targeted in this contribution, the thermal properties of PVdF-HFP and the ionogels based on single ILs and binary [EMIm][FSI]$_{0.5}$[BF$_4$]$_{0.5}$ mixture were first investigated by DSC from 20 to -140 °C, upon cooling and heating. As shown in Figures 29a and 29b, the thermograms of PVdF-HFP are totally flat during cooling and heating (see the magnification in Figure 29c), which is in good agreement with ref. [221]. When an IL is confined in the PVdF-HFP network, the thermograms of the ionogel-[EMIm][FSI], ionogel-[EMIm][BF$_4$], and ionogel-binary are comparable to those of the corresponding liquids [57]. For example, the ionogel-[EMIm][FSI] presents crystallization (T$_f$) and melting (T$_m$) peaks at onset temperatures of -32 °C and -15 °C during cooling and heating, respectively, consistent with the data presented for the neat IL in the refs. [57, 222]. Upon cooling, The ionogel-[EMIm][BF$_4$] does not show any freezing peak, yet, it displays a glass transition (T$_g$ = -96 °C), cold crystallization (T$_{cc}$ = -44 °C) and melting (T$_m$ = 7 °C) during heating, in line with the observations done on the thermogram of the neat [EMIm][BF$_4$] [57]. Similar to the thermogram of the liquid state binary [EMIm][BF$_4$]$_{0.5}$[FSI]$_{0.5}$ mixture, the trace of the ionogel-binary shows only a glass transition observed at -101 °C during cooling and heating [57]. Hence, the low-temperature thermal properties of the ionogels based on single and binary ILs are comparable with the liquid state IL electrolytes. Therefore, due to

the high T_m of ionogel-[EMIm][FSI] and ionogel-[EMIm][BF$_4$], only the ionogel-binary is adapted as solid-state electrolyte for targeting the low-temperature operation of EDLCs.

As expected, the conductivity of the IL binary mixture and ionogel-binary increases with the temperature from -50 °C to 80 °C (Figure 29d). Above -30 °C, the conductivity of the IL binary mixture is higher than for the ionogel-binary (e.g., at 20 °C, $\sigma = 12.6$ mS cm^{-1} for the IL mixture and $\sigma = 5.8$ mS cm^{-1} for the ionogel-binary). Below -30 °C, the reverse situation is observed (i.e. $\sigma = 0.42$ mS cm^{-1} for the IL mixture and $\sigma = 0.75$ mS cm^{-1} for the ionogel-binary at -40 °C). A similar situation has already been reported for the ionogels based on a silica matrix [202]. The inset of Figure 29d shows that the dependence of conductivity on temperature follows the Vogel-Tamman-Fulcher (VTF) model, in agreement with previous findings [57].
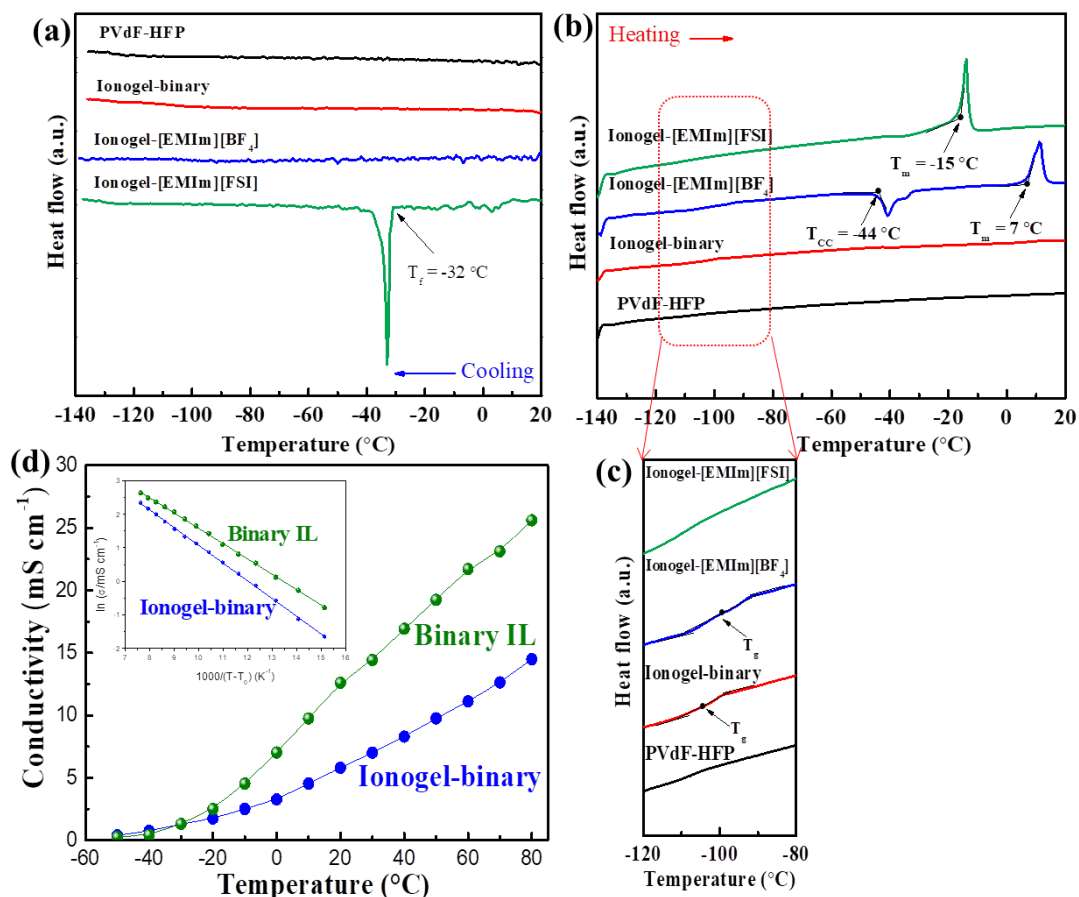
Figure 29. DSC thermograms of PVdF-HFP, ionogel-binary, ionogel-[EMIm][BF$_4$] and ionogel-[EMIm][FSI] during (a) cooling and (b) heating at 10 °C min^{-1}; (c) magnification of the second-order transition region in (b); (d) conductivity of the binary IL mixture and ionogel-binary; the corresponding VTF plots are shown in the inset.

The morphology and microstructure of the PVdF-HFP and ionogel-binary films were investigated by scanning electron microscopy (SEM). As shown in Figures 30a, the surface morphology of the PVdF-HFP film is a wavy-like structure with small holes of 0.6 ~ 3 μm [223], which were created by the evaporation of DMF. The surface of the ionogel-binary is rough without pores (Figure 30b), confirming that the IL occupies the pores of PVdF-HFP where it is confined, in good agreement with the observation done on film made of 60 wt% of 1,2-dimethyl-3-propylimidazolium bis(trifluoromethylsulfonyl) imide (DMPImTFSI) confined in PVdF-HFP [223]. Figure 30c shows the energy-dispersive X-ray analysis (EDX) of the ionogel-binary and PVdF-HFP films. Comparing to the EDX of the PVdF-HFP film showing only C and F, additional peaks of S, O, and N are observed for the ionogel-binary, fitting well with the elemental composition of $[EMIm][FSI]_{0.5}BF_4]_{0.5}$. The mapping of the various elements in the ionogel-binary film (Figure 30d) confirm their homogeneous distribution inside the PVdF-HFP network.
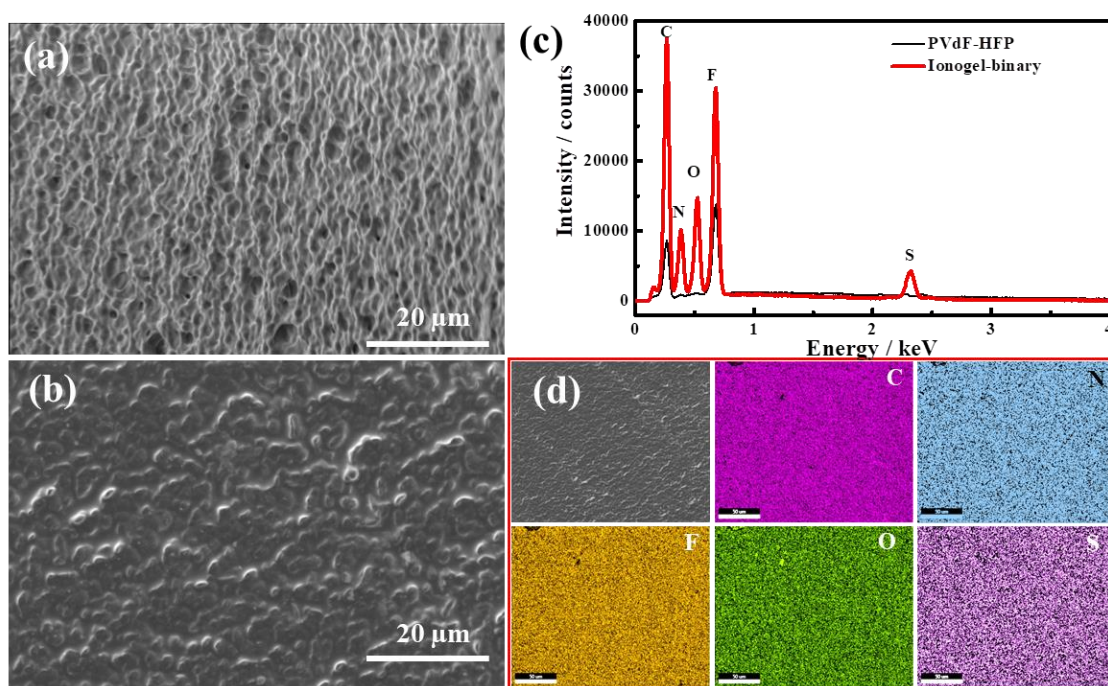
Figure 30. SEM images of (a) a PVdF-HFP film and (b) an ionogel-binary film at a magnification of 5,000X; (c) EDX spectra of the PVdF-HFP and ionogel-binary films; (d) element mapping of C, O, N, F and S in the ionogel-binary film.

The Raman spectra of DMF, PVdF-HFP film, binary IL mixture, and ionogel-binary are shown in Figure 31. The characteristic peaks of DMF at 657 and 866 cm^{-1} ascribed to the O=C-N

in-plane bending and C-N stretching, respectively [224], are totally absent from the spectra of PVdF-HFP and ionogel-binary (Figure 31a), proving a very effective evaporation of DMF from the two films. The characteristic peaks at 725 and 764 cm^{-1} in binary IL mixture and ionogel-binary correspond to the SNS scissoring of the [FSI]$^-$ anion and symmetric stretching mode (A$_{1g}$) of the [BF$_4$]$^-$ anion, respectively [225]. By deconvoluting the region ranging from 777 to 680 cm^{-1} (Figure 31b), it can be seen that the Raman spectrum of the binary IL is composed of three peaks at 764, 725 and 702 cm^{-1}, which are associated to the free [BF$_4$]$^-$ anion, free [FSI]$^-$ anion and [EMIm]$^+$ cation, respectively [51]. In comparison, the same three peaks are observed for the ionogel-binary in the same region, with a small additional peak appearing at 741 cm^{-1} (Figure 31c), which might be attributed to FSI associated with another ion when confined in the PVdF-HFP network; similar results were already observed with the FSI$^-$ anion associated with Li$^+$ cation [51, 226]. Overall, the ionogel-binary shows relatively comparable thermal and physicochemical properties with the liquid binary IL electrolyte and can be a good candidate as a solid-state electrolyte for EDLC.
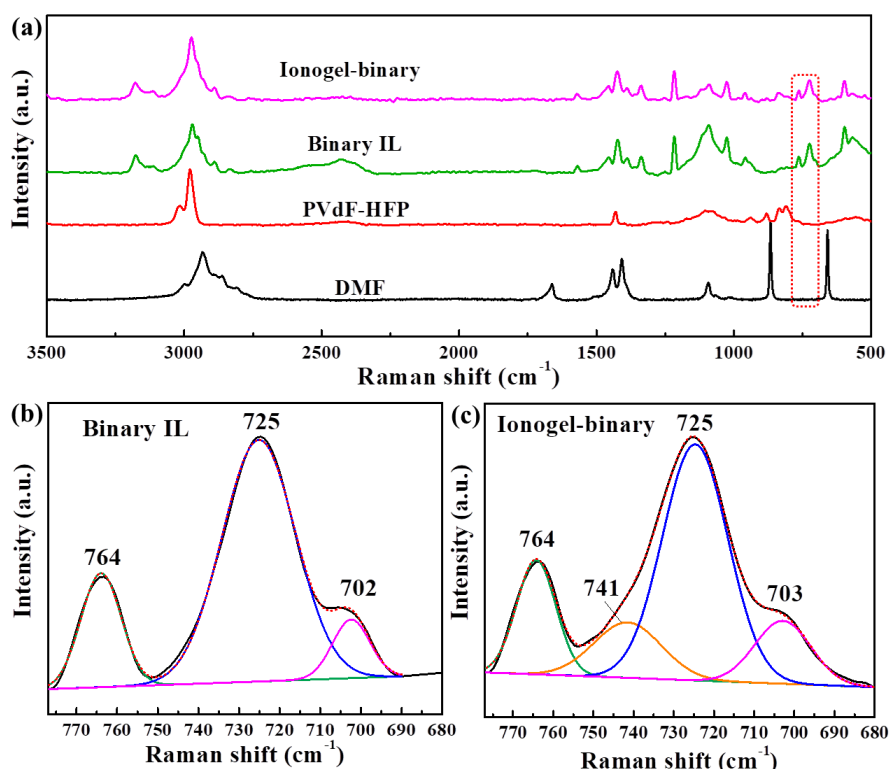
Figure 31. (a) Raman spectra of DMF, PVdF-HFP, binary IL and ionogel-binary; spectra of (a) the binary IL and (c) ionogel-binary in the range from 777 to 680 cm^{-1} (limited by a dotted rectangle in figure 31a) and their deconvolution.

3.2. Electrochemical properties of solid-state EDLCs at low temperatures

The electrochemical properties of MP98B/MP98B pouch cells have been studied by cyclic voltammetry (CV) and galvanostatic charge/discharge (GC/GD) from 20 °C to -50 °C. Figure 32 shows the CV (at 5 mV s^{-1}) and GC/GD (at 500 mA g^{-1}) characteristics of the devices with GF/A separator (260 µm thick) soaked with the liquid binary IL mixture and ionogel-binary films (200 µm or 100 µm thick) up to 3.0 V. For the cells based on the liquid electrolyte (Figure 32 a, d) and 200 µm thick ionogel-binary (Figure 32 b, e), the rectangular CVs and isosceles triangular GC/GD characteristics of charging an electrical double-layer (EDL) are observed at temperatures higher than - 40 °C. Surprisingly, when using the 200 µm thick ionogel-binary, the device demonstrated slightly lower capacitive properties (C = 93 F g^{-1} at -30 °C) at lower temperatures than the cell made of liquid-state electrolyte (C = 101 F g^{-1} at -30 °C). Considering the above-mentioned higher conductivity value of the ionogel-binary below -20 °C, as compared to the liquid electrolyte, better capacitive properties of the ionogel-binary-based cell were expected. Since an opposite situation was observed, we have decided to reduce the thickness of the film. The results obtained with the cell made with the 100 µm thick ionogel-binary (Figure 32 c, f) show comparable capacitive properties with the device made with liquid IL mixture down to -30 °C; it offers a better performance at -40 °C (Figure 32c, f), yet still preserves some EDL characteristics even at -50 °C.

Overall, comparable specific capacitance values of 132 F g^{-1}, 128 F g^{-1} and 124 F g^{-1} at 20 °C, were observed for the cells based on the liquid electrolyte, 100 µm thick ionogel-binary and 200 µm thick ionogel-binary, respectively; at -40 °C, the three cells retained ~65 % of their capacitance compared to the room temperature values. Interestingly, the capacitor made with 100 µm thick ionogel-binary still kept 51 % of its initial capacitance value at -50 °C, whereas the performance of the two other cells deteriorated at this temperature. Based on these results, only the cells based on the 100 µm thick ionogel and liquid IL mixture were considered for further comparisons of the electrochemical properties.
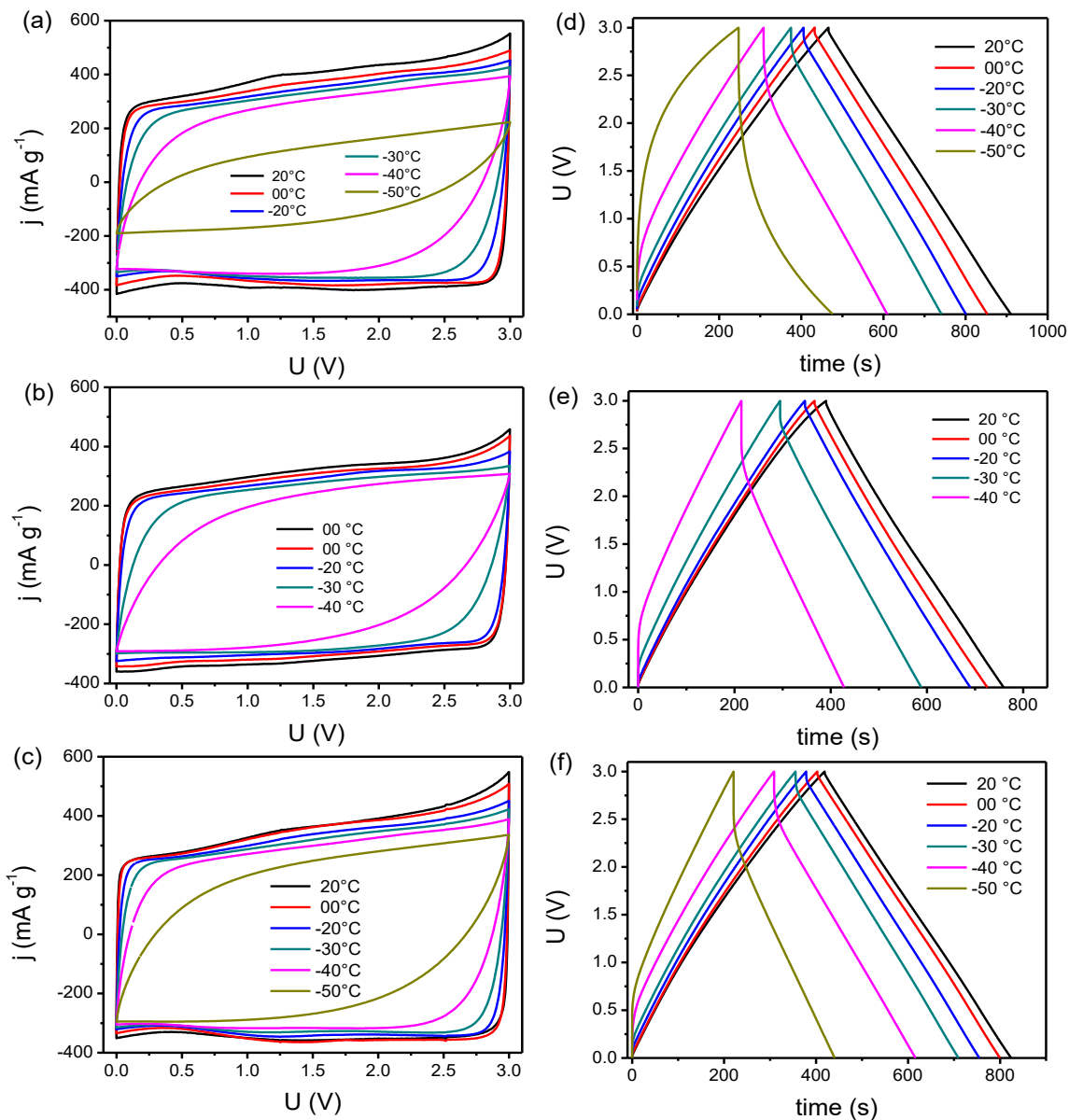
Figure 32. Cyclic voltammograms (5 mV s^{-1}) and galvanostatic (500 mA g^{-1}, per average active mass in one electrode) charge/discharge (GC/GD) characteristics of MP98B/MP98B cells based on (a,d) IL liquid mixture with GF/A separator and (b,e) 200 µm thick ionogel-binary and (c,f) 100 µm thick ionogel-binary.

Electrochemical impedance spectroscopy (EIS) has also been used to evaluate the properties of the MP98B/MP98B cells with liquid state IL mixture electrolyte and the 100 µm thick ionogel-binary. The obtained Nyquist plots at 0.0 V from 20 °C to - 50 °C are presented in Figure 33. The almost vertical lines in the low-frequency region, from 20 to - 30 °C for the

cell-based on the liquid-state electrolyte (Figure 33a) and from 20 °C to -40 °C for the EDLC using the ionogel-binary (Figure 33b) demonstrate a capacitive behavior. Interestingly, even at -50 °C, the lower frequency characteristics of the cell based on the ionogel-binary is still relatively parallel with the vertical axis; the deviation from the verticality when lowering the temperatures is associated with the conductivity decrease of the two electrolytes [144]. The deviation is more pronounced at low temperatures for the cell using the liquid-state electrolyte, in line with the data presented in Figure 29d, showing that the conductivity of ionogel-binary drops more slowly when decreasing temperature; below -30 °C, it becomes even higher than that obtained with the liquid IL (Figure 33d).

The high-frequency region of the Nyquist plots (insets in Figure 33) is characterized by the absence of semi-circles from 20 °C to - 40 °C, what is ascribed to the excellent contact between the aluminum current collectors and the carbon electrodes. The equivalent series resistance (ESR), the equivalent distributed resistance (EDR), and the ionic resistance (R_{ionic}) values of the two devices are reported in Table 3. At 20 and 0 °C, the cell-based on liquid state IL electrolyte demonstrated a lower ESR compared to the device using the ionogel-binary; the situation is opposite from -20 to -40 °C. Since the ESR depends on the electrolyte resistance, the higher ESR of the cell based on ionogel-binary from 20 to 0 °C is undoubtedly related to the lower conductivity of the ionogel, e.g., at 20°C, 5.8 and 12.1 mS cm^{-1} for the cells with ionogel-binary and liquid state electrolyte, respectively. When the temperature is decreased to -40 °C, the ESR value is 6.15 Ω for the capacitor using the liquid state IL electrolyte and 3.85 Ω for the ionogel-based cell, fitting well with the reverse situation observed with the conductivity at this temperature (0.75 mS cm^{-1} for ionogel and 0.42 mS cm^{-1} for the liquid state electrolyte). The EDR - related to the ions transport through the porous texture of the electrode material - is more than twice higher for the cell based on the liquid electrolyte at all the investigated temperatures. This behaviour can be linked to the better contact between the ionogel-binary film and the MP98B carbon electrodes, and thus good charge propagation in the mesopores of the electrode materials for the formation of the double-layer [227]. The advantage of ionogel-binary for better ions diffusion through the MP98B porous electrodes is confirmed by the R_{ionic}, which is always lower for the cell made with the solid-state electrolyte.

Table 3: Temperature dependence of ESR, EDR, and R_{ionic} (determined by subtracting R_{start} from R_{end} at the extremities of the Warburg element) for the pouch-type capacitors based on the ionogel-binary and binary liquid IL electrolytes.

		20 °C	0 °C	-20 °C	-30 °C	-40 °C
ESR	ionogel	0.41	0.48	0.97	1.75	3.85
(Ω)	liquid IL	0.29	0.34	1.38	2.47	6.15
EDR	ionogel	0.93	1.5	3.6	7.1	15.3
(Ω)	liquid IL	3.5	5.4	8.6	15.1	36.3
R_{ionic}	ionogel	0.4	0.9	2.3	5.1	9.8
(Ω)	liquid IL	2.4	4.1	7.8	12.9	26.7
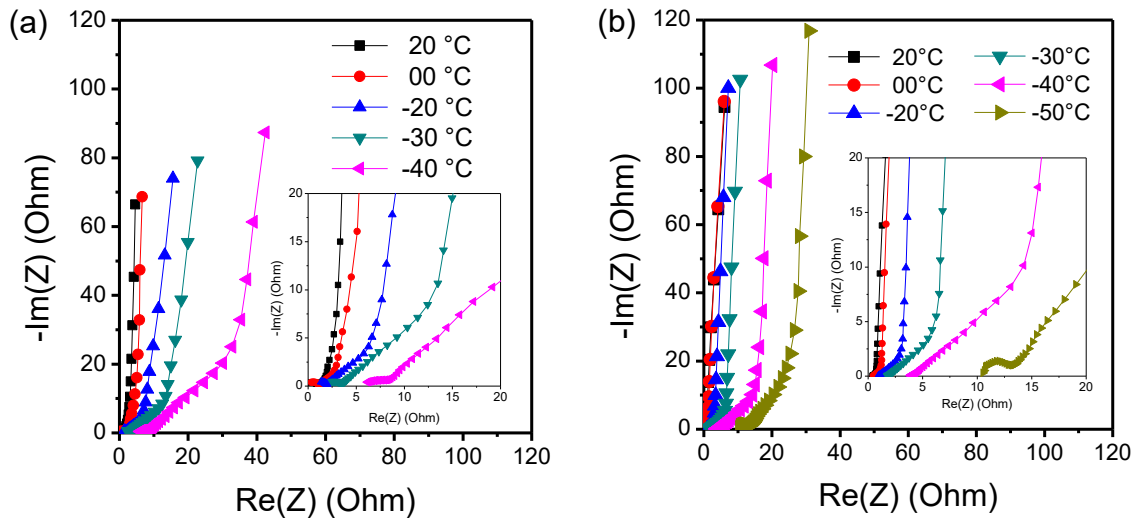
Figure 33. Nyquist plots at 0.0 V for the MP98B/MP98B pouch-type cells with (a) liquid IL binary mixture and (b) 100 µm thick ionogel-binary with the temperature decreasing from 20 °C to - 50°C. The insets represent a magnification of the high-frequency region.

Constant power Ragone plots have been realized as recommended in ref [219] by discharging the MP98B/MP98B cells with the binary ionic liquid (Figure 34a) and ionogel-binary (Figure 34b) electrolytes from 3.0 V to 1.5 V at power densities between 50 and 1500 W kg^{-1} (expressed per total mass of electrodes). From 20 to -20 °C, the specific energy of the two cells is almost constant up to a power of 700 W kg^{-1} (per total mass of electrodes), and above this value, it gradually diminishes. In parallel, at a given power, the specific energy density gradually decreases with lowering the temperature. Nonetheless, in the temperature range from

-20 to -50°C, the capacitor using ionogel-binary demonstrated slightly higher energy values (Figure 34b) up to a high power of 1000 W kg^{-1} (per total mass of electrodes) compared to the cell made with the liquid-state IL binary mixture electrolyte (Figure 34a), which energy declines dramatically when the temperature is lower than -30 °C. The specific energy at 1000 W kg^{-1} of the cells based on the two kinds of electrolytes is comparable at 20 °C (26.9 Wh kg^{-1} for the cell with liquid electrolyte and 25.3 Wh kg^{-1} for the cell with ionogel-binary). At -40 °C and a power density of 1000 W kg^{-1}, the device based on the ionogel-binary exhibits a specific energy output of 3.8 Wh kg^{-1}, which is more than two times higher than the 1.1 Wh kg^{-1} obtained with the liquid state electrolyte at the same temperature.
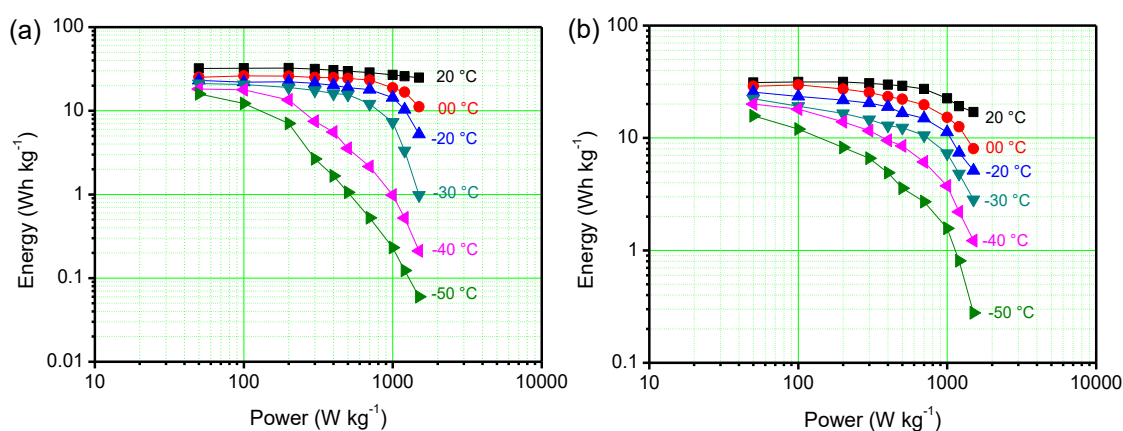
Figure 34. Constant power Ragone plots of the MP98B/MP98B pouch-type cells at temperatures ranging from 20 to -50 °C, using (a) the IL binary mixture with GF/A separator and (b) the ionogel-binary. The cells were discharged at constant power from 3.0 V to 1.5 V.

To evaluate the viability of the two cells, their life span has been assessed by measuring their capacitance and resistance during 200 hours of potentiostatic floating at 20 °C (Figure 35a) and -30 °C (Figure 35b) up to U = 3.0 V. In Figure 35a, it can be seen that the capacitance of the cell using the liquid state IL electrolyte slightly decreases, whilst its resistance slightly increases during the first 40 hours; then, both parameters remain relatively stable. After 200 hours of floating, the relative capacitance (C/C$_0$) reached 89 %, and the relative resistance (R/R$_0$) increased by 23 % compared to its initial value. By contrast, for the cell-based on the ionogel-binary, C/C$_0$ slightly decreases by 5 % after 20 hours of floating and stays constant with 95 % retention of its initial value after 200 hours. In parallel, R/R$_0$ is almost constant, with only a 7 % increase of its initial value after 200 hours of floating. Interestingly, at -30 °C

(Figure 35b), the two devices demonstrated a remarkable life span, with 89 % and 82 % of capacitance retention for the cell-based on ionogel-binary and liquid IL electrolyte, respectively. At this temperature of -30 °C, one may also observe that the increase of the relative resistance of the capacitor based on solid-state electrolyte is twice lower than with the device using the liquid electrolyte. Nevertheless, as an EDLC is considered out of usage when its capacitance retention is lower than 80 % and/or its resistance higher than 200 % of its initial value [228], it can be concluded that the capacitors based on MP98B electrodes in the liquid state IL electrolyte and the ionogel-binary are in good state of health after 200 hours of potentiostatic floating at U = 3.0 V and 20 or -30 °C.
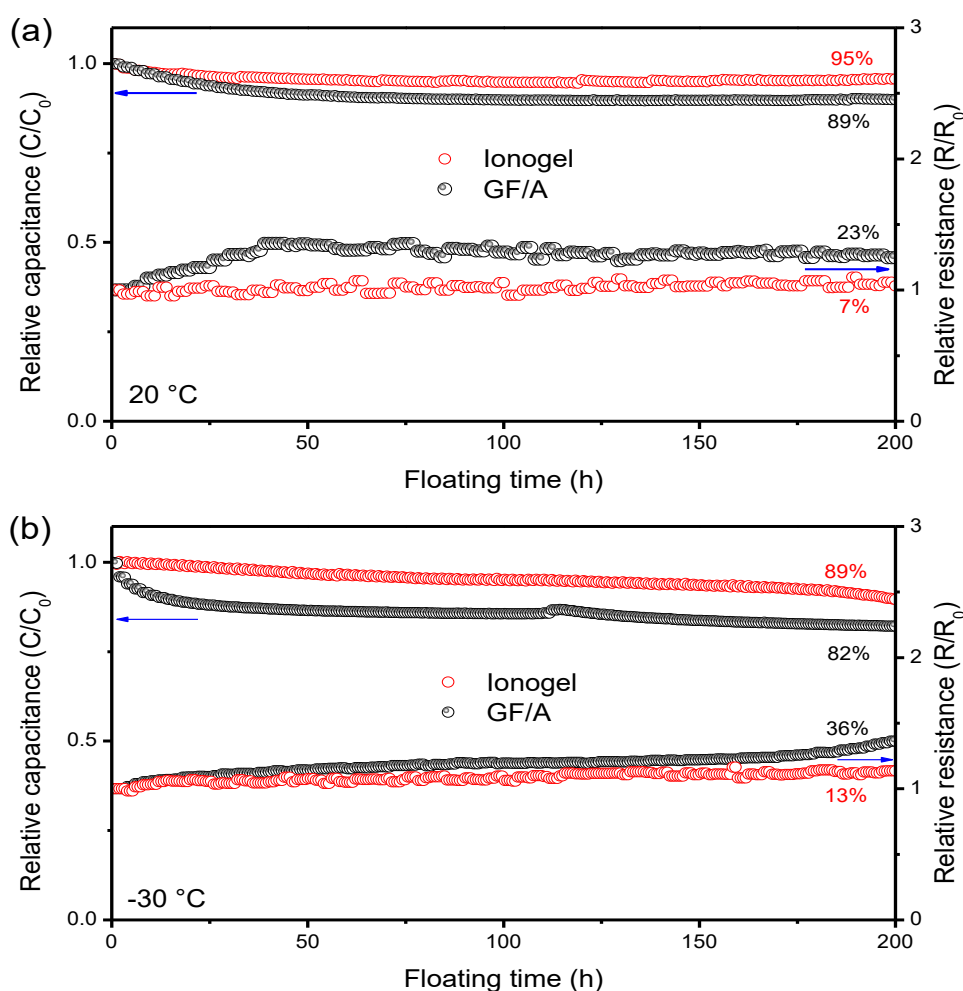
Figure 35. Relative capacitance and resistance of MP98B/MP98B capacitors in liquid IL binary mixture and ionogel-binary during 200 hours of potentiostatic floating U = 3.0 V, at (a) 20 °C and (b) -30 °C. The values are calculated from the galvanostatic (500 mA g^{-1}) charge/discharge characteristics recorded after repeated 2 hour floating periods.

4. Conclusion

Flexible solid-state ionogel films of different thicknesses (~100 and 200 µm) have been designed with an equimolar binary mixture of [EMIm][BF$_4$] and [EMIm][FSI] encapsulated into a poly(vinylidene fluoride) (PVdF-HFP) network. The thermal and physicochemical characterizations disclosed comparable properties of the two electrolytes. The MP98B/MP98B cells with the liquid IL mixture and 200 µm thick ionogel-binary demonstrated comparable electrochemical performance down to -30 °C. Below this temperature, a 100 µm thick ionogel-binary film was necessary to construct an EDLC which could outperform the device made with the liquid IL electrolyte in terms of capacitance, energy and cycle life.

General conclusion

The research presented in this manuscript was focused on the development of high energy electrical double-layer capacitors (EDLCs) operating efficiently at low temperatures (down to ca. -40 °C), while being safer and more environmentally friendly than commercial devices incorporating organic electrolytes. For this purpose, ionic liquids (ILs) were used as solvent-free electrolytes together with carbonaceous electrodes of 'tailored' porous texture. The choice of ILs was motivated by their high electrochemical stability window (ESW), relatively high conductivity, low toxicity, negligible vapor pressure, high thermal stability, and non-flammability. However, the ILs which have been so far examined for EDLCs display a too high melting point to be implemented at sub-zero temperatures, whereas the carbons commonly used in EDLCs are essentially microporous; literally, they are compatible with organic electrolytes, yet ill-suited for ILs which entail the problem of (effective) ion transportation for charging/discharging the cells. Besides, though ILs provide several advantages in comparison to organic electrolytes, the risk of electrolyte leakage remains a concern.

Some binary mixtures of ILs exhibiting a liquid state below zero degree Celsius have already been successfully applied to EDLCs for their low-temperature operation, yet they suffered from poor transport properties causing mediocre performance of the resulting cells. Accordingly, this research showed that binary IL electrolytes with enhanced transport properties are obtained when starting from neat ILs, which display a low viscosity and a high conductivity, such as [EMIm][TFSI], [EMIm][FSI] and [EMIm][BF_4]. Furthermore, it confirmed as well that the formulation of binary mixtures is an effective strategy for depressing the melting point of ionic liquid electrolytes, e.g., 17 out the 27 prepared binary mixtures showed only a glass transition (ca. -90 °C), whereas the other mixtures presented a temperature downshift of all their thermal events (crystallization, cold crystallization and melting) compared to the neat parent ILs. Overall, the preparation of ILs' binary mixtures is a simple way for obtaining new electrolytes with more adjusted physicochemical properties, e.g., [EMIm][TFSI]$_{0.5}$[FSI]$_{0.5}$ was found to be the superior one as it displayed a conductivity of 12.1 mS cm^{-1} at 20°C and 0.42 mS cm^{-1} at -40°C.

Knowing that a good match between the electrolyte and the porosity of the carbon used as electrode material (particularly that mesopores are beneficial for the transportation of ions) is important for designing high performance EDLCs operating at low temperature, this study investigated the influence of these factors using the selected [EMIm][TFSI]$_{0.5}$[FSI]$_{0.5}$ binary mixture electrolyte and two micro/mesoporous carbons of comparable specific surface areas,

yet different porous textures. The research revealed that electrodes made of a hierarchical carbon with interconnected micro- and mesopores, e.g., a MgO-templated carbon (named MP98B) enable EDLCs to exhibit a high specific capacitance and a high specific energy, together with an excellent retention against temperature lowering, contrarily to the cell implementing a carbon black (SC2A by Cabot) where the mesopores are constituted by the agglomeration of the particles, and are consequently not well connected with the micropores. To improve the volumetric outputs of IL-based EDLCs, as well as their retention at low-temperature, the properties of the IL electrolyte and carbonaceous electrodes were further modulated. The investigations showed that mixing [EMIm][TFSI], [EMIm][FSI] and [EMIm][TCB] in various proportions allows to formulate a $[EMIm][FSI]_{0.6}[BF_4]_{0.1}[TCB]_{0.3}$ ternary mixture displaying only a glass transition below -90 °C, as well as a lower viscosity and higher conductivity than the previously proposed $[EMIm][TFSI]_{0.5}[FSI]_{0.5}$ binary mixture. Moreover, a hierarchical SiO_2-templated micro/mesoporous carbon (named TC-2) with a narrower distribution of mesopore size and higher density was developed. The EDLCs incorporating these components showed an enhanced performance, with high and almost preserved specific and volumetric outputs down to -20 °C, and still a retention of 43% down to -40 °C.

Finally, the risk of electrolyte leakage was elimnated by confining the $[EMIm][TFSI]_{0.5}[FSI]_{0.5}$ mixture into a PVdF polymeric host to form a solid-state electrolyte (so-called ionogel). Down to -20 °C, an EDLC using a 100 µm thick ionogel film as separator and MP98B electrodes provides similar specific energy output and cycle life as a device made with the liquid IL mixture. Below this temperature, the solid-state capacitor exhibits even a better capacitance and specific energy output than the one with the 'traditional' liquid IL electrolyte, revealing that after adjusting the properties of the electrolyte and electrodes, the selection of a proper separator is crucial for a complete optimization of the EDLC construction.

Overall, we have demonstrated that by tuning the electrode porous texture and IL electrolyte physicochemical properties, the EDLCs performance might surpass that of so far reported analogous constructions based on lightweight mesoporous materials, which suffered from poor volumetric metrics. The presented EDLCs hold a promise of confronting even their low-temperature performance with cells made of traditional organic electrolytes. Hence, this work evinces a critical path towards designing carbon-based capacitors utilizing IL electrolytes. It can serve as a groundwork for researchers and engineers to optimize the

performance of electrochemical energy storage systems by creating alternative cost-effective, high conductivity, and eco-friendly low-temperature IL-based electrolytes, as well as porous carbons compatible with them.

Considering the outcomes of this research, as well as recent reports on EDLC developments, future investigations should focus on: i) obtaining denser hierarchical carbons to boost the specific and volumetric outputs of EDLCs from room to low temperature, and it could be realized by optimizing the templating methods; ii) improving the properties of IL mixture electrolytes by using high conductive components; iii) enhancing the ionogel conductivity by incorporating nonionic additive in the poly(vinylidene fluoride) (PVDF) matrix; iv) improving the low-temperature electrochemical properties of solid-state EDLCs by adjusting the ionogel thickness.

Abreviations and symbols

- **List of abbreviations**

AC – activated carbon

ACN – acetonitrile

AgQRE – silver-wire quasi reference electrode

BET – Brunauer-Emmett-Teller

BDM - Bockris, Devanathan and Müller

BP - Black Pearls

CB – carbon black

C65 - acetylene black

CDC – carbide derived carbons

CNTs – carbon nanotubes

CE – counter electrode

CV – cyclic voltammetry/voltammogram

DFT – density functional theory

DMDMS - dimethyl-dimethoxy silane

DMF - N, N-Dimethylformamide

DSC - differential scanning calorimetry

EDL – electrical double-layer

EDLCs – electrical double-layer capacitors

ECs – electrochemical capacitors

EIS – electrochemical impedance spectroscopy

ESR – equivalent series resistance

ESDs – Energy Storage Devices

ESW – electrochemical stability window

GC/GD – galvanostatic charge/discharge

HPC - hierarchical porous carbon

HRTEM - high-resolution transmission electron microscopy

IHP – inner Helmholtz plane

OHP – outer Helmholtz plane

OLCs – onion like carbons

IEA - International Energy Agency

ILs – ionic liquids

IUPAC – International Union of Pure and Applied Chemistry

GC - glassy carbon

LIBs – lithium-ion batteries

MgO – Manganese oxide

NLDFT - Non-Local Density Functional Theory

NZE2050 - net-zero emission by 2050

PC – propylene carbonate

PSD – pore size distribution

PTFE – polytetrafluoroethylene

PVDF - poly(vinylidene fluoride)

QSDFT- Quenched Solid Density Functional Theory

RE – reference electrode

TEM - transmission electron microscopy

SDS - Sustainable Development Scenario

SN - succinonitrile

SEM - scanning electron microscopy

SSA – specific surface area

S_{BET} – specific surface area calculated based on BET model

S_{DFT} – total specific surface area calculated based on DFT model

TMOS - tetra methoxy-silane

VTF – Vogel–Tammann–Fulcher

WE – working electrode

2D-NLDFT – two dimensional nonlocal density functional theory

2D-HS-SLIT - two dimensional heterogeneous slit model

[FSI] – bis(fluorosulfonyl)imide

[FTFSI] – fluorosulfonyl-(trifluoromethanesulfonyl)imide

[BF_4] - tetrafluoroborate

[TCB] – tetracyanoborate

[CF_3CO_2] – trifluoroacetate

[CF_3SO_3] – trifluoromethanesulfonate

[$Pyrr_{14}$] – 1-methyl-1-butylpyrrolidinium

[Pip_{13}]+ – 1-methyl-1-propylpyrrolidinium

[BMPyr] –1-butyl-4-methylpyridinium

[BMIm] - 1-butyl-3-methylimidazolium

[MPPip] –1-methyl-1-propylpiperidinium

$[Im]^+$ – imidazolium

$[Pip]^+$ – piperidinium

$[Pyrr]^+$ – pyrrolidinium

- **List of symbols**

A – surface area

C – capacitance

C_s – specific capacitance

C_v – volumetric capacitance

C_{dl} –capacitance of the double layer

C_{diff} – capacitance of the diffusion region

C_H – Helmholtz double-layer capacitance

C_+ – capacitance of positive electrode

C_- – capacitance of negative electrode

CO_2 -carbon dioxide

d – distance or diameter

f – frequency

ESR – equivalent series resistance

E – energy

E_s – specific energy

E_v – volumetric energy

L_0 – average pore size

m – mass

P – power

P_s – specific power

P_v – volumetric power

P/P_0 - relative pressure

Q_+ and Q_- – charges during the anodic and cathodic scans, respectively

R – gas constant (8.314 $J \cdot K \cdot mol^{-1}$)

R_S – equivalent series resistance

t – time

τ - time constant

T – temperature

T_0 – temperature at which the conductivity or viscosity goes to zero ideal or glass transition temperature

T_c – crystallization temperature

T_{cc} – cold crystallization temperature

T_g – glass transition temperature

T_m – melting temperature

U – cell voltage

ε_r – relative permittivity

ε_0 – vacuum permittivity

Φ_E - potential drop

ρ – density

σ – ionic conductivity

η – viscosity

Λ - molar conductivity

α – degree of ionicity

References

[1] P. Simon, Y. Gogotsi, Perspectives for electrochemical capacitors and related devices, Nat Mater, 19 (2020) 1151-1163.

[2] H.v. Helmholtz, Ueber einige Gesetze der Vertheilung elektrischer Ströme in körperlichen Leitern, mit Anwendung auf die thierisch-elektrischen Versuche (Schluss.), Ann.Phys., 165 (1853) 353-377.

[3] M. Gouy, Sur la constitution de la charge électrique à la surface d'un électrolyte, Journal de Physique Théorique et Appliquée, 9 (1910) 457-468.

[4] D.L. Chapman, LI. A contribution to the theory of electrocapillarity, The London, Edinburgh, and Dublin philosophical magazine and journal of science, 25 (1913) 475-481.

[5] O. Stern, Zur theorie der elektrolytischen doppelschicht, Zeitschrift für Elektrochemie und angewandte physikalische Chemie, 30 (1924) 508-516.

[6] H. Shao, Y.C. Wu, Z. Lin, P.L. Taberna, P. Simon, Nanoporous carbon for electrochemical capacitive energy storage, Chem Soc Rev, 49 (2020) 3005-3039.

[7] D.C. Grahame, The electrical double layer and the theory of electrocapillarity, Chem. rev., 41 (1947) 441-501.

[8] Z. Ahmad, Principles of Corrosion Engineering and Corrosion Control, Elsevier, (2006) 57-119.

[9] J. O'M. Bockris, M.A.V. Devanathan, K. Muller, On the structure of charged interfaces, Proc. R. Soc. Lond. A, 274 (1963) 55-79.

[10] P. Ratajczak, M.E. Suss, F. Kaasik, F. Béguin, Carbon electrodes for capacitive technologies, Energy Stor. Mater., 16 (2019) 126-145.

[11] P. Simon, Y. Gogotsi, Materials for electrochemical capacitors, Nat. Mater., (2009) 320-329.

[12] H.D. Yoo, E. Markevich, G. Salitra, D. Sharon, D. Aurbach, On the challenge of developing advanced technologies for electrochemical energy storage and conversion, Mater Today, 17 (2014) 110-121.

[13] A. Balducci, D. Belanger, T. Brousse, J.W. Long, W. Sugimoto, Perspective—A Guideline for Reporting Performance Metrics with Electrochemical Capacitors: From Electrode Materials to Full Devices, J. Electrochem. Soc., 164 (2017) A1487-A1488.

[14] E. Lust, A. Jänes, M. Arulepp, Influence of solvent nature on the electrochemical parameters of electrical double layer capacitors, J. Electroanal. Chem., 562 (2004) 33-42.

[15] H. Shi, Activated carbons and double layer capacitance, Electrochim. Acta, 41 (1996) 1633-1639.

[16] D. Qu, H. Shi, Studies of activated carbons used in double-layer capacitors, J. Power Sources, 74 (1998) 99-107.

[17] O. Barbieri, M. Hahn, A. Herzog, R. Kötz, Capacitance limits of high surface area activated carbons for double layer capacitors, Carbon, 43 (2005) 1303-1310.

[18] M. Inagaki, H. Konno, O. Tanaike, Carbon materials for electrochemical capacitors, J. Power Sources, 195 (2010) 7880-7903.

[19] X. Li, B. Wei, Supercapacitors based on nanostructured carbon, Nano Energy, 2 (2013) 159-173.

[20] M. Inagaki, Pores in carbon materials-importance of their control, New Carbon Mater, 24 (2009) 193-232.

[21] M. Inagaki, M. Toyoda, Y. Soneda, S. Tsujimura, T. Morishita, Templated mesoporous carbons: Synthesis and applications, Carbon, 107 (2016) 448-473.

[22] Y. Kado, Y. Soneda, H. Hatori, M. Kodama, Advanced carbon electrode for electrochemical capacitors, J. Solid State Electrochem., 23 (2019) 1061-1081.

[23] A.G. Pandolfo, A.F. Hollenkamp, Carbon properties and their role in supercapacitors, J. Power Sources, 157 (2006) 11-27.

[24] L. Demarconnay, E. Raymundo-Pinero, F. Béguin, A symmetric carbon/carbon supercapacitor operating at 1.6 V by using a neutral aqueous solution, Electrochem. Commun., 12 (2010) 1275-1278.

[25] P. Ratajczak, K. Jurewicz, P. Skowron, Q. Abbas, F. Béguin, Effect of accelerated ageing on the performance of high voltage carbon/carbon electrochemical capacitors in salt aqueous electrolyte, Electrochim. Acta, 130 (2014) 344-350.

[26] Q. Abbas, P. Ratajczak, P. Babuchowska, A.L. Comte, D. Bélanger, T. Brousse, F. Béguin, Strategies to Improve the Performance of Carbon/Carbon Capacitors in Salt Aqueous Electrolytes, Journal of The Electrochemical Society, 162 (2015) A5148-A5157.

[27] F. Béguin, M. Friebe, K. Jurewicz, C. Vix-Guterl, J. Dentzer, E. Frackowiak, State of hydrogen electrochemically stored using nanoporous carbons as negative electrode materials in an aqueous medium, Carbon, 44 (2006) 2392-2398.

[28] K. Jurewicz, E. Frackowiak, F. Béguin, Towards the mechanism of electrochemical hydrogen storage in nanostructured carbon materials, Applied Physics A, 78 (2004) 981-987.

[29] L. Suo, O. Borodin, T. Gao, M. Olguin, J. Ho, X. Fan, C. Luo, C. Wang, K. Xu, "Water-in-salt" electrolyte enables high-voltage aqueous lithium-ion chemistries, Science, 350 (2015) 938-943.

[30] D. Reber, R.-S. Kühnel, C. Battaglia, High-voltage aqueous supercapacitors based on NaTFSI, Sustainable Energy & Fuels, 1 (2017) 2155-2161.

[31] E. Pameté Yambou, F. Beguin, Effect of salt concentration in LiTFSI electrolytes on the performance of carbon-based electrochemical capacitors, Electrochim. Acta, 389 (2021) 138687.

[32] X. Bu, L. Su, Q. Dou, S. Lei, X. Yan, A low-cost "water-in-salt" electrolyte for a 2.3 V high-rate carbon-based supercapacitor, J. Mater. Chem. A, 7 (2019) 7541-7547.

[33] C. Zhong, Y.D. Deng, W.B. Hu, J.L. Qiao, L. Zhang, J.J. Zhang, A review of electrolyte materials and compositions for electrochemical supercapacitors, Chem Soc Rev, 44 (2015) 7484-7539.

[34] P. Simon, Y. Gogotsi, Capacitive Energy Storage in Nanostructured Carbon Electrolyte Systems, Acc. Chem. Res., 46 (2011) 1094-1103.

[35] C. Ramirez-Castro, C. Schütter, S. Passerini, A. Balducci, On the development of activated carbons with high affinity for high voltage propylene carbonate based electrolytes, J. Power Sources, 270 (2014) 379-385.

[36] P.W. Ruch, D. Cericola, A. Foelske, R. Kötz, A. Wokaun, A comparison of the aging of electrochemical double layer capacitors with acetonitrile and propylene carbonate-based electrolytes at elevated voltages, Electrochimica Acta, 55 (2010) 2352-2357.

[37] P.W. Ruch, D. Cericola, A. Foelske-Schmitz, R. Kötz, A. Wokaun, Aging of electrochemical double layer capacitors with acetonitrile-based electrolyte at elevated voltages, Electrochim. Acta, 55 (2010) 4412-4420.

[38] P. Liu, M. Verbrugge, S. Soukiazian, Influence of temperature and electrolyte on the performance of activated-carbon supercapacitors, J. Power Sources, 156 (2006) 712-718.

[39] E. Iwama, P.-L. Taberna, P. Azais, L. Brégeon, P. Simon, Characterization of commercial supercapacitors for low temperature applications, J. Power Sources, 219 (2012) 235-239.

[40] M. Armand, F. Endres, D.R. MacFarlane, H. Ohno, B. Scrosati, Ionic-liquid materials for the electrochemical challenges of the future, in: Materials For Sustainable Energy: A Collection of Peer-Reviewed Research and Review Articles from Nature Publishing Group, World Scientific, 2011, pp. 129-137.

[41] A. Eftekhari, Supercapacitors utilising ionic liquids, Energy Stor. Mater., 9 (2017) 47-69.

[42] D.R. MacFarlane, N. Tachikawa, M. Forsyth, J.M. Pringle, P.C. Howlett, G.D. Elliott, J.H. Davis, M. Watanabe, P. Simon, C.A. Angell, Energy applications of ionic liquids, Energy Environ. Sci., 7 (2014) 232-250.

[43] K.N. Marsh, J.A. Boxall, R. Lichtenthaler, Room temperature ionic liquids and their mixtures—a review, Fluid Phase Equilibria, 219 (2004) 93-98.

[44] G. Chatel, J.F.B. Pereira, V. Debbeti, H. Wang, R.D. Rogers, Mixing ionic liquids – "simple mixtures" or "double salts"?, Green Chemistry, 16 (2014) 2051.

[45] M. Galiński, A. Lewandowski, I. Stępniak, Ionic liquids as electrolytes, Electrochimica Acta, 51 (2006) 5567-5580.

[46] F. Mizuno, J.P. Belieres, N. Kuwata, A. Pradel, M. Ribes, C.A. Angell, Highly decoupled ionic and protonic solid electrolyte systems, in relation to other relaxing systems and their energy landscapes, Journal of Non-Crystalline Solids, 352 (2006) 5147-5155.

[47] P. Hapiot, C. Lagrost, Electrochemical Reactivity in Room-Temperature Ionic Liquids, Chem. Rev. , 108 (2008) 2238–2264.

[48] C.A. Angell, Y. Ansari, Z. Zhao, Ionic liquids: past, present and future, Faraday Discuss., 154 (2012) 9-27.

[49] R. Lin, P.-L. Taberna, S. Fantini, V. Presser, C.R. Pérez, F. Malbosc, N.L. Rupesinghe, K.B.K. Teo, Y. Gogotsi, P. Simon, Capacitive Energy Storage from −50 to 100 °C Using an Ionic Liquid Electrolyte, J. Phys. Chem. Lett., 2 (2011) 2396-2401.

[50] J. Jacquemin, P. Husson, A.A.H. Padua, V. Majer, Density and viscosity of several pure and water-saturated ionic liquids, Green Chem., 8 (2006) 172-180.

[51] M. Kerner, N. Plylahan, J. Scheers, P. Johansson, Ionic liquid based lithium battery electrolytes: fundamental benefits of utilising both TFSI and FSI anions?, Phys Chem Chem Phys, 17 (2015) 19569-19581.

[52] S.A.S. Amiril, E.A. Rahim, S. Syahrullail, A review on ionic liquids as sustainable lubricants in manufacturing and engineering: Recent research, performance, and applications, Journal of Cleaner Production, 168 (2017) 1571-1589.

[53] J. Jacquemin, P. Husson, A.A. Padua, V. Majer, Density and viscosity of several pure and water-saturated ionic liquids, Green Chem., 8 (2006) 172-180.

[54] P. Hapiot, C. Lagrost, Electrochemical reactivity in room-temperature ionic liquids, Chem. Rev., 108 (2008) 2238-2264.

[55] T.-Y. Wu, L. Hao, P.-R. Chen, J.-W. Liao, Ionic conductivity and transporting properties in LiTFSI-doped bis (trifluoromethanesulfonyl) imide-based ionic liquid electrolyte, Int. J. Electrochem. Sci., (2013).

[56] B. Gorska, L. Timperman, M. Anouti, F. Béguin, Effect of low water content in protic ionic liquid on ions electrosorption in porous carbon: application to electrochemical capacitors,

Phys. Chem. Chem. Phys., 19 (2017) 11173-11186.

[57] E. Pameté Yambou, B. Gorska, F. Béguin, Binary mixtures of ionic liquids based on EMIm cation and fluorinated anions: physico-chemical characterization in view of their application as low-temperature electrolytes, J. Mol. Liq., 298 (2020) 111959.

[58] P. Bonhote, A.-P. Dias, N. Papageorgiou, K. Kalyanasundaram, M. Grätzel, Hydrophobic, highly conductive ambient-temperature molten salts, Inorg. Chem., 35 (1996) 1168-1178.

[59] A.B. McEwen, H.L. Ngo, K. LeCompte, J.L. Goldman, Electrochemical properties of imidazolium salt electrolytes for electrochemical capacitor applications, J. Electrochem. Soc., 146 (1999) 1687-1695.

[60] J. Sun, M. Forsyth, D. MacFarlane, Room-temperature molten salts based on the quaternary ammonium ion, J. Phys. Chem. B, 102 (1998) 8858-8864.

[61] A. Noda, K. Hayamizu, M. Watanabe, Pulsed-gradient spin− echo 1H and 19F NMR ionic diffusion coefficient, viscosity, and ionic conductivity of non-chloroaluminate room-temperature ionic liquids, J. Phys. Chem. B, 105 (2001) 4603-4610.

[62] H.A. Every, A.G. Bishop, D.R. MacFarlane, G. Orädd, M. Forsyth, Transport properties in a family of dialkylimidazolium ionic liquids, Phys. Chem. Chem. Phys., 6 (2004) 1758-1765.

[63] H. Tokuda, K. Hayamizu, K. Ishii, M.A.B.H. Susan, M. Watanabe, Physicochemical properties and structures of room temperature ionic liquids. 1. Variation of anionic species, J. Phys.Chem. B, 108 (2004) 16593-16600.

[64] H. Tokuda, K. Hayamizu, K. Ishii, M.A.B.H. Susan, M. Watanabe, Physicochemical properties and structures of room temperature ionic liquids. 2. Variation of alkyl chain length in imidazolium cation, J. Phys. Chem. B, 109 (2005) 6103-6110.

[65] K. Liu, Y.-X. Zhou, H.-B. Han, S.-S. Zhou, W.-F. Feng, J. Nie, H. Li, X.-J. Huang, M. Armand, Z.-B. Zhou, Ionic liquids based on (fluorosulfonyl)(pentafluoroethanesulfonyl)imide with various oniums, Electrochimica Acta, 55 (2010) 7145-7151.

[66] M. Kerner, N. Plylahan, J. Scheers, P. Johansson, Ionic liquid based lithium battery electrolytes: fundamental benefits of utilising both TFSI and FSI anions?, Phys. Chem. Chem. Phys., 17 (2015) 19569-19581.

[67] L. Dagousset, G.T. Nguyen, F. Vidal, C. Galindo, P.-H. Aubert, Ionic liquids and γ-butyrolactone mixtures as electrolytes for supercapacitors operating over extended temperature ranges, RSC Adv., 5 (2015) 13095-13101.

[68] D.R. MacFarlane, M. Forsyth, E.I. Izgorodina, A.P. Abbott, G. Annat, K. Fraser, On the concept of ionicity in ionic liquids, Phys Chem Chem Phys, 11 (2009) 4962-4967.

[69] D.R. MacFarlane, M. Forsyth, E.I. Izgorodina, A.P. Abbott, G. Annat, K. Fraser, On the concept of ionicity in ionic liquids, Phys. Chem. Chem. Phys., 11 (2009) 4962-4967.

[70] M. Moreno, E. Simonetti, G. Appetecchi, M. Carewska, M. Montanino, G.-T. Kim, N. Loeffler, S. Passerini, Ionic Liquid Electrolytes for Safer Lithium Batteries I. Investigation around Optimal Formulation, J. Electrochem. Soc., 164 (2017) A6026-A6031.

[71] M. Montanino, M. Moreno, F. Alessandrini, G. Appetecchi, S. Passerini, Q. Zhou, W. Henderson, Physical and electrochemical properties of binary ionic liquid mixtures:(1− x) PYR14TFSI–(x) PYR14IM14, Electrochim. Acta, 60 (2012) 163-169.

[72] T.G. Tucker, C.A. Angell, Approaches to, and problems with, ionic liquid electrolytes for alkali metal electrochemical devices: The case of low-melting chloroaluminate binary solutions, J. Electrochem. Soc., 161 (2014) H796-H801.

[73] Z. Wojnarowska, M. Paluch, Recent progress on dielectric properties of protic ionic liquids, J. Phy. Cond. Matt., 27 (2015) 073202.

[74] R. Zarrougui, R. Hachicha, R. Rjab, O. Ghodbane, 1-Allyl-3-methylimidazolium-based ionic liquids employed as suitable electrolytes for high energy density supercapacitors based on graphene nanosheets electrodes, J. Mol. Liq., 249 (2018) 795-804.

[75] M. Kunze, S. Jeong, G.B. Appetecchi, M. Schönhoff, M. Winter, S. Passerini, Mixtures of ionic liquids for low temperature electrolytes, Electrochim. Acta, 82 (2012) 69-74.

[76] Masahiro Yoshizawa, Wu Xu, C.A. Angell, Ionic Liquids by Proton Transfer; Vapor Pressure, Conductivity, and the Relevance of ΔpKa from Aqueous Solutions, J. Am. Chem. Soc., 125 (2003) 15411–15419.

[77] T. Sato, G. Masuda, K. Takagi, Electrochemical properties of novel ionic liquids for electric double layer capacitor applications, Electrochimica Acta, 49 (2004) 3603-3611.

[78] K. Xu, S.P. Ding, T.R. Jow, Toward reliable values of electrochemical stability limits for electrolytes, J. Electrochem. Soc., 146 (1999) 4172-4178.

[79] D. Weingarth, H. Noh, A. Foelske-Schmitz, A. Wokaun, R. Kötz, A reliable determination method of stability limits for electrochemical double layer capacitors, Electrochimica Acta, 103 (2013) 119-124.

[80] D. Weingarth, H. Noh, A. Foelske-Schmitz, A. Wokaun, R. Kötz, A reliable determination method of stability limits for electrochemical double layer capacitors, Electrochim. Acta, 103 (2013) 119-124.

[81] C.O. Ania, J. Pernak, F. Stefaniak, E. Raymundo-Piñero, F. Béguin, Solvent-free ionic liquids as in situ probes for assessing the effect of ion size on the performance of electrical

double layer capacitors, Carbon, 44 (2006) 3126-3130.

[82] C. Largeot, C. Portet, J. Chmiola, P.-L. Taberna, Y. Gogotsi, P. Simon, Relation between the ion size and pore size for an electric double-layer capacitor, J. Am. Chem. Soc., 130 (2008) 2730-2731.

[83] F. Beguin, V. Presser, A. Balducci, E. Frackowiak, Carbons and electrolytes for advanced supercapacitors, Adv. Mater., 26 (2014) 2219-2251, 2283.

[84] K.S. Sing, D. Everett, R. Haul, L. Moscou, R. Pierotti, J. Rouquerol, T. Siemieniewska, Reporting physisorption data for gas/solid systems with special reference to the determination of surface area and porosity (Recommendations 1984), Pure appl. chem, 57 (1985) 603-619.

[85] M. Thommes, K. Kaneko, A.V. Neimark, J.P. Olivier, F. Rodriguez-Reinoso, J. Rouquerol, K.S. Sing, Physisorption of gases, with special reference to the evaluation of surface area and pore size distribution (IUPAC Technical Report), Pure Appl. Chem., 87 (2015) 1051-1069.

[86] R. Bardestani, G.S. Patience, S. Kaliaguine, Experimental methods in chemical engineering: specific surface area and pore size distribution measurements—BET, BJH, and DFT, The Canadian Journal of Chemical Engineering, 97 (2019) 2781-2791.

[87] M. Thommes, Physical Adsorption Characterization of Nanoporous Materials, 82 (2010) 1059-1073.

[88] J. Landers, G.Y. Gor, A.V. Neimark, Density functional theory methods for characterization of porous materials, Colloids and Surfaces A: Physicochemical and Engineering Aspects, 437 (2013) 3-32.

[89] J.P. Olivier, Modeling physical adsorption on porous and nonporous solids using density functional theory, J. Porous Mater., 2 (1995) 9-17.

[90] T.X. Nguyen, S.K. Bhatia, Characterization of Pore Wall Heterogeneity in Nanoporous Carbons Using Adsorption: the Slit Pore Model Revisited, J. Phys.Chem. B, 108 (2004).

[91] J.P. Olivier, Improving the models used for calculating the size distribution of micropore volume of activated carbons from adsorption data, Carbon, 36 (1998) 1469-1472.

[92] J. Jagiello, J.P. Olivier, A simple two-dimensional NLDFT model of gas adsorption in finite carbon pores. Application to pore structure analysis, J. Phys. Chem. C, 113 (2009) 19382-19385.

[93] T.X. Nguyen, S.K. Bhatia, Probing the Pore Wall Structure of Nanoporous Carbons Using Adsorption, Langmuir, 20 (2004) 3532-3535.

[94] P. Ravikovitch, A.V. Neimark, Density Functional Theory Model of Adsorption on Amorphous and Microporous Silica Materials, Langmuir 22 (2006) 11171-11179.

[95] J. Jagiello, J.P. Olivier, 2D-NLDFT adsorption models for carbon slit-shaped pores with surface energetical heterogeneity and geometrical corrugation, Carbon, 55 (2013) 70-80.

[96] J. Jagiello, J.P. Olivier, Carbon slit pore model incorporating surface energetical heterogeneity and geometrical corrugation, Adsorption, 19 (2013) 777-783.

[97] J. Jagiello, A. Chojnacka, S.E.M. Pourhosseini, Z. Wang, F. Beguin, A dual shape pore model to analyze the gas adsorption data of hierarchical micro-mesoporous carbons, Carbon, 178 (2021) 113-124.

[98] E. Frackowiak, Carbon materials for supercapacitor application, Phys Chem Chem Phys, 9 (2007) 1774-1785.

[99] F. de Clippel, M. Dusselier, S. Van de Vyver, L. Peng, P.A. Jacobs, B.F. Sels, Tailoring nanohybrids and nanocomposites for catalytic applications, Green Chem., 15 (2013) 1398.

[100] H.P. Boehm, Some aspects of the surface chemistry of carbon blacks and other carbons, Carbon, 32 (1994) 759-769.

[101] Salame, II, T.J. Bandosz, Surface Chemistry of Activated Carbons: Combining the Results of Temperature-Programmed Desorption, Boehm, and Potentiometric Titrations, J Colloid Interface Sci, 240 (2001) 252-258.

[102] J.L. Figueiredo, M.F. Pereira, M.M. Freitas, J.J. Órfão, Characterization of active sites on carbon catalysts, Ind. Eng. Chem. Res., 46 (2007) 4110-4115.

[103] P. Przygocki, P. Ratajczak, F. Beguin, Quantification of the Charge Consuming Phenomena under High-Voltage Hold of Carbon/Carbon Supercapacitors by Coupling Operando and Post-Mortem Analyses, Angew Chem Int Ed Engl, 58 (2019) 17969-17977.

[104] V. Gomez-Serrano, P. M. Alvarez, J. Jaramillo, F. J. Beltran, Formation of oxygen complexes by ozonation of carbonaceous materials prepared from cherry stones: I. Thermal effects, Carbon, 40 (2002) 513-522.

[105] B. Puri, Surface complexes on carbons, Chemistry and physics of carbon, 6 (1970) 191-282.

[106] V. Presser, M. Heon, Y. Gogotsi, Carbide-Derived Carbons - From Porous Networks to Nanotubes and Graphene, Advanced Functional Materials, 21 (2011) 810-833.

[107] L. Wei, M. Sevilla, A.B. Fuertes, R. Mokaya, G. Yushin, Polypyrrole-Derived Activated Carbons for High-Performance Electrical Double-Layer Capacitors with Ionic Liquid Electrolyte, Advanced Functional Materials, 22 (2012) 827-834.

[108] G. Yushin, A. Nikitin, Y. Gogotsi, Carbide derived carbon, Carbon nanomaterials, (2006) 211-254.

[109] S. Osswald, J. Chmiola, Y. Gogotsi, Structural evolution of carbide-derived carbons upon vacuum annealing, Carbon, 50 (2012) 4880-4886.

[110] M. Rose, Y. Korenblit, E. Kockrick, L. Borchardt, M. Oschatz, S. Kaskel, G. Yushin, Hierarchical micro- and mesoporous carbide-derived carbon as a high-performance electrode material in supercapacitors, Small, 7 (2011) 1108-1117.

[111] N.L. Wu, S.Y. Wang, Conductivity percolation in carbon-carbon supercapacitor electrodes, J. Power Sources, 10 (2002) 233-236.

[112] C. Portet, P.L. Taberna, P. Simon, E. Flahaut, C. Laberty-Robert, High power density electrodes for Carbon supercapacitor applications, Electrochim. Acta, 50 (2005) 4174-4181.

[113] V.L. Martins, R.M. Torresi, A.J.R. Rennie, Design considerations for ionic liquid based electrochemical double layer capacitors, Electrochimica Acta, 270 (2018) 453-460.

[114] A. Laheäär, A. Arenillas, F. Béguin, Change of self-discharge mechanism as a fast tool for estimating long-term stability of ionic liquid based supercapacitors, J. Power Sources, 396 (2018) 220-229.

[115] C. Arbizzani, S. Beninati, M. Lazzari, F. Soavi, M. Mastragostino, Electrode materials for ionic liquid-based supercapacitors, Journal of Power Sources, 174 (2007) 648-652.

[116] C. Wolff, S. Jeong, E. Paillard, A. Balducci, S. Passerini, High power, solvent-free electrochemical double layer capacitors based on pyrrolidinium dicyanamide ionic liquids, Journal of Power Sources, 293 (2015) 65-70.

[117] H. Kurig, M. Vestli, A. Jänes, E. Lust, Electrical Double Layer Capacitors Based on Two 1-Ethyl-3-Methylimidazolium Ionic Liquids with Different Anions, Electrochem. Solid State Lett., 14 (2011) A120.

[118] M. Lazzari, F. Soavi, M. Mastragostino, High voltage, asymmetric EDLCs based on xerogel carbon and hydrophobic IL electrolytes, Journal of Power Sources, 178 (2008) 490-496.

[119] A.J.R. Rennie, V.L. Martins, R.M. Torresi, P.J. Hall, Ionic Liquids Containing Sulfonium Cations as Electrolytes for Electrochemical Double Layer Capacitors, The Journal of Physical Chemistry C, 119 (2015) 23865-23874.

[120] F.B. Sillars, S.I. Fletcher, M. Mirzaeian, P.J. Hall, Variation of electrochemical capacitor performance with Room Temperature Ionic Liquid electrolyte viscosity and ion size, Phys Chem Chem Phys, 14 (2012) 6094-6100.

[121] T. Nishida, Y. Tashiro, M. Yamamoto, Physical and electrochemical properties of 1-alkyl-3-methylimidazolium tetrafluoroborate for electrolyte, Journal of Fluorine Chemistry, 120

(2003) 135-141.

[122] Y. Kado, K. Imoto, Y. Soneda, N. Yoshizawa, Highly enhanced capacitance of MgO-templated mesoporous carbons in low temperature ionic liquids, J. Power Sources, 271 (2014) 377-381.

[123] A. Platek, C. Nita, C.M. Ghimbeu, E. Frąckowiak, K. Fic, Electrochemical capacitors operating in aqueous electrolyte with volumetric characteristics improved by sustainable templating of electrode materials, Electrochim. Acta, 338 (2020) 135788.

[124] C. Vix-Guterl, E. Frackowiak, K. Jurewicz, M. Friebe, J. Parmentier, F. Béguin, Electrochemical energy storage in ordered porous carbon materials, Carbon, 43 (2005) 1293-1302.

[125] L. Zhang, X. Yang, F. Zhang, G. Long, T. Zhang, K. Leng, Y. Zhang, Y. Huang, Y. Ma, M. Zhang, Controlling the effective surface area and pore size distribution of sp2 carbon materials and their impact on the capacitance performance of these materials, J. Am. Chem. Soc., 135 (2013) 5921-5929.

[126] P.J. Hall, M. Mirzaeian, S.I. Fletcher, F.B. Sillars, A.J. Rennie, G.O. Shitta-Bey, G. Wilson, A. Cruden, R. Carter, Energy storage in electrochemical capacitors: designing functional materials to improve performance, Energy Environ. Sci., 3 (2010) 1238-1251.

[127] M.E. Suss, T.F. Baumann, M.A. Worsley, K.A. Rose, T.F. Jaramillo, M. Stadermann, J.G. Santiago, Impedance-based study of capacitive porous carbon electrodes with hierarchical and bimodal porosity, J. Power Sources, 241 (2013) 266-273.

[128] M. Enterria, A. Castro-Muniz, F. Suarez-Garcia, A. Martinez-Alonso, J. Tascon, T. Kyotani, Effects of the mesostructural order on the electrochemical performance of hierarchical micro–mesoporous carbons, J. Mat. Chem. A, 2 (2014) 12023-12030.

[129] A. Kumar, K. Sharma, A.R. Dixit, A review on the mechanical properties of polymer composites reinforced by carbon nanotubes and graphene, Carbon Letters, (2020).

[130] M. Zeiger, N. Jäckel, D. Weingarth, V. Presser, Vacuum or flowing argon: What is the best synthesis atmosphere for nanodiamond-derived carbon onions for supercapacitor electrodes?, Carbon, 94 (2015) 507-517.

[131] M. Zeiger, N. Jäckel, V.N. Mochalin, V. Presser, Review: carbon onions for electrochemical energy storage, Journal of Materials Chemistry A, 4 (2016) 3172-3196.

[132] S.-M. Bak, K.-H. Kim, C.-W. Lee, K.-B. Kim, Mesoporous nickel/carbon nanotube hybrid material prepared by electroless deposition, J. Mater. Chem., 21 (2011) 1984-1990.

[133] A. Shaikh, B.K. Singh, D. Mohapatra, S. Parida, Nitrogen-Doped Carbon Nano-Onions

as a Metal-Free Electrocatalyst, Electrocatalysis, 10 (2019) 222-231.

[134] R. Lin, P.-L. Taberna, S. Fantini, V. Presser, C.R. Pérez, F. Malbosc, N.L. Rupesinghe, K.B. Teo, Y. Gogotsi, P. Simon, Capacitive energy storage from− 50 to 100 C using an ionic liquid electrolyte, J. Phys. Chem. Lett., 2 (2011) 2396-2401.

[135] R.M. Reilly, Carbon nanotubes: potential benefits and risks of nanotechnology in nuclear medicine, J Nucl Med, 48 (2007) 1039-1042.

[136] A.G. Olabi, M.A. Abdelkareem, T. Wilberforce, E.T. Sayed, Application of graphene in energy storage device – A review, Renew. Sust. Energ. Rev., 135 (2021) 110026.

[137] Z. Liu, H. Zhang, S. Song, Y. Zhang, Improving thermal conductivity of styrene-butadiene rubber composites by incorporating mesoporous silica@solvothermal reduced graphene oxide hybrid nanosheets with low graphene content, Composites Science and Technology, 150 (2017) 174-180.

[138] L. Zhang, F. Zhang, X. Yang, G. Long, Y. Wu, T. Zhang, K. Leng, Y. Huang, Y. Ma, A. Yu, Y. Chen, Porous 3D graphene-based bulk materials with exceptional high surface area and excellent conductivity for supercapacitors, Sci Rep, 3 (2013) 1408.

[139] S.I. Wong, H. Lin, J. Sunarso, B.T. Wong, B. Jia, Optimization of ionic-liquid based electrolyte concentration for high-energy density graphene supercapacitors, Applied Materials Today, 18 (2020) 100522.

[140] Q. Shao, J. Tang, Y. Lin, J. Li, F. Qin, K. Zhang, J. Yuan, L.-C. Qin, Ionic liquid modified graphene for supercapacitors with high rate capability, Electrochimica Acta, 176 (2015) 1441-1446.

[141] Y. Chen, Y. Jiang, Z. Liu, L. Yang, Q. Du, K. Zhuo, Hierarchical porous N-doped graphene aerogel with good wettability for high-performance ionic liquid-based supercapacitors, Electrochimica Acta, 366 (2021) 137414.

[142] E.A. Arkhipova, A.S. Ivanov, K.I. Maslakov, S.V. Savilov, Nitrogen doping of mesoporous graphene nanoflakes as a way to enhance their electrochemical performance in ionic liquid-based supercapacitors, Journal of Energy Storage, 30 (2020) 101464.

[143] Y. Zhou, M. Ghaffari, M. Lin, H. Xu, H. Xie, C.M. Koo, Q. Zhang, High performance supercapacitor under extremely low environmental temperature, RSC Adv., 5 (2015) 71699-71703.

[144] Z. Lin, P.-L. Taberna, P. Simon, Graphene-Based Supercapacitors Using Eutectic Ionic Liquid Mixture Electrolyte, Electrochim. Acta, 206 (2016) 446-451.

[145] W.-Y. Tsai, R. Lin, S. Murali, L. Li Zhang, J.K. McDonough, R.S. Ruoff, P.-L. Taberna,

Y. Gogotsi, P. Simon, Outstanding performance of activated graphene based supercapacitors in ionic liquid electrolyte from −50 to 80°C, Nano Energy, 2 (2013) 403-411.

[146] P. Simon, Y. Gogotsi, Capacitive energy storage in nanostructured carbon–electrolyte systems, Acc. Chem. Res., 46 (2012) 1094-1103.

[147] Stephen J. Harris, A.M. Weiner, Chemical kinetics of soot particle growth, Ann. Rev. Phys. Chem., 36 (1985) 31.

[148] M.L. Studebaker, The Chemistry of Carbon Black and Reinforcement, Rubber Chemistry and Technology, 30 (1957) 1400-1483.

[149] P.J.F. Harris, New Perspectives on the Structure of Graphitic Carbons, Critical Reviews in Solid State and Materials Sciences, 30 (2005) 235-253.

[150] Y. Wang, A. Du Pasquier, D. Li, P. Atanassova, S. Sawrey, M. Oljaca, Electrochemical double layer capacitors containing carbon black additives for improved capacitance and cycle life, Carbon, 133 (2018) 1-5.

[151] S. Ban, K. Malek, C. Huang, Z. Liu, A molecular model for carbon black primary particles with internal nanoporosity, Carbon, 49 (2011) 3362-3370.

[152] W. Zhu, D.E. Miser, W. Geoffrey Chan, M.R. Hajaligol, HRTEM investigation of some commercially available furnace carbon blacks, Carbon, 42 (2004) 1841-1845.

[153] P.J.F. Harris, Z. Liu, K. Suenaga, Imaging the atomic structure of activated carbon, Journal of Physics: Condensed Matter, 20 (2008) 362201.

[154] J. Biscoe, B.E. Warren, An X-Ray Study of Carbon Black, J Appl Phys, 13 (1942) 364-371.

[155] F. Tuinstra, J.L. Koenig, Raman Spectrum of Graphite, The Journal of Chemical Physics, 53 (1970) 1126-1130.

[156] G. Pognon, T. Brousse, D. Bélanger, Effect of molecular grafting on the pore size distribution and the double layer capacitance of activated carbon for electrochemical double layer capacitors, Carbon, 49 (2011) 1340-1348.

[157] F. Béguin, V. Pavlenko, P. Przygocki, M. Pawlyta, P. Ratajczak, Melting point depression of ionic liquids by their confinement in carbons of controlled mesoporosity, Carbon, 169 (2020) 501-511.

[158] N. Fechler, T.P. Fellinger, M. Antonietti, "Salt templating": a simple and sustainable pathway toward highly porous functional carbons from ionic liquids, Adv Mater, 25 (2013) 75-79.

[159] X. Liu, M. Antonietti, Molten salt activation for synthesis of porous carbon

nanostructures and carbon sheets, Carbon, 69 (2014) 460-466.

[160] E. Masika, R. Mokaya, High surface area metal salt templated carbon aerogels via a simple subcritical drying route: preparation and CO2 uptake properties, RSC Advances, 3 (2013) 17677.

[161] D. Qiu, T. Cao, J. Zhang, S.-W. Zhang, D. Zheng, H. Wu, W. Lv, F. Kang, Q.-H. Yang, Precise carbon structure control by salt template for high performance sodium-ion storage, J Energy Chem, 31 (2019) 101-106.

[162] Y. Xia, Z. Yang, R. Mokaya, Templated nanoscale porous carbons, Nanoscale, 2 (2010) 639-659.

[163] Sangjin Han, Kwonnam Sohn, T. Hyeon, Fabrication of New Nanoporous Carbons through Silica Templates and Their Application to the Adsorption of Bulky Dyes, Chem. Mater., 12 (2000) 3337-3341.

[164] T. Morishita, T. Tsumura, M. Toyoda, J. Przepiórski, A.W. Morawski, H. Konno, M. Inagaki, A review of the control of pore structure in MgO-templated nanoporous carbons, Carbon, 48 (2010) 2690-2707.

[165] N. Bhandari, R. Dua, L. Estevez, R. Sahore, E.P. Giannelis, A combined salt–hard templating approach for synthesis of multi-modal porous carbons used for probing the simultaneous effects of porosity and electrode engineering on EDLC performance, Carbon, 87 (2015) 29-43.

[166] M. Leżańska, A. Olejniczak, J.P. Łukaszewicz, Hierarchical porous carbon templated with silica spheres of a diameter of 14 nm from pure chitosan or a chitosan/ZnCl2 solution, J. Porous Mater., 25 (2018) 1633-1648.

[167] X. Liu, M. Antonietti, Moderating black powder chemistry for the synthesis of doped and highly porous graphene nanoplatelets and their use in electrocatalysis, Adv Mater, 25 (2013) 6284-6290.

[168] N. Fechler, S.-A. Wohlgemuth, P. Jäker, M. Antonietti, Salt and sugar: direct synthesis of high surface area carbon materials at low temperatures via hydrothermal carbonization of glucose under hypersaline conditions, Journal of Materials Chemistry A, 1 (2013) 9418.

[169] S. Dutta, A. Bhaumik, K.C.W. Wu, Hierarchically porous carbon derived from polymers and biomass: effect of interconnected pores on energy applications, Energy Environ. Sci., 7 (2014) 3574-3592.

[170] M. Kruk, M. Jaroniec, Characterization of Ordered Mesoporous Carbons Synthesized Using MCM-48 Silicas as Templates, J. Phys. Chem. B, 104 (2000) 7960-7968.

[171] H. Darmstadt, C. Roy, S. Kaliaguine, T.-W. Kim, R. Ryoo, Surface and pore structure of CMK-5 ordered mesoporous carbons by adsorption and surface chemistry, Chem. Mater., 15 (2003) 3300–3307.

[172] T.T. M. Kaneda, A. Carlsson, Y. Sakamoto, T. Ohsuna, O. Terasaki Structural study of mesoporous MCM-48 and carbon networks synthesized in the spaces of MCM-48 by electron crystallography, J. Phys. Chem. B, 106 (2002) 1256–1266.

[173] P.M. Barata-Rodrigues, T.J. Mays, G.D. Moggridge, Structured carbon adsorbents from clay, zeolite and mesoporous aluminosilicate templates, Carbon, 41 (2003) 2231-2246.

[174] Y. Kado, K. Imoto, Y. Soneda, N. Yoshizawa, Correlation between the pore structure and electrode density of MgO-templated carbons for electric double layer capacitor applications, J. Power Sources, 305 (2016) 128-133.

[175] Y. Soneda, M. Kodama, Effect of Mesopore in MgO Templated Mesoporous Carbon Electrode on Capacitor Performance, Electrochemistry, 81 (2013) 845-848.

[176] Y. Zhou, M. Ghaffari, M. Lin, H. Xu, H. Xie, C.M. Koo, Q.M. Zhang, High performance supercapacitor under extremely low environmental temperature, RSC Advances, 5 (2015) 71699-71703.

[177] R.-w. Fu, Z.-h. Li, Y.-r. Liang, F. Li, F. Xu, D.-c. Wu, Hierarchical porous carbons: design, preparation, and performance in energy storage, New Carbon Mater., 26 (2011) 171-179.

[178] D. Lee, J.-Y. Jung, M.-J. Jung, Y.-S. Lee, Hierarchical porous carbon fibers prepared using a SiO2 template for high-performance EDLCs, Chem Eng J, 263 (2015) 62-70.

[179] M. Brachet, D. Gaboriau, P. Gentile, S. Fantini, G. Bidan, S. Sadki, T. Brousse, J. Le Bideau, Solder-reflow resistant solid-state micro-supercapacitors based on ionogels, Journal of Materials Chemistry A, 4 (2016) 11835-11843.

[180] B. Asbani, C. Douard, T. Brousse, J. Le Bideau, High temperature solid-state supercapacitor designed with ionogel electrolyte, Energy Storage Materials, 21 (2019) 439-445.

[181] S.N. Syahidah, S.R. Majid, Ionic liquid-based polymer gel electrolytes for symmetrical solid-state electrical double layer capacitor operated at different operating voltages, Electrochimica Acta, 175 (2015) 184-192.

[182] Z. Song, H. Duan, L. Li, D. Zhu, T. Cao, Y. Lv, W. Xiong, Z. Wang, M. Liu, L. Gan, High-energy flexible solid-state supercapacitors based on O, N, S-tridoped carbon electrodes and a 3.5 V gel-type electrolyte, Chem Eng J, 372 (2019) 1216-1225.

[183] Y. Ding, J. Zhang, L. Chang, X. Zhang, H. Liu, L. Jiang, Preparation of High-

Performance Ionogels with Excellent Transparency, Good Mechanical Strength, and High Conductivity, Adv Mater, 29 (2017).

[184] G.A. Tiruye, D. Muñoz-Torrero, J. Palma, M. Anderson, R. Marcilla, Performance of solid state supercapacitors based on polymer electrolytes containing different ionic liquids, Journal of Power Sources, 326 (2016) 560-568.

[185] G.P. Pandey, S.A. Hashmi, Performance of solid-state supercapacitors with ionic liquid 1-ethyl-3-methylimidazolium tris(pentafluoroethyl) trifluorophosphate based gel polymer electrolyte and modified MWCNT electrodes, Electrochimica Acta, 105 (2013) 333-341.

[186] A.I. Horowitz, M.J. Panzer, Poly(dimethylsiloxane)-supported ionogels with a high ionic liquid loading, Angew Chem Int Ed Engl, 53 (2014) 9780-9783.

[187] L. Nègre, B. Daffos, P.L. Taberna, P. Simon, Solvent-Free Electrolytes for Electrical Double Layer Capacitors, J. Electrochem. Soc., 162 (2015) A5037-A5040.

[188] M. Brachet, T. Brousse, J. Le Bideau, All Solid-State Symmetrical Activated Carbon Electrochemical Double Layer Capacitors Designed with Ionogel Electrolyte, ECS Electrochemistry Letters, 3 (2014) A112-A115.

[189] D. Membreno, L. Smith, K.-S. Shin, C.O. Chui, B. Dunn, A high-energy-density quasi-solid-state carbon nanotube electrochemical double-layer capacitor with ionogel electrolyte, Transl. Mater. Res., 2 (2015) 015001.

[190] B. Asbani, B. Bounor, K. Robert, C. Douard, L. Athouël, C. Lethien, J. Le Bideau, T. Brousse, Reflow Soldering-Resistant Solid-State 3D Micro-Supercapacitors Based on Ionogel Electrolyte for Powering the Internet of Things, J. Electrochem. Soc., 167 (2020) 100551.

[191] S. Zhu, P.-L. Taberna, N. Zhao, P. Simon, Salt-template synthesis of mesoporous carbon monolith for ionogel-based supercapacitors, Electrochemistry Communications, 96 (2018) 6-10.

[192] C.J. Smith, 2nd, D.V. Wagle, H.M. O'Neill, B.R. Evans, S.N. Baker, G.A. Baker, Bacterial Cellulose Ionogels as Chemosensory Supports, ACS Appl Mater Interfaces, 9 (2017) 38042-38051.

[193] S. Guo, K. Zhao, Z. Feng, Y. Hou, H. Li, J. Zhao, Y. Tian, H. Song, High performance liquid crystalline bionanocomposite ionogels prepared by in situ crosslinking of cellulose/halloysite nanotubes/ionic liquid dispersions and its application in supercapacitors, Appl Surf Sci, 455 (2018) 599-607.

[194] B. Zhang, G. Sudre, G. Quintard, A. Serghei, L. David, J. Bernard, E. Fleury, A. Charlot, Guar gum as biosourced building block to generate highly conductive and elastic ionogels with

poly(ionic liquid) and ionic liquid, Carbohydr Polym, 157 (2017) 586-595.

[195] T.J. Trivedi, D. Bhattacharjya, J.S. Yu, A. Kumar, Functionalized Agarose Self-Healing Ionogels Suitable for Supercapacitors, ChemSusChem, 8 (2015) 3294-3303.

[196] J. Liu, H. Song, Z. Wang, J. Zhang, J. Zhang, X. Ba, Stretchable, self-healable, and reprocessable chemical cross-linked ionogels electrolytes based on gelatin for flexible supercapacitors, J. Mater. Sci., 55 (2019) 3991-4004.

[197] C.-W. Liew, S. Ramesh, A.K. Arof, Characterization of ionic liquid added poly(vinyl alcohol)-based proton conducting polymer electrolytes and electrochemical studies on the supercapacitors, International Journal of Hydrogen Energy, 40 (2015) 852-862.

[198] N. Yadav, K. Mishra, S.A. Hashmi, Optimization of porous polymer electrolyte for quasi-solid-state electrical double layer supercapacitor, Electrochimica Acta, 235 (2017) 570-582.

[199] V. Chaudoy, F. Tran Van, M. Deschamps, F. Ghamouss, Ionic liquids in a poly ethylene oxide cross-linked gel polymer as an electrolyte for electrical double layer capacitor, Journal of Power Sources, 342 (2017) 872-878.

[200] P.F.R. Ortega, J.P.C. Trigueiro, G.G. Silva, R.L. Lavall, Improving supercapacitor capacitance by using a novel gel nanocomposite polymer electrolyte based on nanostructured SiO 2 , PVDF and imidazolium ionic liquid, Electrochimica Acta, 188 (2016) 809-817.

[201] G.P. Pandey, T. Liu, C. Hancock, Y. Li, X.S. Sun, J. Li, Thermostable gel polymer electrolyte based on succinonitrile and ionic liquid for high-performance solid-state supercapacitors, Journal of Power Sources, 328 (2016) 510-519.

[202] L. Negre, B. Daffos, V. Turq, P.L. Taberna, P. Simon, Ionogel-based solid-state supercapacitor operating over a wide range of temperature, Electrochimica Acta, 206 (2016) 490-495.

[203] M. Suleman, Y. Kumar, S.A. Hashmi, Structural and electrochemical properties of succinonitrile-based gel polymer electrolytes: role of ionic liquid addition, J Phys Chem B, 117 (2013) 7436-7443.

[204] J. Gamby, P.L. Taberna, P. Simon, J.F. Fauvarque, M. Chesneau, Studies and characterisations of various activated carbons used for carbon/carbon supercapacitors, J. Power Sources, 101 (2001) 109-116.

[205] A. Noori, M.F. El-Kady, M.S. Rahmanifar, R.B. Kaner, M.F. Mousavi, Towards establishing standard performance metrics for batteries, supercapacitors and beyond, Chem Soc Rev, 48 (2019) 1272-1341.

[206] A. Eftekhari, Supercapacitors utilising ionic liquids, Energy Storage Mater., 9 (2017) 47-

69.

[207] R. Lin, P.-L. Taberna, S. Fantini, V. Presser, C.R. Pérez, F. Malbosc, N.L. Rupesinghe, K.B.K. Teo, Y. Gogotsi, P. Simon, Capacitive Energy Storage from −50 to 100 °C Using an Ionic Liquid Electrolyte, J. Phys. Chem. Lett., 2 (2011) 2396-2401.

[208] W.-Y. Tsai, R. Lin, S. Murali, L.L. Zhang, J.K. McDonough, R.S. Ruoff, P.-L. Taberna, Y. Gogotsi, P. Simon, Outstanding performance of activated graphene based supercapacitors in ionic liquid electrolyte from −50 to 80 °C, Nano Energy, 2 (2013) 403-411.

[209] E. Pameté Yambou, B. Gorska, V. Pavlenko, F. Béguin, Fitting the porous texture of carbon electrodes to a binary ionic liquid electrolyte for the realization of low temperature EDLCs, Electrochim. Acta, 350 (2020) 136416.

[210] A.I. Horowitz, M.J. Panzer, High-performance, mechanically compliant silica-based ionogels for electrical energy storage applications, Journal of Materials Chemistry, 22 (2012) 16534.

[211] K.P. Safna Hussan, M.S. Thayyil, T.V. Jinitha, J. Kolte, Development of an ionogel membrane PVA/[EMIM] [SCN] with enhanced thermal stability and ionic conductivity for electrochemical application, Journal of Molecular Liquids, 274 (2019) 402-413.

[212] J. Wu, G. Xia, S. Li, L. Wang, J. Ma, A Flexible and Self-Healable Gelled Polymer Electrolyte Based on a Dynamically Cross-Linked PVA Ionogel for High-Performance Supercapacitors, Industrial & Engineering Chemistry Research, 59 (2020) 22509-22519.

[213] C.-W. Liew, S. Ramesh, A.K. Arof, Investigation of ionic liquid-doped ion conducting polymer electrolytes for carbon-based electric double layer capacitors (EDLCs), Materials & Design, 92 (2016) 829-835.

[214] P.K. Singh, K.C. Sabin, X. Chen, Ionic liquid–solid polymer electrolyte blends for supercapacitor applications, Polymer Bulletin, 73 (2015) 255-263.

[215] L.-Q. Fan, Q.-M. Tu, C.-L. Geng, Y.-L. Wang, S.-J. Sun, Y.-F. Huang, J.-H. Wu, Improved redox-active ionic liquid-based ionogel electrolyte by introducing carbon nanotubes for application in all-solid-state supercapacitors, International Journal of Hydrogen Energy, 45 (2020) 17131-17139.

[216] J. Le Bideau, L. Viau, A. Vioux, Ionogels, ionic liquid based hybrid materials, Chem Soc Rev, 40 (2011) 907-925.

[217] P.J. Alarco, Y. Abu-Lebdeh, A. Abouimrane, M. Armand, The plastic-crystalline phase of succinonitrile as a universal matrix for solid-state ionic conductors, Nat Mater, 3 (2004) 476-481.

[218] X. Pan, A. Chojnacka, F. Béguin, Advantageous carbon deposition during the irreversible electrochemical oxidation of Na2C4O4 used as a presodiation source for the anode of sodium-ion systems, Energy Storage Materials, 40 (2021) 22-30.

[219] J. Zhao, Y. Gao, A.F. Burke, Performance testing of supercapacitors: Important issues and uncertainties, J. Power Sources, 363 (2017) 327-340.

[220] A. Laheäär, P. Przygocki, Q. Abbas, F. Béguin, Appropriate methods for evaluating the efficiency and capacitive behavior of different types of supercapacitors, Electrochem. Commun., 60 (2015) 21-25.

[221] K.-S.K. Sun-Hwa Yeon, Sukjeong Choi, Jong-Ho Cha, Huen Lee, Jaeseung Oh and Byoung-Bae Lee Poly (vinylidenefluoride) -hexafluoropropylene gel electrolytes based on N-(2-hydroxyethyl) -N-methyl morpholinium ionic liquids, Korean Journal of Chemical Engineering 23 (2006) 940-947.

[222] F. Béguin, V. Pavlenko, P. Przygocki, M. Pawlyta, P. Ratajczak, Melting point depression of ionic liquids by their confinement in carbons of controlled mesoporosity, Carbon, (2020).

[223] R. Singh, B. Bhattacharya, M. Gupta, Rahul, Z.H. Khan, S.K. Tomar, V. Singh, P.K. Singh, Electrical and structural properties of ionic liquid doped polymer gel electrolyte for dual energy storage devices, International Journal of Hydrogen Energy, 42 (2017) 14602-14607.

[224] G. Gururajan, C.B. Giller, C.M. Snively, D.B. Chase, J.F. Rabolt, Molecular orientation evolution and solvent evaporation during electrospinning of atactic polystyrene using real-time Raman spectroscopy, Applied spectroscopy, 65 (2011) 858-865.

[225] V.H. Paschoal, L.F.O. Faria, M.C.C. Ribeiro, Vibrational Spectroscopy of Ionic Liquids, Chemical reviews, 117 (2017) 7053-7112.

[226] A. Lahiri, T.J. Schubert, B. Iliev, F. Endres, LiTFSI in 1-butyl-1-methylpyrrolidinium bis(fluorosulfonyl)amide: a possible electrolyte for ionic liquid based lithium ion batteries, Phys. Chem. Chem. Phys., 17 (2015) 11161-11164.

[227] G. Pandey, S. Hashmi, Performance of solid-state supercapacitors with ionic liquid 1-ethyl-3-methylimidazolium tris (pentafluoroethyl) trifluorophosphate based gel polymer electrolyte and modified MWCNT electrodes, Electrochim. Acta, 105 (2013) 333-341.

[228] D. Weingarth, A. Foelske-Schmitz, R. Kötz, Cycle versus voltage hold – Which is the better stability test for electrochemical double layer capacitors?, J. Power Sources, 225 (2013) 84-88.

Scientific achievements

1. Publications

1) **E. Pameté Yambou**, F. Béguin, Electrochim. Acta, 389 (2021) 138687. *Impact Factor: 6.215; MNiSW Points: 100*

2) **E. Pameté Yambou**, B. Gorska, F. Béguin, ChemSusChem, 14 (2021) 1196 - 1208. *Impact Factor: 7.962; MNiSW Points: 140*

3) **E. Pameté Yambou**, B. Gorska, P. Ratajczak, F. Béguin, J. Mater. Chem. A, 8 (2020) 13548 - 13557. *Impact Factor: 11.301; MNiSW Points: 140*

4) **E. Pameté Yambou**, B. Gorska, V. Pavlenko, F. Béguin, Electrochim. Acta, 350 (2020) 136416. *Impact Factor: 6.215; MNiSW Points: 100*

5) **E. Pameté Yambou**, B. Gorska, F. Béguin, J. Mol. Liq., 298 (2020) 111959. *Impact Factor: 5.065; MNiSW Points: 100*

$$\sum IF = \mathbf{36.758} \qquad\qquad \sum MNiSW\ Points = \mathbf{580}$$

2. Awards

1) **Award for the best creative work in 2020** in "Science and Earth Sciences" by the Polish Academy of Sciences (PAN) Branch in Poznań, June 29th, Poland 2021.

2) **Best Poster Prize** during the 71st Annual Meeting of the International Society of Electrochemistry (ISE), 30 August - 4 September, Belgrade Online, Serbia 2020.

3) **Best Oral Presentation Award** during the 8th International Conference on Carbon for Energy Storage and Environmental Protection (CESEP'19), 21-24th October, Alicante, Spain 2019.

3. Oral presentations at international conferences

1) **E. Pameté Yambou**, Z. Wang and F. Béguin, An all-solid-state electrical double-layer capacitor operating down to -40 °C with the help of an ionogel electrolyte and a hierarchical micro-mesoporous carbon, 72nd Annual Meeting of the International Society of Electrochemistry; from 29th August to 3rd September, Jeju Island, Korea 2021.

2) P. Przygocki, **E. Pameté Yambou**, B. Gorska and F. Béguin, Carbon-based hybrid capacitors in environmentally friendly aqueous electrolyte competing with EDLCs in organic electrolyte, The 10th Asian conference on Electrochemical Power Sources: November 24th to 27th, Kaohsiung, Taiwan 2019.

3) **E. Pameté Yambou**, B. Górska and F. Béguin, Low temperature performance of carbon/carbon EDLCs down to -50 °C in ionic liquid binary mixture , 8th international conference on Carbon for Energy Storage and Environment Protection(CESEP'19): October 20th to 24th, Alicante, Spain 2019.

4) P. Przygocki, **E. Pameté Yambou**, B. Gorska and F. Béguin, How next generations of electrochemical capacitors can be developed with help of carbon porosity? ; 8th international conference on Carbon for Energy Storage and Environment Protection (CESEP'19): October 20th to 24th, Alicante, Spain 2019.

5) **E. Pameté Yambou**, B. Górska and F. Béguin, Low temperature (-50 °C) extended operation of ionic liquid-based EDLCs by implementing binary mixtures and carbons with optimised porous texture, the 10th edition of the Journées de Chimie Analytique: September 04th to 06th, Yaoundé, Cameroon 2019.

6) **E. Pameté Yambou**, B. Górska, V. Pavlenko and F. Béguin, Low temperature (-50°C) extended operation of ionic liquid-based EDLCs by implementing binary mixtures and carbons with optimised porous texture, 70th Annual Meeting of the International Society of Electrochemistry: August 04th to 09th, Durban, South Africa 2019.

7) P. Ratajczak, B. Górska, **E. Pameté Yambou**, P. Przygocki, E. Frackowiak, F. Béguin, Electrochemical energy storage with nanoporous carbons, The World Conference on Carbon Lexington (Carbon 2019), KY, July 14–19, USA 2019

8) V. Pavlenko, **E. Pameté Yambou**, B. Górska and F. Béguin, Effect of ionic liquids confinement in carbon nanopores on their thermal properties**,** Satellite Symposium to CARBON 2019: Beyond Adsorption II, 20th July, New York City, USA 2019.

9) B. Górska, **E. Pameté Yambou** and F. Béguin, Remarkable low temperature performance of carbon/carbon EDLCs in ionic liquid binary mixture**,** 06th International Symposium on Enhanced Electrochemical Capacitors: May 06th to 10th, Nantes, France 2019.

10) V. Pavlenko, **E. Pameté Yambou**, B. Górska, F. Béguin, Effect of ionic liquid confinement in carbon nanopores on electrical double-layer charging**,** MATERIALS RESEARCH SOCIETY® Spring Meeting: April 22nd to 26th, Phoenix, Arizona, USA 2019.

4. Poster presentations at international conferences

1) **E. Pameté Yambou**, B. Górska and F. Béguin, Electrical double-layer capacitors performing at low temperature with the help of carbons with tuned porous texture and ionic liquid mixtures**,** 72nd Annual Meeting of the International Society of Electrochemistry; from 29th August to 3rd September, Jeju Island, Korea 2021.

2) **E. Pameté Yambou**, B. Górska, P. Ratajczak and F. Béguin, Hybrid Capacitor with Anthraquinone-Grafted Carbon as Battery-Type Electrode Operating in Low pH Aqueous Salt Solution, 71st Annual Meeting of the International Society of Electrochemistry: August 31st to September 04th, Belgrade Online, Belgrade, Serbia 2020.

3) **E. Pameté Yambou** and F. Béguin, Reduction of faradaic contributions in carbon/carbon cells using a "water-in-salt" electrolyte, 71st Annual Meeting of the International Society of Electrochemistry: August 31st to September 04th, Belgrade Online, Belgrade, Serbia 2020.

4) **E. Pameté Yambou**, B. Górska and F. Béguin, Hybrid capacitor with anthraquinone grafted carbon operating in low pH aqueous salt solution as faradaic battery-like component, 08th international conference on Carbon for Energy Storage and Environment Protection (CESEP'19): October 20th to 24th, Alicante, Spain 2019.

5) **E. Pameté Yambou**, Q. Abbas and F. Béguin, Effect of lithium hydration degree on carbon electrodes performance in "water-in-salt" electrolyte, the 10th edition of the Journées de Chimie Analytique: September 04th to 06th, Yaoundé, Cameroon 2019.

6) **E. Pameté Yambou**, B. Górska and F. Béguin, Anthraquinone-grafted carbon electrode as faradaic battery-like component for hybrid capacitor operating in low pH aqueous salt solution, the 10th edition of the Journées de Chimie Analytique: September 04th to 06th, Yaoundé, Cameroon 2019.

7) **E. Pameté Yambou**, B. Górska and F. Béguin, Hybrid capacitor based on a faradaic anthraquinone-grafted carbon electrode operating in low pH aqueous salt solution, 70th Annual Meeting of the International Society of Electrochemistry: August 04th to 09th, Durban, South Africa 2019.

8) **E. Pameté Yambou,** B. Górska and F. Béguin, Anthraquinone grafted carbon as negative electrode for hybrid capacitor operating in low pH aqueous salt solution**,** 06th International Symposium on Enhanced Electrochemical Capacitors: May 06th to 10th, Nantes, France 2019.

9) Q. Abbas, **E. Pameté Yambou**, P. Ratajczak, F. Béguin, Reduced faradaic contributions in carbon/carbon supercapacitors using highly concentrated neutral aqueous electrolytes, 69th Annual Meeting of the International Society of Electrochemistry: September 02nd to 07th, Bologna, Italy 2018

Abstract

Electrical double-layer capacitors (EDLCs) are energy storage devices characterized by high power outputs, yet moderate specific and volumetric energy. Therefore, a primary goal of the development of EDLCs is boosting their energy. At the same time, these devices should operate in a wide temperature range (-40/70+ °C), have a great life span ($>10^6$ cycles) as well as provide a safet use. Besides, the materials for constructing EDLCs should be eco-friendly.

Generally, the energy (*E*) of EDLCs depends on their capacitance (*C*) and operational voltage (*U*) as expressed by the formula E = ½ C U^2, wherein i) the capacitance is mainly determined by the effective surface area of the electrical double-layer formed at the electrode/electrolyte interface, and this is related to the accessible surface area of the electrodes, whereas ii) the voltage largely depends on the electrochemical stability window (ESW) of the electrolyte. Accordingly, EDLCs constructed from electrodes which are made of carbons with a well-developed porosity, accounted for enhancing the capacitance, and from ionic liquid (IL) electrolytes displaying a high electrochemical stability (>3 V on porous carbonaceous electrodes with a 'clean' surface), for voltage extending, have emerged as an attractive alternative to the commercial devices. Nonetheless, the research on EDLCs with carbon electrodes and IL-electrolytes did not move beyond the laboratory stage so far. It is related to a few problems: i) a high melting point of the electrochemically stable ILs acknowledged for the application in EDLCs precluding their use at low temperature; (ii) ill-suited carbonaceous materials for the realization of IL-based EDLCs displaying realistic specific and volumetric outputs over a wide temperature range; iii) risk of cell failure due to electrolyte leakage.

In this context, the research conducted in the frame of this doctoral dissertation focused on advancing in the construction of EDLCs based on carbonaceous electrodes and IL electrolytes. To solve the above-listed issues, the main objectives were: i) obtaining IL electrolytes which retain a liquid state at low temperatures, at least -40 °C; ii) the selection of well-suited carbonaceous materials for their coupling with IL-electrolyte to enable an effective operation of EDLCs at sub-ambient conditions; iii) increasing the operational safety of EDLCs.

The dissertation itself includes five parts. The first chapter outlines the current state of the art within the field of EDLCs. It discusses the EDL models on 2D electrodes, starting from the first and simplest one by Helmholtz and finishing with the most advanced one proposed by Bockris, Devanathan, and Müller. The working principles of EDLCs are explained, while their construction and operation parameters are described. A special attention is paid to the influence

of the carbonaceous electrode materials, i.e., their specific surface area and porous texture, on the performance of EDLCs. Another part is dedicated to the liquid electrolytes: aqueous and organic. In the latter case, the effect of (low) temperature on the EDLCs operation is highlighted. Then, ILs are introduced as a promising class of solvent-free electrolytes. Their physical and electrochemical properties are discussed in view of their application to EDLCs. Afterward, the influence of the properties (texture and morphology) of various carbonaceous materials on the operation of IL-based EDLCs, especially in view of low-temperature applications, is depicted. Finally, conclusions and perspectives for future research are presented.

To provide IL-electrolyte retaining a liquid state at low-temperature, the well-known strategy of ILs' melting point depression through the formulation of their binary mixture was harnessed. For this purpose, three ILs with an imidazolium-type cation, $[EMIm]^+$, and fluorinated anions, $[BF_4]^-$, $[FSI]^-$ or $[TFSI]^-$, were preselected and their mixtures characterized as presented in Chapter II. Importantly, the mixtures showed a downshift of the thermal events, crystallization and melting, as compared to the neat ILs, whereas in some cases, only a glass transition below -90 °C. Accordingly, for the mixtures retaining the liquid state in such a broad range of low temperatures, the transport properties were determined. These investigations revealed $[EMIm][FSI]_{0.6}[BF_4]_{0.4}$ and $[EMIm][FSI]_{0.5}[BF_4]_{0.5}$ binary mixtures to exhibit the lowest viscosity (~31 mPa s at 20 °C) and the highest conductivity (~12 mS cm^{-1} at 20 °C), making them prospective IL-binary mixture electrolytes for the development of EDLCs operating at low temperatures.

Chapter III shows an implementation of the electrolyte selected in Chapter II to EDLCs, while the focus was providing appropriate electrode materials. Keeping in mind that, for IL-based EDLCs operating at low temperatures, the presence of mesopores in the electrode materials is favorable, two micro/mesoporous carbons were harnessed. Their texture and morphology were characterized to elucidate their influence on the electrochemical performance of the EDLCs. These carbons had a similar specific surface area (S_{DFT} ~1500 m^2 g^{-1}), yet different types of porosity: MP98B was a hierarchical MgO-templated carbon with micropores interconnected with narrow mesopores (average mesopore size of 3.5 nm), whereas the carbon black SC2A had so-called open mesopores (in a relatively broad range from 3 to 17 nm) poorly interconnected with the micropores. Briefly, the electrodes made of the nanoarchitectured carbon MP98B enabled the resulting EDLC to exhibit higher gravimetric outputs

(C_s = 140 F g^{-1} and E_s = 21 Wh kg^{-1} at 20 °C) compared to the cell with the carbon black SC2A (C_s = 115 F g^{-1} and E_s = 16 Wh kg^{-1} at 20 °C) as well as greater retention of the specific capacitance (87 % vs. 71 % at -40 °C) and energy (23 % vs. 7 % at -30 °C) along with the temperature lowering. Contrarily, the carbon black allowed for obtaining greater volumetric metrics ($C_{v(SC2A)}$ = 54 F cm^{-3} vs. $C_{v(MP98B)}$ = 34 F cm^{-3} and $E_{v(SC2A)}$ = 7.5 Wh L^{-1} vs. $E_{v(MP98B)}$ = 5 Wh L^{-1} at 20 °C). Therefore, a mixture of these two carbons was used as electrode material, leading the EDLC with such electrodes to display both high gravimetric and volumetric energy as well as their good retention at -40 °C (39 %).

Nevertheless, a single electrode material enabling to obtain a good EDLC performance appears to be required: therefore, a further advancement in the EDLCs construction was realized, as presented in Chapter IV. Another hierarchical carbon was synthesized by selecting a templating technique and proper substrates - colloidal silica with particle sizes of 12nm. The thereof obtained carbon was denser than the above-mentioned MP98B, with a well-adapted mesopore size of 9 nm. Moreover, ternary mixtures of [EMIm][FSI], [EMIm][BF$_4$] and [EMIm][TCB] with various molar ratio were prepared, and it was found that [EMIm][FSI]$_{0.6}$[BF$_4$]$_{0.1}$[TCB]$_{0.3}$ has a low viscosity (η=23.6 mP s at 20 °C) and a high conductivity (σ = 14.2 mS cm^{-1} at 20°C). These materials were incorporated in an EDLC, which displayed realistic gravimetric and volumetric energy outputs (E_s = 31 Wh kg^{-1} and E_v = 12.2 Wh L^{-1} at 20 °C), even at -40 °C, where 43 % of initial values was retained.

Finally, to increase the device's safety, solid-state electrolytes based on ILs, called ionogels, were prepared. The films consisted of the optimal binary IL mixture, [EMIm][FSI]$_{0.5}$[BF$_4$]$_{0.5}$, encapsulated in a poly(vinylidene fluoride (PVDF) matrix. The resulting EDLCs, with electrodes made of the hierarchical MP98B carbon, exhibited a high operational voltage and comparable capacitive properties with a reference cell made of the liquid IL mixture electrolyte. Furthermore, the capacitor using the solid-state electrolyte demonstrated an excellent life span at low temperatures and 'mild' experimental conditions, with a higher specific energy (E_s = 3.8 Wh kg^{-1} at -40°C) than the device based on the liquid IL mixture (E_s = 1.1 Wh kg^{-1} at -40°C) at a constant power of 1000 W kg^{-1}.

Streszczenie

Kondensatory podwójnej warstwy elektrycznej to urządzenia do magazynowania energii charakteryzujące się dużą mocą wyjściową przy umiarkowanej gęstości energii. Z tego względu, głównym celem rozwoju kondensatorów podwójnej warstwy elektrycznej jest zwiększenie gęstości ich energii. Jednocześnie urządzenia te powinny pracować w szerokim zakresie temperatur (-40/70+ °C), charakteryzować się dobrą pracą cykliczną (>10^6 cykli) oraz zapewniać bezpieczeństwo użytkowania. Poza tym materiały do budowy kondensatorów podwójnej warstwy elektrycznej powinny być przyjazne dla środowiska.

Zasadniczo, energia (E) kondensatorów podwójnej warstwy elektrycznej zależy od ich pojemności (C) i napięcia pracy (U) zgodnie z wzorem E = ½ C U^2, gdzie i) pojemność zależy głównie od powierzchni podwójnej warstwy elektrycznej utworzonej na granicy faz elektroda/elektrolit, co jest związane z dostępną powierzchnią elektrod, natomiast ii) napięcie w dużej mierze zależy od stabilności elektrochemicznej elektrolitu. W związku z tym kondensatory podwójnej warstwy elektrycznej zbudowane z i) elektrod wykonanych z węgli o dużej porowatości, odpowiedzialnych za wzrost pojemności, oraz z cieczy jonowych jako elektrolitów wykazujących wysoką stabilność elektrochemiczną (>3 V na porowatych elektrodach węglowych pozbawionych grup funkcyjnych), odpowiedzialnych za zwiększenie napięcia pracy, stały się atrakcyjną alternatywą dla urządzeń komercyjnych. Niemniej jednak badania nad kondensatorami podwójnej warstwy elektrycznej z elektrodami węglowymi i cieczami jonowymi jako elektrolitami pozostają na etapie badań laboratoryjnych. Wiąże się to z kilkoma problemami: i) wysoka temperatura topnienia elektrochemicznie stabilnych cieczy jonowych stosowanych w kondensatorach podwójnej warstwy elektrycznej, uniemożliwiająca ich działanie w niskiej temperaturze; ii) materiały węglowe niedostosowane do wytwarzania kondensatorów podwójnej warstwy elektrycznej z cieczami jonowymi jako elektrolitami uniemożliwiające wysokie wartości gęstości energii w szerokim zakresie temperatur; iii) ryzyko awarii kondensatora z powodu wycieku elektrolitu.

W związku z powyższym badania prowadzone w ramach niniejszej rozprawy doktorskiej koncentrowały się na ulepszeniu konstrukcji kondensatorów podwójnej warstwy elektrycznej na bazie elektrod węglowych i cieczy jonowych jako elektrolitów. Aby rozwiązać powyższe problemy, głównymi celami badań były: i) otrzymanie elektrolitów na bazie cieczy jonowych, które zachowują ciekły stan skupienia w niskich temperaturach, co najmniej -40 °C; ii) dobór elektrodowych materiałów węglowych tak by umożliwiały wydajne działanie kondensatorów podwójnej warstwy elektrycznej na bazie cieczy jonowych jako elektrolitów w niskich

temperaturach; iii) zwiększenie bezpieczeństwa pracy kondensatorów podwójnej warstwy elektrycznej.

Niniejsza rozprawa doktorska składa się z pięciu części. Pierwszy rozdział przedstawia aktualny stan wiedzy o kondensatorach podwójnej warstwy elektrycznej. Omówiono modele podwójnej warstwy elektrycznej na dwuwymiarowych elektrodach, od pierwszego i najprostszego modelu autorstwa Helmholtza, a kończąc na najbardziej zaawansowanym zaproponowanym przez Bockrisa, Devanathana i Müllera. Wyjaśnione zostały zasada działania kondensatorów podwójnej warstwy elektrycznej, ich konstrukcja oraz parametry pracy. Szczególną uwagę zwrócono na wpływ elektrodowych materiałów węglowych, tj. ich powierzchni właściwej i porowatej tekstury, na działanie kondensatorów podwójnej warstwy elektrycznej. Kolejna część poświęcona jest ciekłym elektrolitom wodnym i organicznym. W tym drugim przypadku kładziono nacisk na wpływ (niskiej) temperatury na działanie kondensatorów podwójnej warstwy elektrycznej. Następnie przedstawiono ciecze jonowe jako obiecujące bezrozpuszczalnikowe elektrolity. Ich właściwości fizyczne i elektrochemiczne omówiono pod kątem zastosowania w kondensatorach podwójnej warstwy elektrycznej. Następnie przedstawiono wpływ właściwości (tekstury i morfologii) różnych materiałów węglowych na działanie kondensatorów podwójnej warstwy elektrycznej na bazie cieczy jonowych, zwłaszcza w ujęciu ich zastosowania w niskich temperaturach. Na koniec przedstawiono wnioski i perspektywy przyszłych badań.

W celu otrzymania cieczy jonowych występujących w stanie ciekłym w niskiej temperaturze, wykorzystano dobrze znaną strategię obniżania ich temperatury topnienia poprzez wytwarzanie ich mieszanin dwuskładnikowych. Do tych celów wyselekcjonowano trzy ciecze jonowe z kationem imidazoliowym $[EMIm]^+$ i fluorowanymi anionami $[BF_4]^-$, $[FSI]^-$ lub $[TFSI]^-$, a następnie scharakteryzowano ich mieszaniny, i przedstawiono w rozdziale II. Co ważne, w porównaniu do czystych cieczy jonowych, ich mieszaniny wykazywały obniżenie temperatur przemian fazowych, krystalizacji i topnienia, a w niektórych przypadkach jedynie zeszklenie poniżej -90 °C. Dla mieszanin zachowujących stan ciekły w tak szerokim zakresie niskich temperatur zbadano ich właściwości transportowe. Mieszaniny dwuskładnikowe $[EMIm][FSI]_{0,6}[BF4]_{0,4}$ i $[EMIm][FSI]_{0,5}[BF4]_{0,5}$ wykazały najniższą lepkość (~31 mPa·s w 20 °C) i najwyższe przewodnictwo (~12 mS cm^{-1} w 20 °C), co czyni je potencjalnymi elektrolitami dla kondensatorów podwójnej warstwy elektrycznej działających w niskich temperaturach.

Rozdział III przedstawia zastosowanie elektrolitu wybranego w rozdziale II w kondensatorach podwójnej warstwy elektrycznej, jednocześnie prowadząc badania nad doborem odpowiednich materiałów elektrodowych. Mając na uwadze, że w przypadku kondensatorów podwójnej warstwy elektrycznej na bazie cieczy jonowych, które działają w niskich temperaturach, morwowate materiały węglowe wpływają korzystnie na działanie takich urządzeń, wstępnie wybrano dwa typy takich materiałów. Scharakteryzowano ich teksturę i morfologię, aby wyjaśnić ich wpływ na parametry pracy kondensatorów podwójnej warstwy elektrycznej. Węgle te miały podobną powierzchnię właściwą (S_{DFT} ~1500 m^2 g^{-1}), ale różne typy porowatości: MP98B był węglem o strukturze hierarchicznej otrzymanym poprzez odwzorowanie z MgO jako matrycy w którym mikropory są połączone z wąskimi mezoporami (średnia wielkość mezoporów 3,5 nm), podczas gdy sadza o wysoko rozwiniętej powierzchni właściwej SC2A miał tzw. otwarte mezopory (w stosunkowo szerokim zakresie od 3 do 17 nm) słabo połączone z mikroporami. Zastosowanie elektrod wykonanych z węgla MP98B umożliwiło wytworzenie kondensatora podwójnej warstwy elektrycznej o lepszych parametrach pracy (Cs = 140 F g^{-1} i Es = 21 Wh kg^{-1} w 20 °C), w porównaniu do ogniwa z sadzą SC2A (Cs = 115 F g^{-1} i Es = 16 Wh kg^{-1} w 20 °C), oraz lepszą retencją pojemności (87% vs 71 % w -40 °C) i energii (23% vs 7 % przy -30 °C) w przeliczeniu na masę elektrod wraz z obniżeniem temperatury. Natomiast użycie elektrod wykonanych z sadzy pozwoliło uzyskać większe wartości pojemności (Cv(SC2A) = 54 F cm^{-3} vs. Cv(MP98B) = 34 F cm^{-3}) i energii (Ev(SC2A) = 7,5 Wh L^{-1} vs. Ev(MP98B)) = 5 Wh L^{-1} w 20 °C) w przeliczeniu na objętość elektrod. W związku z powyższym jako materiał elektrodowy zastosowano mieszaninę tych dwóch węgli, dzięki czemu kondensator podwójnej warstwy elektrycznej wykazywał zarówno wysoką gęstość energii w przeliczeniu na masę i objętość elektrod, a także jej zachowanie w temperaturze -40 °C (39%).

Niemniej jednak wydaje się, że potrzebny jest jeden materiał elektrodowy umożliwiający uzyskanie dobrych parametrów pracy kondensatorów podwójnej warstwy elektrycznej. Dalsze prace w tym obszarze przedstawiono w rozdziale IV. Kolejny węgiel o strukturze hierarchicznej z zsyntetyzowano odwzorowując strukturę krzemionki koloidalnej o wielkości cząstek 12 nm. Otrzymany węgiel był gęstszy niż wspomniany powyżej MP98B, z dobrze dostosowanym rozmiarem mezoporów o średniej wielkości 9 nm. Ponadto, przygotowano trójskładnikowe mieszaniny [EMIm][FSI], [EMIm][BF4] i [EMIm][TCB] o różnym stosunku molowym i stwierdzono, że [EMIm][FSI]$_{0,6}$[BF4]$_{0,1}$[TCB]$_{0,3}$ ma niską lepkość (η=23,6 mP s

w 20 °C) i wysokie przewodnictwo (σ = 14,2 mS cm^{-1} w 20 °C). Materiały te zostały użyte do wykonania kondensatora podwójnej warstwy elektrycznej uzyskując wyższą gęstość energii (Es = 31 Wh kg^{-1} i Ev = 12,2 Wh L^{-1} w 20 °C), nawet w temperaturze -40 °C, gdzie 43 % początkowej wartości energii zostało zachowane.

Na zakończenie, w celu zwiększenia bezpieczeństwa urządzenia, przygotowano kondensatory podwójnej warstwy elektrycznej z elektrolitami stałymi na bazie cieczy jonowych, zwane jonożelami. Elektrolity w formie foli wykonano z optymalnej mieszaniny dwuskładnikowej cieczy jonowych [EMIm][FSI]$_{0,5}$[BF$_4$]$_{0,5}$ oraz poli(fluorku winylidenu (PVdF) jako żelowej matrycy. Kondensatory podwójnej warstwy elektrycznej na bazie tychże ionożeli i elektrod z węgla MP98B o strukturze hierarchicznej miały wysokie napięcie pracy i wykazywały paprametry pracy zbliżone do kondensatora wykonanego z ciekłego elektrolitu i takich samych elektrod. Ponadto, kondensator wykorzystujący elektrolit stały wykazał wysoką trwałość cykliczną w niskich temperaturach i „łagodnych" warunkach doświadczalnych, a jednocześnie, przy stałej mocy 1000 W kg^{-1}, wyższą gęstość energii w przeliczeniu na masę elektrod (Es = 3,8 Wh kg^{-1} przy 40 °C) niż urządzenie oparte na elektrolicie ciekłym (Es = 1,1 Wh kg^{-1} przy -40 °C).